Fryer, P., Pearce, J. A., Stokking, L. B., et al., 1990
Proceedings of the Ocean Drilling Program, Initial Reports, Vol. 125

14. SITE 786[1]

Shipboard Scientific Party[2]

HOLE 786A

Date occupied: 2 April 1989

Date departed: 4 April 1989

Time on hole: 2 days, 6 hr, 45 min

Position: 31°52.48′N, 141°13.58′E

Bottom felt (rig floor; m; drill-pipe measurement): 3069.5

Distance between rig floor and sea level (m): 11.40

Water depth (drill-pipe measurement from sea level; m): 3058.1

Total depth (rig floor; m): 3236.00

Penetration (m): 166.50

Number of cores: 19

Total length of cored section (m): 166.50

Total core recovered (m): 84.95

Core recovery (%): 51

Oldest sediment cored:
Depth (mbsf): 115.71
Nature: nannofossil marl
Earliest age: middle Eocene

Hard rock:
Depth (mbsf): 124.90
Nature: metabasalt

HOLE 786B

Date occupied: 4 April 1989

Date departed: 16 April 1989

Time on hole: 12 days, 2 hr, 45 min

Position: 31°52.45′N, 141°13.59′E

Bottom felt (rig floor; m, drill-pipe measurement): 3082.4

Distance between rig floor and sea level (m): 11.40

Water depth (drill-pipe measurement from sea level; m): 3071.0

Total depth (rig floor; m): 3911.00

Penetration (m): 828.60

Number of cores: 72

Total length of cored section (m): 666.10

Total core recovered (m): 190.07

Core recovery (%): 28.5

Oldest sediment cored:
Nature: sedimentary breccias, sandstones, siltstones, and claystones interbedded with igneous rocks
Earliest age: early Eocene

Hard rock:
Depth (mbsf): 162.5
Nature: pillowed and massive flows, breccias, dikes and sills of picrites, high-magnesian basalts, boninites, basalts, andesites, dacites, and rhyolites

Principal results: Site 786 (proposed Site BON-6C) is located in the center of the Izu-Bonin forearc basin about 120 nmi east of the active volcano Myojin Sho.

The stratigraphic section recovered at Site 786 has been assigned to four lithologic units (I through IV). Units I through III are defined only in Hole 786A, in which the sedimentary sequence at the site was recovered. Unit IV is defined in both Holes 786A and 786B. Unit I, from 0 to 83.46 meters below seafloor (mbsf), consists of nannofossil marls and clays and is of early Pleistocene to middle Miocene age. Unit II (83.46–103.25 mbsf) is late Oligocene to middle Eocene age, nannofossil marl and nannofossil-rich clay. Also present is a volcanogenic component containing vitric ash and mineral fragments. Unit III (103.25–124.90 mbsf) is a sequence of volcaniclastic breccia, of middle Eocene age. Unit IV (124.9–166.5 mbsf in Hole 786A and 162.5–826.6 mbsf in Hole 786B) consists of volcaniclastic and sedimentary breccias, vitric siltstones and sandstones, lavas, dikes, and pyroclastic flows.

The rocks in the bottom of Hole 786A and the top of Hole 786B are considered to be the same material. Sedimentation rates were highest in the Pliocene (8.6 m/m.y.) and decreased (to 4.2 m/m.y.) between the latest Miocene and middle Miocene. A hiatus exists between the middle Miocene and the late Oligocene. The igneous basement has mainly massive and brecciated flows, ash flows, and intercalated sediment in an upper part and pillow lavas and dikes or sills below. Rock types include high-magnesian basalts, boninites, basalts, andesites, dacites, and rhyolites. There are several prominent shear zones and hydrothermal breccias within the sequence. Studies of physical properties show that the average bulk densities are 1.65 g/cm^3 in the sediments and 1.8 to 2.1 g/cm^3 in the volcanic sequences; the average grain density of 2.65 g/cm^3 varied little between the sediments and the volcanic rocks. Preliminary interpretation of the paleomagnetic data indicates little translation since the late Miocene.

BACKGROUND AND SCIENTIFIC OBJECTIVES

Site 786 is located on the outer half of the Izu-Bonin forearc, about 120 km east of the active arc volcano of Myojin Sho and about 70 km west of the axis of the Izu-Bonin Trench (Fig. 1). This site was originally designated as a contingency site to augment or fulfill the objectives of Sites 782 and 785. Thus, the objectives of this site are the same as those of Sites 782 and 785, namely to determine the following:

1. The stratigraphy of the forearc and hence the temporal variations in sedimentation, depositional environment, paleoceanography, and intensity and chemistry of the volcanism in the active arc;
2. The uplift/subsidence history of the outer half of the forearc to provide information about forearc flexure and basin development as well as about the extent of any vertical tectonic activity that may have taken place since formation of the forearc terrane;
3. The nature of igneous basement forming the forearc, to answer questions concerning the nature of volcanism in the

[1] Fryer, P., Pearce, J. A., Stokking, L. B., et al., 1990. *Proc. ODP, Init. Repts.*, 125: College Station, TX (Ocean Drilling Program).

[2] Shipboard Scientific Party is as given in the list of participants preceding the contents.

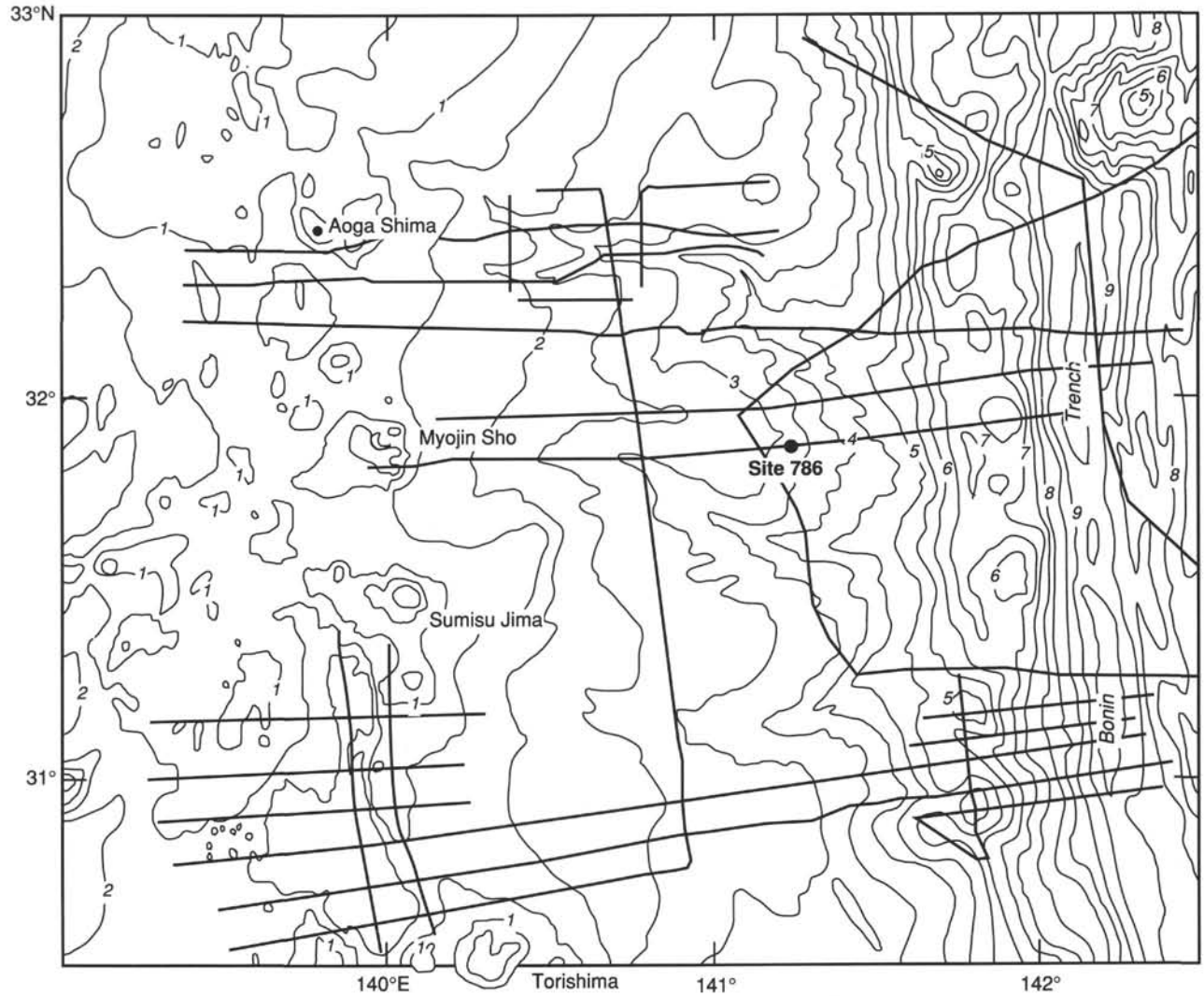

Figure 1. Location of Site 786 within the Izu-Bonin forearc. Contours are in kilometers below sea level.

initial stages of subduction, the origin of boninites, and formation of the 200-km-wide arc-type forearc crust; and

4. The microstructural deformation and the large-scale rotation and translation of the forearc terrane since the Eocene.

Details of the approach for achieving these objectives are described in the "Background and Scientific Objectives" section, "Site 782" chapter (this volume).

OPERATIONS

Transit to Site 786 (proposed Site BON-6C)

Time was available to drill Site 786 (proposed Site BON-6C) because the pumice layer at Site 785 could not be penetrated. The 64-nmi transit to Site 786 was made in 10.5 hr and included a 4.75-hr site survey. A beacon was deployed at 2015UTC, 1 April 1989, to establish Site 786.

Hole 786A

A standard advanced hydraulic piston corer/extended core barrel (APC/XCB) bottom-hole assembly (BHA) with a lockable flapper valve, nonmagnetic drill collar, and soft-formation bit was assembled and deployed. Three APC water cores were taken to a depth of 29 mbsf (from the bottom depth indicated by the precision depth recorder). The BHA was raised 7.5 m and another APC shot recovered 9.7 m of core. Hole 786A was officially spudded at 0815UTC, 2 April, and the mud line was established at 3058.1 m below sea level (mbsl).

From the first three APC core barrels we recovered 29.6 m of core for a recovery rate of 103%. The XCB was then deployed from Cores 125-786A-4X to 125-786A-19X (28.7–166.5 mbsf, total depth), where 55.3 m of core was recovered for a recovery rate of 40.1%. A total of 166.5 m was cored in Hole 786A in 19 runs that recovered 85 m of core for a total recovery of 51% (Table 1). Heat flow was measured at 28.7 and 76.8 mbsf. Upon reaching basement, a round trip was made so that Hole 786B could be drilled into basement using the rotary core barrel (RCB). Hole 786A officially ended at 0300UTC, 4 April, when the bit was back on deck.

Hole 786B

A standard RCB BHA was prepared with a mechanical bit release and a medium-formation bit. The vessel was offset 30 m to the south as the BHA was tripped in. Hole 786B was officially spudded when the seafloor was tagged at a depth of 3071.0 mbsl at 0845UTC, 4 April. The hole was washed to a depth of 162.6 mbsf before coring began.

Table 1. Coring summary for Site 786.

Core no.	Date (April 1989)	Time (UTC)	Depth (mbsf)	Length cored (m)	Length recovered (m)	Recovery (%)
125-786-A-						
1H	2	0830	0.0–9.7	9.7	9.73	100.0
2H	2	0930	9.7–19.2	9.5	9.94	104.0
3H	2	1030	19.2–28.7	9.5	9.96	105.0
4X	2	1350	28.7–38.2	9.5	2.18	22.9
5X	2	1445	38.2–47.6	9.4	5.47	58.2
6X	2	1535	47.6–57.1	9.5	6.70	70.5
7X	2	1700	57.1–67.1	10.0	7.51	75.1
8X	2	1755	67.1–76.8	9.7	1.16	11.9
9X	2	2215	76.8–86.4	9.6	8.61	89.7
10X	2	2300	86.4–96.0	9.6	8.45	88.0
11X	3	0005	96.0–105.7	9.7	8.96	92.4
12X	3	0145	105.7–115.3	9.6	2.27	23.6
13X	3	0430	115.3–124.9	9.6	0.41	4.3
14X	3	0630	124.9–134.6	9.7	0.41	4.2
15X	3	0910	134.6–144.3	9.7	0.25	2.6
16X	3	1140	144.3–154.0	9.7	0.63	6.5
17X	3	1450	154.0–155.0	1.0	0.47	47.0
18X	3	1715	155.0–164.0	9.0	1.36	15.1
19X	3	2035	164.0–166.5	2.5	0.48	19.2
Coring totals				166.5	84.95	51.0
125-786-B-						
1R	4	0030	162.5–169.5	7.0	0.70	10.0
2R	4	0300	169.5–179.2	9.7	0.62	6.4
3R	4	0500	179.2–189.0	9.8	0.87	8.9
4R	4	0600	189.0–198.6	9.6	0.82	8.5
5R	5	0753	198.6–208.2	9.6	1.83	19.0
6R	5	0925	208.2–217.8	9.6	2.70	28.1
7R	5	1030	217.8–227.6	9.8	0.20	2.0
8R	5	1150	227.6–237.1	9.5	0.74	7.8
9R	5	1345	237.1–246.6	9.5	2.16	22.7
10R	5	1530	246.6–256.3	9.7	1.70	17.5
11R	5	1720	256.3–266.0	9.7	1.53	15.8
12R	5	1910	266.0–275.7	9.7	2.21	22.8
13R	5	2130	275.7–285.4	9.7	2.49	25.7
14R	5	2315	285.4–295.0	9.6	0.88	9.2
15R	6	0100	295.0–304.6	9.6	2.55	26.5
16R	6	0300	304.6–314.3	9.7	2.06	21.2
17R	6	0430	314.3–323.9	9.6	0.90	9.4
18R	6	0600	323.9–333.6	9.7	0.86	8.9
19R	6	0800	333.6–343.3	9.7	0.76	7.8
20R	6	0910	343.3–353.0	9.7	0.96	9.9
21R	6	1045	353.0–362.6	9.6	2.10	21.9
22R	6	1210	362.6–372.3	9.7	3.88	40.0
23R	6	1325	372.3–381.9	9.6	0.12	1.3
24R	6	1455	381.9–391.5	9.6	1.81	18.8
25R	6	1700	391.5–401.2	9.7	0.77	7.9
26R	6	1840	401.2–410.8	9.6	1.03	10.7
27R	6	2018	410.8–420.4	9.6	1.85	19.3
28R	6	2215	420.4–430.1	9.7	1.17	12.0
29R	7	0100	430.1–439.7	9.6	0.64	6.7
30R	7	0415	439.7–449.4	9.7	2.95	30.4
31R	7	0730	449.4–459.0	9.6	2.32	24.1
32R	7	0905	459.0–468.7	9.7	1.94	20.0
33R	7	1040	468.7–478.3	9.6	0.95	9.9
34R	7	1515	478.3–488.0	9.7	4.63	47.7
35R	7	1720	488.0–497.7	9.7	4.04	41.6
36R	7	1940	497.7–507.4	9.7	0.85	8.8
37R	8	0000	507.4–517.1	9.7	2.68	27.6
38R	8	0245	517.1–526.8	9.7	1.19	12.2
39R	8	0500	526.8–536.3	9.5	3.00	31.6
40R	8	0800	536.3–545.9	9.6	3.63	37.8
41R	8	0940	545.9–555.6	9.7	4.35	44.8
42R	8	1345	555.6–565.0	9.4	4.40	46.8
43R	8	1650	565.0–574.6	9.6	2.15	22.4
44R	8	2015	574.6–584.3	9.7	1.35	13.9
45R	8	2215	584.3–593.9	9.6	1.25	13.0
46R	9	0100	593.9–603.5	9.6	3.00	31.2
47R	9	0300	603.5–613.2	9.7	1.27	13.1
48R	9	0545	613.2–622.9	9.7	2.57	26.5
49R	9	0745	622.9–632.5	9.6	4.67	48.6
50R	9	0920	632.5–642.2	9.7	1.80	18.5
51R	9	1100	642.2–651.9	9.7	1.38	14.2
52R	9	1300	651.9–661.6	9.7	2.83	29.2
53R	9	1500	661.6–671.2	9.6	1.68	17.5
54R	9	1705	671.2–680.8	9.6	5.54	57.7
55R	9	2030	680.8–690.1	9.3	4.03	43.3
56R	10	0130	690.1–699.8	9.7	7.64	78.7
57R	10	0700	699.8–709.4	9.6	9.53	99.3
58R	10	1035	709.4–714.4	5.0	5.49	110.0
59R	10	1350	714.4–719.0	4.6	5.35	94.5
60R	10	2000	719.0–728.7	9.7	8.32	85.8
61R	10	0130	728.7–738.4	9.7	7.80	80.4
62R	10	0600	738.4–748.0	9.6	3.51	36.5
63R	10	1025	748.0–757.7	9.7	1.63	16.8
64R	10	1310	757.7–767.4	9.7	3.52	36.3
65R	10	1530	767.4–777.1	9.7	2.79	28.7
66R	10	1800	777.1–786.7	9.6	3.26	33.9
67R	11	0030	786.7–796.3	9.6	0.76	7.9
68R	11	0215	796.3–797.3	1.0	0.60	60.0
69R	11	0730	797.3–806.9	9.6	8.13	84.7
70R	11	1145	806.9–815.6	8.7	4.40	50.6
71R	11	1750	815.6–823.6	8.0	4.56	57.0
72R	11	2200	823.6–828.6	5.0	2.42	48.4
Coring totals				66.1	190.07	28.5

The RCB was deployed 72 times, coring 666.1 m and recovering 190.1 m of core for a recovery rate of 28.5%. Total depth was 828.6 mbsf, when coring was halted so that the remainder of the time allotted to Leg 125 could be used for logging.

The BHA was pulled to 3172.6 mbsl, and the logging line was prepared. Six suites of logging tools were used in Hole 786B. The first suite of logging tools, consisting of the dual induction tool (DIT), the digital sonic tool (SDT), and the natural gamma-ray spectrometry tool (NGT), was run from 3520.0 mbsl (the depth of a bridge that the tools could not penetrate) to the top of the hole. The second suite, consisting of the lithodensity tool (LDT), the compensated neutron tool (CNT), and the NGT, was run to 3458.1 mbsl. Another bridge encountered at that depth could not be penetrated by these tools, so the hole was logged from there to the top.

The Schlumberger equipment was rigged down, and the pipe was run in the hole to clear the bridges. The hole was clear from 3516.6 to 3808.6 mbsl, and the BHA was raised to 3519.6 mbsl so that the lower section of the hole could be logged.

The third logging suite, consisting of the DIT, LDT, CNT, and SDT, was deployed to 3892.0 mbsl, and the hole was logged from that point upward to 3535.2 mbsl. The fourth suite, consisting of the induced gamma-ray spectrometry tool (GST), the aluminum clay tool (ACT), and the NGT, was deployed to 3892.0 mbsl, and the hole then was logged to the mud line. The borehole televiewer (BHTV) was deployed for the fifth logging run, but failed downhole. During the sixth logging run, the spare BHTV was deployed, and we logged 80 m of the hole before logging time expired.

The BHTV was pulled out of the hole and the logging equipment was rigged down. The BHA was pulled to the drill floor at 0800UTC, 16 April, officially ending Hole 786B. The BHA was then inspected and secured in the derrick. With the BHA back on deck, the vessel was under way at 1130UTC, 16 April, and the occupation of Site 786 officially ended.

Site 786 to Tokyo

A survey was performed over Site 786 before steaming north to Tokyo. At 1430UTC, 16 April, the seismic gear was retrieved and the transit began. The 252-nmi transit to Tokyo was made in 35.5 hr. The anchor was dropped at 2300UTC, 17 April 1989, officially ending Leg 125.

LITHOSTRATIGRAPHY

A downhole stratigraphy of nannofossil marls, sedimentary breccias interlayered with nannofossil marls, and igneous rocks defines four lithologic units at Holes 786A and 786B (Table 2). Lithologic Units I through III are lower Pleistocene to middle Eocene sediments. Lithologic Unit IV is early Eocene age volcanic basement present in both holes, with drilling-produced chips and pebbles at Hole 786A and the entire stratigraphic section recovered at Hole 786B. Hole 786B is 30 m south of Hole 786A.

Unit I

Sections 125-786A-1H-1, 0 cm, to 125-786A-9X-5, 66 cm; depth, 0.0–83.46 mbsf.
Age: early Pleistocene to middle Miocene.

Lithologic Unit I is a succession of lower Pleistocene through middle Miocene nannofossil marls and clays with a persistent volcanogenic component. Upper and middle Pleistocene strata are missing, on the basis of an early Pleistocene assemblage of nannofossils in the uppermost sample (125-786A-1H-1, 2 cm). Sediment color varies from very pale brown (10YR 7/3), light brownish gray (2.5Y 6/2), gray (10YR 6/1), and dark grayish brown (2.5Y 4/2) to dark gray (5Y 4/1 and 10YR 4/1). Nannofossils are the dominant biogenic component (present in amounts up to 56%; in one sample up to 70%) forming nannofossil marl (in one sample forming a thin—<1-cm-thick—calcareous ooze), glass-rich nannofossil marl, and nannofossil-rich clay. Foraminifers (trace–30%) and micrite (trace–40%) are also present. Radiolarians (trace–4%), diatoms (trace–3%), and sponge spicules (trace–5%) form the biosiliceous component. Terrigenous detritus is predominantly clay (5%–72%) with some quartz (trace–1%).

Volcaniclastics are ubiquitous as dispersed vitric particles or pumice fragments and in ash layers (Table 3). Locally, concentrations in pelagic sediments are sufficient to define glass-rich nannofossil marls and glass-rich clays, such as in Cores 125-786A-4X and 125-786A-5X. Volcanogenic material is primarily vitric debris (trace–57%) with lesser amounts of pyroxene and feldspar (trace–5%). Pumice is disseminated throughout lithologic Unit I as subrounded to rounded, granule-sized, light brownish gray (2.5Y 6/2) particles. Scattered larger pumice clasts, up to 3 cm in diameter, occurring downhole from about Core 125-786A-3H are brown (7.5YR 5/4), dark gray (5YR 5/1), and white (10YR 8/1). Volcaniclastic layers of predominantly vitric detritus (60%–100%) are common throughout Unit I (see Table 3) and probably represent both pyroclastic air-fall and epiclastic deposits.

Sedimentary structures are rare. A few volcaniclastic layers have normal size grading, and others have poorly defined laminae. A 55-cm-thick layer of feldspar-rich, foraminiferal vitric sand in Section 125-786A-1H-5, 60–115 cm, contains vague laminae. Nonclastic sediment sequences are extensively burrowed; thus, possible sedimentary structures are obliterated. A few synsedimentary normal faults are present, with one prominent example truncating a burrow filled with black (N 4/0) clay (Section 125-786A-2H-7, 28 cm).

Carbonate-cemented pelagic sediment occurs at two levels in Unit I (Sections 125-786A-1H-6, 140 cm, and 125-786A-6X-4, 0–10 cm) as indurated and blocky pieces of black (N 4/0) lithic fragments. A pebble of chlorite-rich, vitric, silty claystone is present in the top 2 cm of Core 125-786A-6X. The lithic fragment is gray (5Y 5/1), with a discoid and rounded shape (3.5 × 3 × 2 cm in size), contains clasts of granule-sized chloritized pumice as well as sand-sized altered igneous rocks, and is cut by numerous chlorite veins. Microfossil assemblages suggest an age of middle Miocene, slightly older than or equivalent to the age of the host sediment (see "Biostratigraphy" section, this chapter).

The basal sediment in lithologic Unit I is a black (10YR 2/1) vitric ash composed of sideromelane and manganese oxide (both in about equal proportions) with trace amounts of calcareous nannofossils. Ferromanganese oxides are present both as disseminated silt-sized particles and as coatings with laminated-botryoidal textures on the edges of blocky sediment clasts. This 10-cm-thick deposit in Section 125-786A-9X, 56–66 cm, represents a hiatus separating middle Miocene and upper Oligocene biozones (see "Biostratigraphy" and "Sediment-Accumulation Rates" sections, this chapter).

Unit II

Sections 125-786A-9X-5, 66 cm, to 125-786A-11X-5, 125 cm; depth, 83.46–103.25 mbsf.
Age: late Oligocene to middle Eocene.

A distinctive color change to reddish brown (10YR 5/4) nannofossil marls marks the change to lithologic Unit II. Gray

Table 2. Lithologic units recovered at Site 786.

Lithologic unit	Cores	Depth (mbsf)	Dominant lithology	Stratigraphic age
I	786A-1H-1, 0 cm, to 786A-9X-5, 66 cm	0.0–83.46	Nannofossil marl, nannofossil-rich clay, glass-rich clay	lower Pleistocene to middle Miocene
II	786A-9X-5, 66 cm, to 786A-11X-5, 125 cm	83.46–103.25	Nannofossil marl, nannofossil-rich clay	upper Oligocene to upper Eocene
III	786A-11X-5, 125 cm, to 786A-13X-CC, 44 cm	103.25–124.90	Volcaniclastic breccia	middle Eocene
IV	786A-14X-1, 0 cm, to 786A-19X-1, 15 cm	124.90–166.50	Igneous rocks	middle Eocene(?)
	786B-1R-1, 0 cm, to 786B-72R-2, 138 cm	162.50–826.60	Volcaniclastic and sedimentary breccias, lava and pyroclastic flows, vitric siltstone and sandstone	middle Eocene

Table 3. Volcaniclastic layers in lithologic Unit I, Hole 786A.

Core, section, interval (cm)	Depth of top of section (mbsf)	True depth (mbsf)	Volcaniclastic layer
125-786A-			
1H-1, 62–77	0	0.62–0.77	1
1H-2, 3–5	1.5	1.53–1.55	2
1H-2, 5–18	1.5	1.55–1.68	3
1H-4, 12–16	4.5	4.62–4.66	4
1H-4, 23.5–25	4.5	4.735–4.75	5
1H-5, 62–111	6	6.62–7.11	6
1H-6, 77–78	7.5	8.27–8.28	7
1H-7, 5–8	9	9.05–9.08	8
2H-1, 10–14	9.7	9.80–9.94	9
2H-1, 29–30	9.7	9.99–10.0	10
2H-1, 80	9.7	10.5	11
2H-2, 99–113	11.2	12.19–12.33	12
2H-2, 143–146	11.2	12.63–12.66	13
2H-3, 145–146	12.7	14.10–14.14	14
2H-4, 36–40	14.2	14.56–14.60	15
2H-4, 84–85	14.2	15.04–15.05	16
2H-4, 93–96	14.2	15.13–15.16	17
2H-4, 141–145	14.2	15.60–15.65	18
2H-5, 28–30	15.7	15.98–16.00	19
2H-5, 122–125	15.7	16.92–16.95	20
2H-6, 14–17	17.2	17.34–17.37	21
3H-1, 41–44	19.2	19.61–19.64	22
3H-1, 54–58	19.2	19.74–19.78	23
3H-1, 87–90	19.2	20.07–20.10	24
3H-2, 100–103	20.7	21.70–21.73	25
3H-3, 116–120	22.2	23.36–23.40	26
3H-3, 116–120	22.2	23.36–23.40	26
3H-5, 79–80.5	25.2	25.99–26.005	27
3H-6, 102–112	26.7	27.72–27.82	28
3H-CC, 10–17	28.89	28.99–29.06	29
3H-CC, 21	28.89	29.1	30
4X-1, 60–61	28.7	29.30–29.31	31
5X-1, 39–41	38.2	38.59–38.61	32
5X-1, 74–76	38.2	38.94–38.96	33
5X-1, 74–76	38.2	38.94–38.96	33
5X-1, 78–79	38.2	38.98–38.99	34
5X-1, 106–107	38.2	39.26–39.27	35
5X-2, 14–15	39.7	39.84–39.85	36
6X-1, 21–25	47.6	47.81–47.85	37
6X-1, 93–94	47.6	48.53–48.54	38
6X-2, 37–46	49.1	49.91–49.92	39
6X-2, 102–103	49.1	50.12–50.13	40
6X-3, 126.5–128	50.6	51.865–51.88	41
6X-5, 8–9	53.6	53.68–53.69	42
6X-5, 22–27	53.6	53.82–53.87	43
6X-5, 36–40	53.6	53.98–54.0	44
7X-1, 138–140	57.1	58.48–58.50	45
7X-2, 125–127	58.6	59.85–59.87	46
7X-3, 3–4	60.1	60.13–60.14	47
7X-3, 15.5–16	60.1	60.255–60.26	48
7X-5, 9–10	63.1	63.19–63.20	49
7X-5, 14–15	63.1	63.24–63.25	50
7X-5, 18–24	63.1	63.28–63.34	51
7X-5, 64–66	63.1	63.74–63.76	52
7X-6, 27–28	64.29	64.56–64.57	53
9X-3, 43–44	79.8	80.23–80.24	54
9X-3, 85–89	79.8	80.65–80.69	55
9X-3, 128–131	79.8	81.08–81.11	56
9X-4, 23–26	81.3	81.53–81.56	57
9X-5, 56–66	82.8	83.36–83.46	58

and greenish gray colors similar to those of lithologic Unit I (5GY 5/1 and 5Y 5/1) reappear downcore (at Section 125-786A-9X-CC, 14.5 cm) in nannofossil marls and sandy nannofossil oozes. These are followed again (Section 125-786A-10X-4, 70 cm) by nannofossil marls and nannofossil-rich clays, which have the same reddish brown color noted at the top of Unit II. This succession of gray and red nannofossil marls and oozes, which defines lithologic Unit II, spans the upper Oligocene to middle Eocene section. Each color change is in close proximity to an unconformity of minor duration (see "Biostratigraphy" and "Sediment-Accumulation Rates" sections).

Sedimentary components are similar to those noted for Unit I. Biogenic components are dominantly nannofossils (2%–60%), with lesser amounts of foraminifers (2%–10%), micrite (1%–35%), and radiolarians (trace–2%). Clays are present in amounts varying between 10% and 50%, opaque minerals between 3% and 15%, and chlorite and serpentine in trace amounts. Volcanogenic components are usually vitric particles (35%–98%) with feldspar (1%–7%) and pyroxene (1%–10%), disseminated in the sediment as detritus or pumice. Volcaniclastic layers are not present. Pumice colors provide a variegated contrast to the pelagic sediment and range from light gray (10YR 4/1), light brownish gray (2.5Y 6/2), white (10YR 8/1), brown (7.5YR 5/4), dark gray (5YR 5/1), and orange to dark yellowish brown (10YR 5/4) and black (N 4/0).

Extensive mottling reflects bioturbation; no sedimentary structures are present. A fault with apparent normal movement (see "Structural Studies" section, this chapter) in Section 125-786A-11X-4, 100 cm, marks an abrupt sediment color change from light reddish brown and reddish brown (5YR 6/3 and 5YR 5/3) to light yellowish brown (2.5YR 6/4). This continues as the dominant background color for about 0.5 m downhole, and then changes between Sections 125-786A-11X-4 and 125-786A-11X-5 to white (2.5Y 8/2) and light gray (2.5Y 7/2). General sediment types (nannofossil oozes and nannofossil marls) and sedimentary components do not change across the fault. Dispersed throughout the sediment below the fault are rounded clasts, 1 to 3 cm in diameter, of glass-rich silt that have a distinctive bright, light greenish gray color (10Y 6/6).

Unit III

Sections 125-786A-11X-5, 125 cm, to 125-786A-13X-CC, 44 cm; depth, 103.25–124.90 mbsf.
Age: middle Eocene.

Increased clast content and an abrupt color change of the matrix sediment to dark brown (2.5YR 4/2) at Section 125-786A-11X-5, 125 cm, define the volcaniclastic breccia that is the dominant lithology of Unit III in Hole 786A; breccia with this color and clast content was not recovered at Hole 786B. Angular to rounded clasts of vitric ash and dacite are green (5GY 6/4), greenish gray (10Y 6/6), dark greenish gray (5BG 4/1), white (N 8/0), dark yellowish brown (10YR 6/8), grayish brown (10YR 5/2), and black (10YR 2/1). The black color is caused by manganese oxides disseminated within the ash. Clast diameters average about 1 cm, with rare larger clasts reaching 4 cm, such as in a moderately well-sorted breccia in Sections 125-786A-11X-6 and 125-786A-11X-CC. Dacite fragments up to 6 cm in diameter form a poorly sorted breccia in Sections 125-786A-12X-1 and 125-786A-12X-2. Clasts float in a matrix of white (2.5Y 8/2) and light gray (2.5Y 7/2) nannofossil marl.

Sedimentary components in the matrix are predominantly nannofossils (up to 65%, locally forming nannofossil oozes); additional components include foraminifers (1%–10%), micrite (1%–35%), radiolarians (trace–2%), clay (10%–50%), and opaque mineral grains (3%–15%).

No sedimentary structures occur in this unit for interpreting depositional and post-depositional processes.

Unit IV

Sections 125-786A-14X-1, 0 cm, to 125-786A-19X-1, 15 cm; depth, 124.90–166.50 mbsf. Age: middle Eocene(?).
Sections 125-786B-1R-1, 0 cm, to 125-786B-72R-2, 138 cm; depth, 162.50–826.60 mbsf.
Age: middle Eocene.

Hole 786A

Lithologic Unit IV at Hole 786A is a mixture of drilling chips and drilling-produced pebbles of igneous rocks and vein material from these rocks, as well as an assortment of volcaniclastic and

sedimentary rocks typical of the clast lithologies in lithologic Unit III. The determination of biostratigraphic age was not attempted because of the uncertain stratigraphic position of the chips and pebbles; however, a middle Eocene age may be assumed for lithologic Unit IV based on the oldest age obtained from similar lithologies in the overlying lithologic unit.

Hole 786B

Sedimentary breccias, sandstones, siltstones, and claystones interbedded within a 666.1-m-thick succession of lava flows, pyroclastic flows, pillow flows, and dikes constitute lithologic Unit IV at Hole 786B. Deposition during the middle to late Eocene is inferred for this unit based upon a limited nannofossil assemblage. Sedimentary rocks form nearly one-half of the stratigraphic sequence if all the volcaniclastic rocks are considered sedimentary. If these rocks are treated as igneous because they may be autobrecciated interflow deposits, then sedimentary rocks represent less than 10% of the stratigraphic succession. In order of abundance, rock types are volcaniclastic breccias, volcaniclastic conglomerates, vitric siltstones, vitric clayey siltstones, and vitric sandstones. The addition of various mineralogic components forms jasper and chlorite siltstones, chlorite vitric sands, chlorite-orthopyroxene-glass-rich sandstones, feldspar-rich vitric silty sandstones and feldspar, and glass-rich silty clays.

The dominant detrital component is volcanogenic, including glass (20%–100%), pyroxene (1%–30%), feldspar (1%–15%), igneous rock fragments (trace–10%), and amphibole (trace–5%). Sideromelane and palagonite are common glass types in interpillow deposits. Pyroxenes (predominantly orthopyroxene) form thick sequences of sand as the matrix within breccias and conglomerates (e.g., in Cores 125-786B-7R to 125-786B-12R). Another detrital component is clay (10%–53%). Clasts in volcaniclastic breccias and conglomerates vary in size from 2 mm (granule size) up to 6 cm (the diameter of the core barrel and thus the limit of megascopic resolution of clasts from flow/sedimentary layers), have shapes that are angular to subrounded, and consist of fragments of vitric and lithic volcanic rocks such as pillow rinds.

Minerals of presumed diagenetic origin, perhaps in connection with hydrothermal fluid circulation, include opaque minerals (1%–50%), chlorite (4%–97%), chert and jasper (2%–44%), zeolites (trace–2%), and sepiolite (trace–100%). Pyrite, chlorite, chert, and jasper are found in the lower part of the section (Cores 125-786B-27R to 125-786B-72R for chlorite and 125-786B-61R and 125-786B-62R for chert and jasper). Chlorite sands with vitric and pyroxene grains exhibit crossbedding and laminae structures (Core 125-786B-27R); it is not clear whether the chlorite here represents a detrital fraction or the post-depositional alteration of detrital vitric grains. Zeolites are found only in the upper part of the middle of the stratigraphic section (Core 125-786B-22R). Section 125-786B-22R-1, 28–42 cm, also includes a spectacular 14-cm-thick sepiolite layer of moderate pink (5R 6/4) to grayish pink (5R 8/2) that may have a hydrothermal origin.

Biogenic components such as nannofossils (trace–5%), radiolarians (trace), and a spicule (trace) are rare. Micrite is present in trace amounts to 4% and may be of either biogenic or authigenic origin.

A marine sedimentary environment is indicated by these biogenic components as well as by small structures interpreted as burrows in Section 125-786B-34R-1. The provenance of clastic particles is assumed to be nearby igneous rocks on the basis of (1) the large size (sand or ash size, gravel or block size) and shapes (usually angular to subangular) of grains and clasts, (2) the high proportion of clasts compared to fine-grained detritus creating poorly sorted deposits, (3) the similarity in lithology between igneous flows/dikes and the volcanogenic detritus, and (4) a predominance of easily abraded, vitric grains. The matrix-supported clast textures of the volcaniclastic breccias and conglomerates suggest either mass-flow or particle-by-particle deposition. Existing criteria are inadequate to differentiate between the two processes in the absence of obvious contacts between these coarse-grained deposits. Sedimentary structures indicative of depositional processes for sandstones and siltstones are scarce, but normal size grading, syndepositional slump structures, cross-bedding, and laminae demonstrate mass-flow and redepositional mechanisms.

Correlation Between Holes 786A and 786B

Lithologic Unit IV is thought to be correlative between Holes 786A and 786B in stratigraphic position and age because (1) of the proximity of the two holes, (2) cores containing this unit were cut at about the same sub-bottom depth, (3) the recovered igneous rocks appear similar in hand specimen and smear slide, and (4) biostratigraphic criteria indicate that both units may be middle Eocene in age. Hole 786B is 30 m south of Hole 786A. The depth of the bottom of Core 125-786A-19X at the base of the hole is 166.50 mbsf; the depth of the top of Core 125-786B-1R is 162.50 mbsf. Rock types from lithologic Unit IV at both sites are dark gray and black, vesicular, olivine- and orthopyroxene-bearing andesites with vesicles commonly filled by a bluish zeolite.

BIOSTRATIGRAPHY

Evidence from calcareous nannofossils, foraminifers, and diatoms assigns an early Pleistocene age to the uppermost sediments in Hole 786A. Nannofossils date the lowermost sediments to the middle Eocene. The sediments interbedded with the lava flows in Hole 786B are assigned an Eocene age based on their nannofossil assemblages. The biostratigraphy from this site is summarized in Figure 2, with the age boundaries based on nannofossil data.

Calcareous Nannofossils

Hole 786A

Pleistocene through middle Eocene nannofossil assemblages from Hole 786A are abundant; their preservation is good to moderate.

The uppermost Sample 125-786A-1H-1, 2 cm, is early Pleistocene (Subzone CN14a) in age on the basis of the co-occurrence of *Pseudoemiliania lacunosa*, *Calcidiscus macintyrei*, *Gephyrocapsa oceanica*, *Gephyrocapsa caribbeanica*, and *Helicosphaera sellii*; thus, upper and middle Pleistocene sediments are missing.

Sample 125-786A-1H-1, 150 cm, is late Pliocene (Subzone CN13b) based on the occurrence of *G. caribbeanica* and the absence of *G. oceanica*. Sample 125-786A-1H-2, 96 cm, has been assigned to Subzone CN12b by the presence of *Discoaster brouweri* and *Discoaster surculus* and the absence of *Discoaster tamalis*. The occurrences of *D. tamalis* together with *Ceratolithus separatus* in Samples 125-786A-1H-4, 92 cm, to 125-786A-2H-CC allow us to assign these sediments to Subzone CN12a (late Pliocene).

Sample 125-786A-3H-CC contains *Reticulofenestra pseudoumbilica*, *Ceratolithus acutus*, and *Sphenolithus* spp. and is therefore early Pliocene in age (Subzone CN10b).

Samples 125-786A-4X-CC and 125-786A-5X-CC are dated as late Miocene (Zones CN9b and CN9a, respectively) by the occurrence of *Discoaster berggrenii* and *Discoaster quinqueramus* in both and also in the former sample of *Amaurolithus*

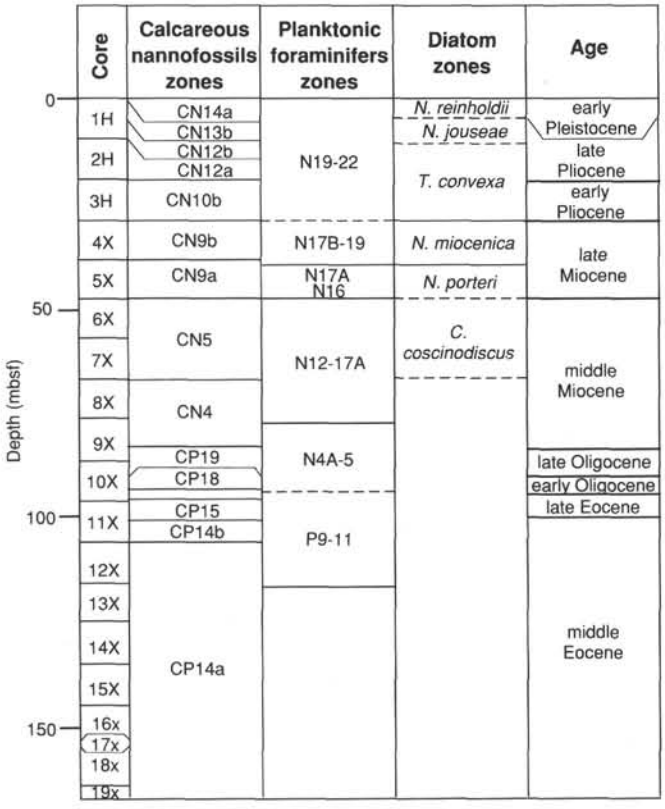

Figure 2. Summary of biostratigraphic data from Hole 786A.

delicatus, *Amaurolithus tricorniculatus*, and *Discoaster blackstockae*. *Discoaster kugleri* and *Discoaster exilis* are present in Samples 125-786A-6X-CC and 125-786A-7X-CC, which are, therefore, middle Miocene in age (Zone CN5). Samples 125-786A-8X-CC to 125-786A-9X-5, 40 cm, are also dated as middle Miocene, but the occurrence of *Sphenolithus heteromorphus*, *D. exilis*, and *C. macintyrei* places these within Zone CN4. The occurrence of specimens of *R. pseudoumbilica* more than 7 mm in size indicates that this is the higher part of Zone CN4. Lower Miocene sediments are missing (Zones CN1 through CN3); a hiatus with a duration of approximately 7.2 m.y. thus is present between the middle Miocene and late Oligocene. A similar hiatus exists between the middle Miocene and the late Oligocene in Hole 782A. The hiatus at Site 786 coincides with a volcanic ash interval at Section 125-786A-9X-5, 56–66 cm.

Abundant, moderately preserved to well-preserved nannofossil assemblages are present from Samples 125-786A-9X-5, 80 cm, to 125-786A-10X-6, 51 cm.

Late Oligocene nannofossil assemblages are found in Samples 125-786A-9X-5, 80 cm, to 125-786A-10X-3, 142 cm; they are characterized by *Dictyococcites bisectus*, *Cyclicargolithus abisectus*, *Helicosphaera recta*, *Sphenolithus ciperoensis*, and *Sphenolithus distentus*, which assigns the assemblages to Zone CP19. Samples 125-786A-10X-4, 42 cm, to 125-786A-10X-5, 95 cm, are dated as early Oligocene (Zone CP18) by the appearance of *Sphenolithus predistentus*. Sample 125-786A-10X-6, 37 cm, is dated by the occurrence of *Ericsonia formosa*, *Reticulofenstra umbilica*, and common *Ericsonia subdisticha* as early Oligocene (Subzone CP16a). A hiatus may occur between Subzones CP18 and CP16a.

Sample 125-786A-10X-CC is near the Oligocene/Eocene boundary. The assemblage contains species usually found in the late Eocene, but the CP15 marker species *Discoaster saipanensis* and *Discoaster barbadiensis* are missing. The last occurrence of these marker species is about 0.5 m.y. before the Oligocene/Eocene boundary. Sample 125-786A-10X-CC is, therefore, latest Eocene in age and is assigned to the base of Subzone CP16a.

The presence of *D. barbadiensis*, *D. saipanensis*, *Cribrocentrum reticulatum*, *Chiasmolithus oamaruensis*, and *Isthmolithus recurvus* dates Sample 125-786A-11X-1, 20 cm, to the late Eocene (Subzone CP15b). The *C. reticulatum* extinction approximates the CP15a/15b boundary; therefore, a short hiatus may be within Subzone CP15b. Samples 125-786A-11X-1, 140 cm, to 125-786A-11X-2, 133 cm, are assigned to the late Eocene (Subzone CP15a) by the occurrence of a late Eocene association and the absence of *Chiasmolithus grandis*, but the genus *Chiasmolithus* is usually rare in samples.

Middle Eocene nannofossil assemblages (Subzone CP14b) (based on the appearance of *C. grandis* together with *D. saipanensis*, *D. barbadiensis*, *C. reticulatum*, *S. predistentus*, and *R. umbilica*) occur in the interval from Samples 125-786A-11X-3, 38 cm, to 125-786A-11X-CC. Nannofossil assemblages from Samples 125-786A-12X-2, 35 cm, to 125-786A-19X-CC are assigned to Subzone CP14a by the occurrence of *Chiasmolithus solitus*, *Sphenolithus furcatolithoides*, and *Reticulofenestra dictyoda*, in association in Sample 125-786A-12X-2, 35 cm, with *D. saipanensis*. The absolute age is between 42.2 and 42.8 m.y., according to Berggren et al. (1985a).

Hole 786B

Rare, poorly to moderately preserved calcareous nannofossils are present in sediments interbedded with the lava flows in Hole 786B.

Samples 125-786B-22R-1, 50 cm, 125-786B-27R-2, 28 cm, and 125-786B-40R-1, 35 cm, are middle to late Eocene in age (CP14-15 Zone), based on the presence of the marker species *Discoaster barbadiensis*, *Discoaster saipanensis*, and *Reticulofenestra umbilica* and the species *Cyclicargolithus floridanus* and *Discoaster deflanderi*.

Nannofossil assemblages were also found in Samples 125-786B-40R-1, 35 cm, 125-786B-41R-3, 60 cm, 125-786B-49R-1, 50 cm, 125-786B-51R-2, 10 cm, and 125-786B-56R-CC. The presence of *Ericsonia formosa*, *Dictyococcites bisectus*, and *Cyclicargolithus floridanus* confines these samples to the middle to late Eocene, although no marker species were found.

Early Eocene nannofossil assemblages are present in Samples 125-786B-61R-6, 26 cm, and 125-786B-63R-1, 92 cm, based on the co-occurrence of *D. barbadiensis*, *Discoaster distinctus*, and *Sphenolithus anarrhopus*.

Foraminifers

The Cenozoic planktonic foraminiferal stratigraphy for Hole 786A is summarized in Table 4. The relatively poor preservation and moderate to low abundance of planktonic foraminifers in most of the cores do not allow an accurate biostratigraphic subdivision of Hole 786A. The presence or absence of the species listed was used to define the age of a sample, but no age determinations using the absence of species were attempted for poorly preserved samples.

The planktonic foraminifers from the sedimentary sequence in Hole 786A were deposited between the Quater-

Table 4. Summary of foraminiferal data, Hole 786A.

Core, section, interval (cm)	Abundance	Preservation	Diagnostic species present	Diagnostic species absent	Nannofossil zone	Age
125-786A-						
1H-6, 140–142	Rare	Poor	*Globorotalia crassaformis*		upper N19–22	middle early Pliocene–Pleistocene
1H-6, 143–144	Rare	Poor	*Globorotalia tosaensis*	—	N21–lower N22	late Pliocene–earliest Pleistocene
1H-CC	Common	Moderate	*Globorotalia tosaensis*	*Globorotalia truncatulinoides*	N21	late Pliocene
2H-CC	Rare	Poor	*Globorotalia crassaformis* *Neogloboquadrina pachyderma*	—	upper N19–21	middle early Pliocene–late Pliocene
3H-CC	Rare	Poor	*Globorotalia crassaformis*	—	upper N19–22	middle early Pliocene–Pleistocene
4X-CC	Rare	Moderate	*Globorotalia plesiotumida* *Sphaeroidinellopsis praedehiscens*	—	N17B–lower N19	middle late Miocene–earliest Pliocene
5X-CC	Rare	Poor	*Globorotalia lenguaensis* *Globigerinoides* cf. *kennetti*	—	N16–17A	early late Miocene–middle late Miocene
6X-CC	Rare	Poor	*Orbulina universa* *Sphaeroidinellopsis seminulina*	—	N9–21	early middle Miocene–late Pliocene
7X-CC	Rare	Poor	*Globorotalia* cf. *lenguaensis*	—	N12–17A	middle middle Miocene–middle late Miocene
8X-CC	Rare	Poor	*Globorotalia* cf. *lenguaensis*	—	N12–17A	middle middle Miocene–middle late Miocene
9X-CC	Abundant	Moderate	*Globigerinoides primordius* *Glogoquadrina praedehiscens*	—	N4A–5	latest Oligocene–earliest Miocene
10X-6, 51–53	Common	Poor	*Catapsydrax dissimilis* *Pseudohastigerina micra*	—	P13–upper P19	middle Eocene–early Oligocene
10X-CC	Common	Moderate	*Cribrohantkenina inflata* *Hantkenina alabamensis*	—	P16–17	latest Eocene
11X-1, 8–10	Few	Poor	*Cribrohantkenina inflata*	—	P16–17	latest Eocene
11X-CC	Few	Poor	*Morozovella aragonensis* *Acarinina bullbrooki*	—	P9–11	latest early Eocene–early middle Eocene
12X-CC	Rare	Poor	*Morozovella aragonensis* *Acarinina bullbrooki*	—	P9–11	latest early Eocene–early middle Eocene

nary (lower Zone P22) and the latest early Eocene (Zones P16 and P17). Evidence from the sparse planktonic foraminiferal assemblages suggests that hiatuses may have existed in the late early Miocene to middle Miocene and the late early Oligocene. The relatively poor preservation and low abundance of planktonic foraminifers in Samples 125-786A-1H-6, 51–53 cm, to 125-786A-12X-CC correlate with the large amounts of volcaniclastic material in these samples.

Diatoms

Rare to common and poorly to well-preserved diatom assemblages are present in the first seven cores of Hole 786A. The samples below Sample 125-786A-7X-CC contain no diatoms.

The uppermost Sample 125-786A-1H-1, 0 cm, is assigned to the *Nitzschia reinholdii* A Zone (Pliocene/Pleistocene boundary) by the co-occurrence of *N. reinholdii*, *Pseudoeunotia doliolus*, and *Rhizosolenia praebergonii*.

The presence of *Nitzschia jouseae* in Sample 125-786A-1H-CC dates this sample as late Pliocene (top of *N. jouseae* Zone).

Zonal marker species were not found in Samples 125-786A-2H-CC and 125-786A-3H-CC. However, Sample 125-786A-3H-CC is tentatively placed in the early Pliocene *Thalassiosira convexa* Zone by the absence of *N. jouseae*.

Nitzschia miocenica is present in Sample 125-786A-4X-CC and *Nitzschia porteri* was found in Sample 125-786A-5X-CC, dating this interval as late Miocene.

Zonal markers were not found in Sample 125-786A-6X-CC, but Sample 125-786A-7X-CC contains *Denticulopsis punctata* f. *hustedtii*, which allows us to assign this sample to the middle Miocene *Craspedodiscus coscinodiscus* Zone.

IGNEOUS AND METAMORPHIC PETROLOGY

From the two holes drilled at Site 786, taken together, we penetrated and recovered strata from 0 to 828 mbsf. In Hole 786A, sediments were recovered from 0 to 100.5 mbsf (Sections 125-786A-1X to 125-786A-11X-5, 100 cm; "Lithostratigraphy" section, this chapter), and a sedimentary breccia marks the transition to basement dominated by igneous strata of boninitic affinity. Predominantly igneous rocks were recovered in this hole from 124.9 to 166.5 mbsf (Sections 125-786A-11X-5, 100 cm, to 125-786A-19X-CC). Hole 786B is offset 30 m toward the south with respect to the preceding hole, and cores were recovered from 162.5 to 828.6 mbsf (Sections 125-786B-1R to 125-786B-72R-2), stratigraphically below the interval penetrated in Hole 786A. The cores of Hole 786B contain lava flows, breccias dominated by igneous clasts, rare sedimentary intervals, and very low-grade metamorphic lavas crosscut by dikes. Biostratigraphic studies ("Biostratigraphy" section) constrain the age of the top of the basement to middle Eocene, and several sedimentary intercalations within the basement also give middle Eocene ages. The deepest sedimentary intercalation dated is in Core 125-786B-61R; local faults and a lack of biostratigraphic data leave the ages below this depth ambiguous.

The igneous and sedimentary sequence in Holes 786A and 786B has been divided into four major lithologic units. The first three units form a lower Pleistocene–middle Eocene sedimentary sequence ("Lithostratigraphy" section). The fourth major unit, basement, is divided into 30 subunits, and is the subject of this section. Intercalated sedimentary strata in lithologic Unit IV are described in the "Lithostratigraphy" section. Unit divisions and rock names are based on macroscopic criteria as well as on major-element chemical analyses. The distinction between boninite series rocks and andesite was not obvious in hand specimen. A nomenclature presented in the "Igneous and Metamorphic Geochemistry" section (this chapter) was developed using the MgO and SiO_2 contents of the rocks. Rock names based on these compositional criteria are given precedence but have not been rigidly applied throughout. Common rock names synonymous with, and commonly more specific than, our compositional nomenclature are used in the hand specimen and thin-section descriptions when they do not conflict with the chemical data, or when no analysis is available. Within these limits, the rock names used in unit descrip-

tions, from analyses, thin section, and hand specimen, are internally consistent.

The following approach is used in the assignment of lithologic units. Multiple volcanic strata of similar character are assigned to a single unit. If two volcanic units are separated by strata of clear sedimentary affinities, the latter are assigned to a separate unit; breccias adjacent to these sediments are assigned to this same unit.

A summary of the petrographic characteristics of the rock types encountered at Site 786 is given in Table 5. The characteristics of the individual units are discussed in the following. The basement lithostratigraphy is illustrated in Figure 3.

Table 5. Petrology of the rock types at Site 786.

Basalt	
Phenocrysts:	Clinopyroxene (3%–5%) + plagioclase (trace–5%) + orthopyroxene (0%–2%)
Groundmass:	Glass (60%–70%) + plagioclase (5%–10%) + clinopyroxene (3%–5%) + opaque minerals (trace–1%)
Comments:	Hyalo-ophitic; Sample 125-786B-40R-2, 54–56 cm, contains 15%–20% olivine
High-magnesian basalt	
Phenocrysts:	Clinopyroxene (5%–8%) + orthopyroxene (4%–7%) + olivine (0%–3%) + spinel (0%–trace)
Groundmass:	Glass (50%–70%) + plagioclase (10%–20%) + clinopyroxene (2%–7%) + orthopyroxene (0%–5%) + opaque minerals (0%–2%)
Comments:	Spinel occurs as inclusions in olivine phenocrysts; glomerophyric texture (olivine + orthopyroxene + clinopyroxene); orthopyroxene has clinopyroxene (100) exsolution lamellae and a clinopyroxene reaction rim
Picrite	
Phenocrysts:	None
Groundmass:	Clinopyroxene (25%–30%) + orthopyroxene (1%–2%) + glass (60%–70%) + opaque minerals (trace–1%)
Boninite	
Phenocrysts:	Orthopyroxene (2%–7%) + clinopyroxene (3%–5%) + plagioclase (5%–7%)
Groundmass:	Glass (70%–80%) + plagioclase (5%–10%) + clinopyroxene (1%–2%) + orthopyroxene (trace–1%) + opaque minerals (0%–trace)
Comments:	Orthopyroxene (2V = −80° to −85°; bronzite) has some (100) clinopyroxene exsolution lamellae and a reaction rim of clinopyroxene
Andesite	
Phenocrysts:	Plagioclase (10%–20%) + clinopyroxene (2%–6%) + orthopyroxene (0%–2%) + opaque minerals (0%–trace)
Groundmass:	Glass (50%–60%) + plagioclase (10%–20%) + opaque minerals (1%–2%)
Comments:	Can be further classified as two-pyroxene (clinopyroxene + orthopyroxene) andesites; glomerocrysts are common
Dacite	
Phenocrysts:	Plagioclase (5%–15%) + clinopyroxene (2%–8%) + orthopyroxene (trace)
Groundmass:	Glass (60%–70%) + plagioclase (10%–20%) + opaque minerals (1%–2%)
Comments:	Porphyritic (partly glomerophyric) and hyalopilitic
Rhyolite	
Phenocrysts:	Plagioclase (2%–3%)
Groundmass:	Glass (40%–50%) + plagioclase + quartz + opaque minerals
Comments:	Predominantly massive rhyolite without flow texture

Unit 1

Sections 125-786A-11X-5, 100 cm, to 125-786A-19X-CC and 125-786B-1R-1, 0 cm, to 125-786B-5R-2, 25 cm.

The top of the igneous sequence from Sections 125-786A-11X-5, 100 cm, through 125-786A-12X-CC is formed by a breccia made up of clasts of basaltic andesite in a matrix of marl. The clasts contain 5%–20% fresh phenocrysts consisting of two pyroxenes with olivine or plagioclase. Some olivine phenocrysts contain chromium-spinel and have reaction rims of orthopyroxene. Most of the groundmass has been altered to a low-grade metamorphic assemblage, but unaltered patches are locally preserved. Clasts increase in size (from a few millimeters to 6 cm) and abundance with depth.

The poor recovery precludes a comprehensive lithologic study of the remainder of this unit. Cores 125-786A-13X-CC through 125-786A-19X-CC are mainly cuttings and clasts in clay of high-magnesian basalts, boninites, and picrites. Orthopyroxene is the dominant phenocryst in these samples, with subordinate clinopyroxene and olivine and rare plagioclase in a glassy groundmass; these are typical petrographic characteristics of rocks of the boninite series (Meijer, 1980). Unit 1 lithologies continue in the interval from Sections 125-786B-1R through 125-786B-5R-2, 25 cm, as oligomictic breccias containing boninite clasts. These contain mainly phenocrysts of orthopyroxene with subordinate clinopyroxene and plagioclase, although the latter can be locally predominant. Glass in the groundmass of the clasts has been largely devitrified or replaced by clay.

Unit 2

Sections 125-786B-5R-2, 25 cm, to 125-786B-8R-1, 0 cm.

The top of Unit 2 comprises a flow of intermingled andesite and basalt overlying basalt. The basalt contains 5% to 7% phenocrysts, made up of olivine, which is replaced by a carbonate/iron oxide assemblage, and minor clinopyroxene and traces of orthopyroxene and plagioclase. The glassy groundmass is variably altered (10%–50%) to clay. The base of the unit is formed by a relatively fresh andesite.

Unit 3

Sections 125-786B-8R-1, 0 cm, to 125-786B-17R-1, 130 cm.

Unit 3 is formed by oligomictic breccias containing a small number of exotic fragments. The breccias at the top of the unit contain andesite clasts petrographically similar to those of the overlying flow of Unit 2 (Sections 125-786B-8R-1 through 125-786B-11R-1, 90 cm). The andesite contains 8% to 30% phenocrysts of plagioclase and clinopyroxene and minor orthopyroxene in a black glassy groundmass, with plagioclase and minor clinopyroxene. Glass is partly to largely replaced by clays. Alteration rims of clasts appear similar to the sandy matrix of the breccia, indicating *in-situ* brecciation. Exotic fragments of pumice and basalt are present in the lower part of the andesite breccia (Sections 125-786B-10R-1 through 125-786B-11R-1, 90 cm). High-magnesian basalts and boninite, classified on the basis of bulk-rock chemistry, are present in Sections 125-786B-11R-1, 90 cm, through 125-786B-14R-1, 0 cm. Basalt clasts contain phenocrysts of two pyroxenes and plagioclase in a fine-grained to glassy groundmass. Clasts alter to material similar to the matrix of the breccia. Boninite clasts also contain phenocrysts of two pyroxenes and plagioclase, but clinopyroxene is subordinate. Sections 125-786B-14R-1 through 125-786B-17R-1, 115 cm, are made up of andesite-dacite breccias. Microdiorite fragments, possibly represent-

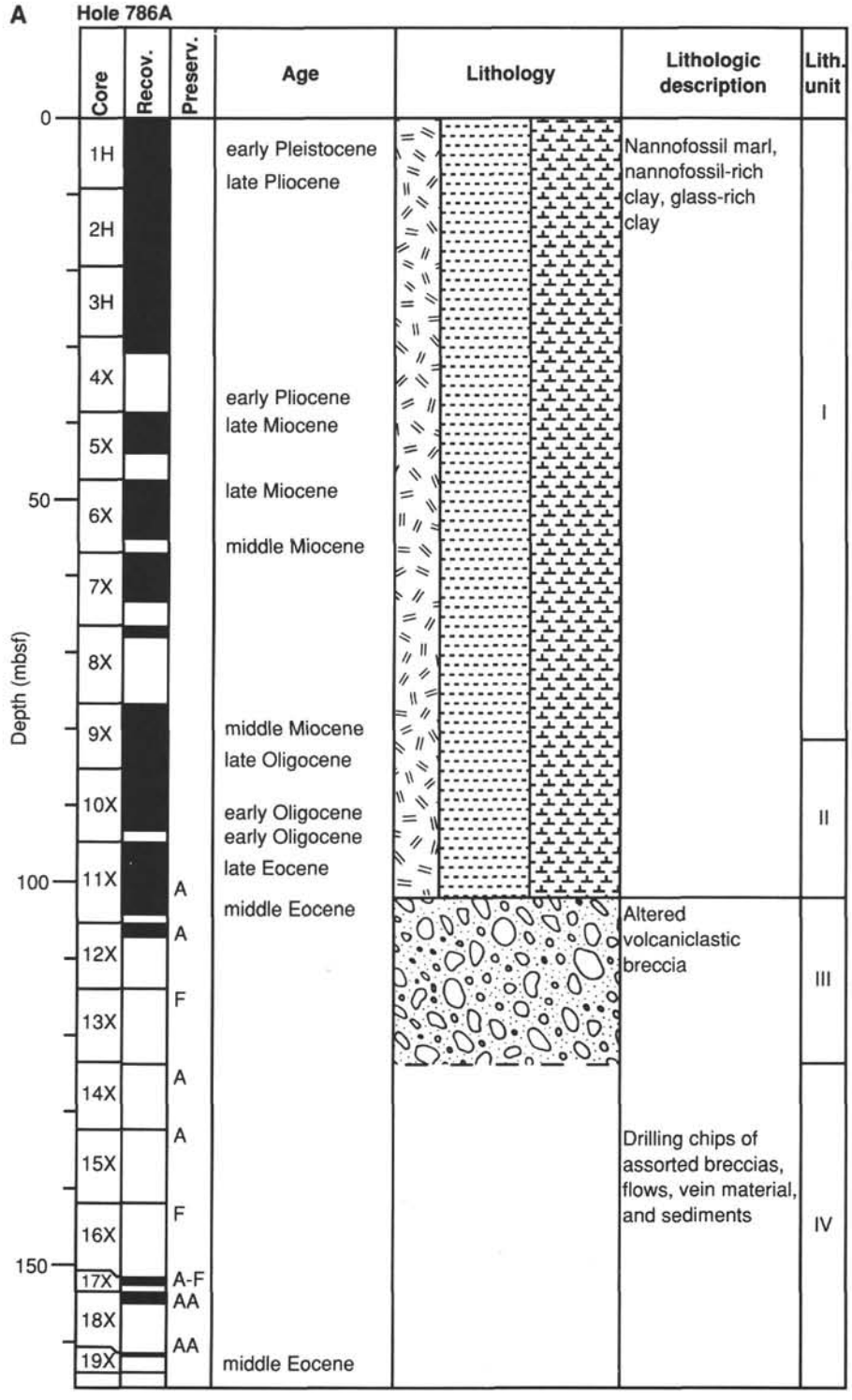

Key for preservation for 7A and 7B

AA= very altered: groundmass and phenocrysts are pervasively altered, only phenocryst traces remaining.

A = altered: groundmass and olivines altered, other phenocrysts largely fresh, some fresh glass.

F = fresh: some alteration of groundmass and phenocrysts, olivine altered.

FF= very fresh: no signs of alteration, vesicles may contain secondary mineralization.

Figure 3. Lithostratigraphy and core recovery at Site 786. **A.** Hole 786A. **B.** Hole 786B.

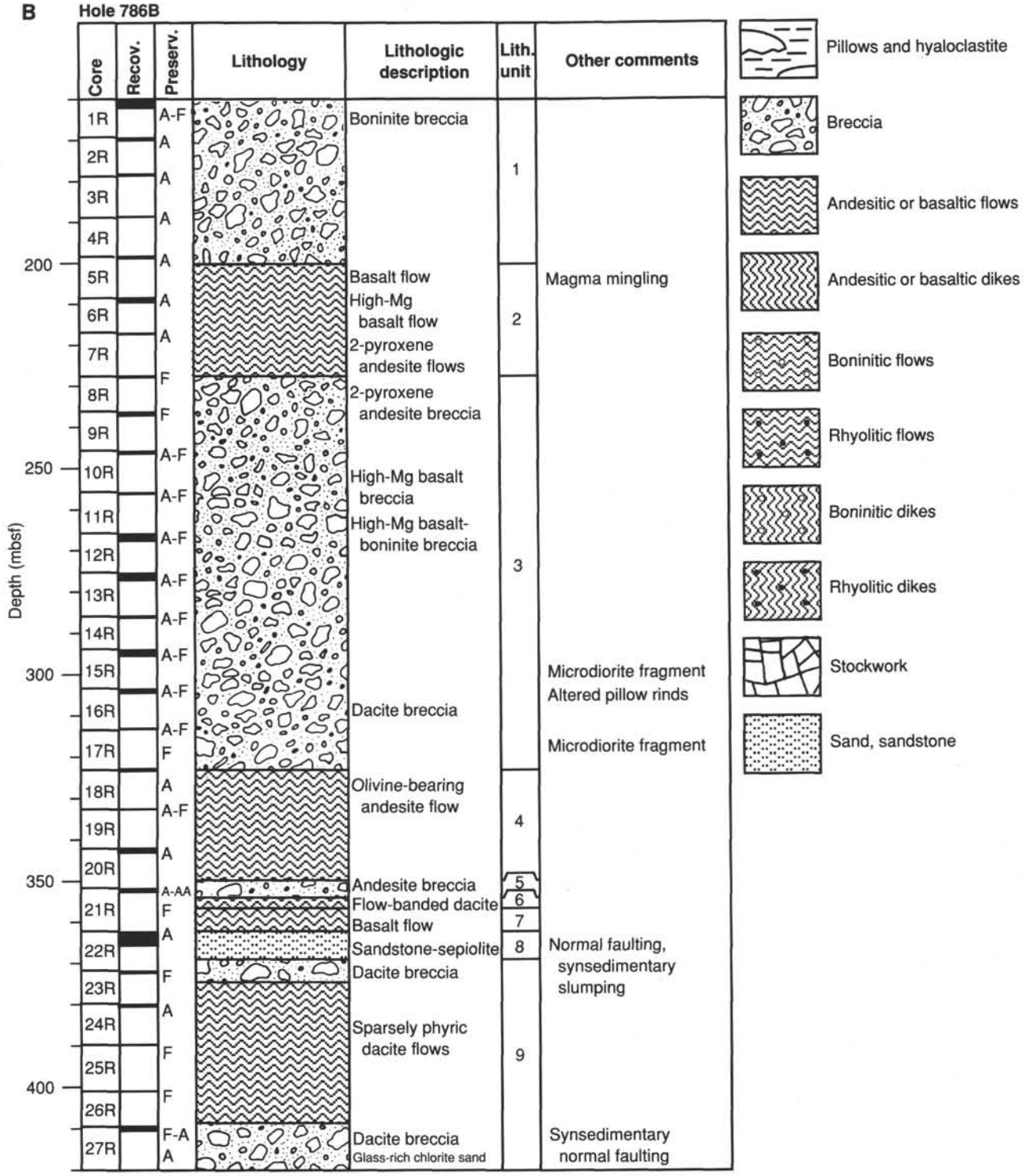

Figure 3 (continued).

ing cumulates, were recovered in Samples 125-786B-15R-1, 0–3 cm, and 125-786B-17R-1, 0–3 cm. Alteration throughout this unit is highly variable.

Unit 4

Sections 125-786B-18R-1, 0 cm, to 125-786B-21R-1, 0 cm.

Unit 4 consists of two flows of variably altered andesite. The top flow occupies Sections 125-786B-17R-1 through 125-786B-19R-1, and the lower flow, Sections 125-786B-20R-1 through 125-786B-21R-1, 0 cm.

Unit 5

Sections 125-786B-21R-1, 0 cm, to 125-786B-21R-1, 50 cm.

Unit 5 is a brecciated andesite having minor alteration to chlorite and clays and grading downward into highly brecci-

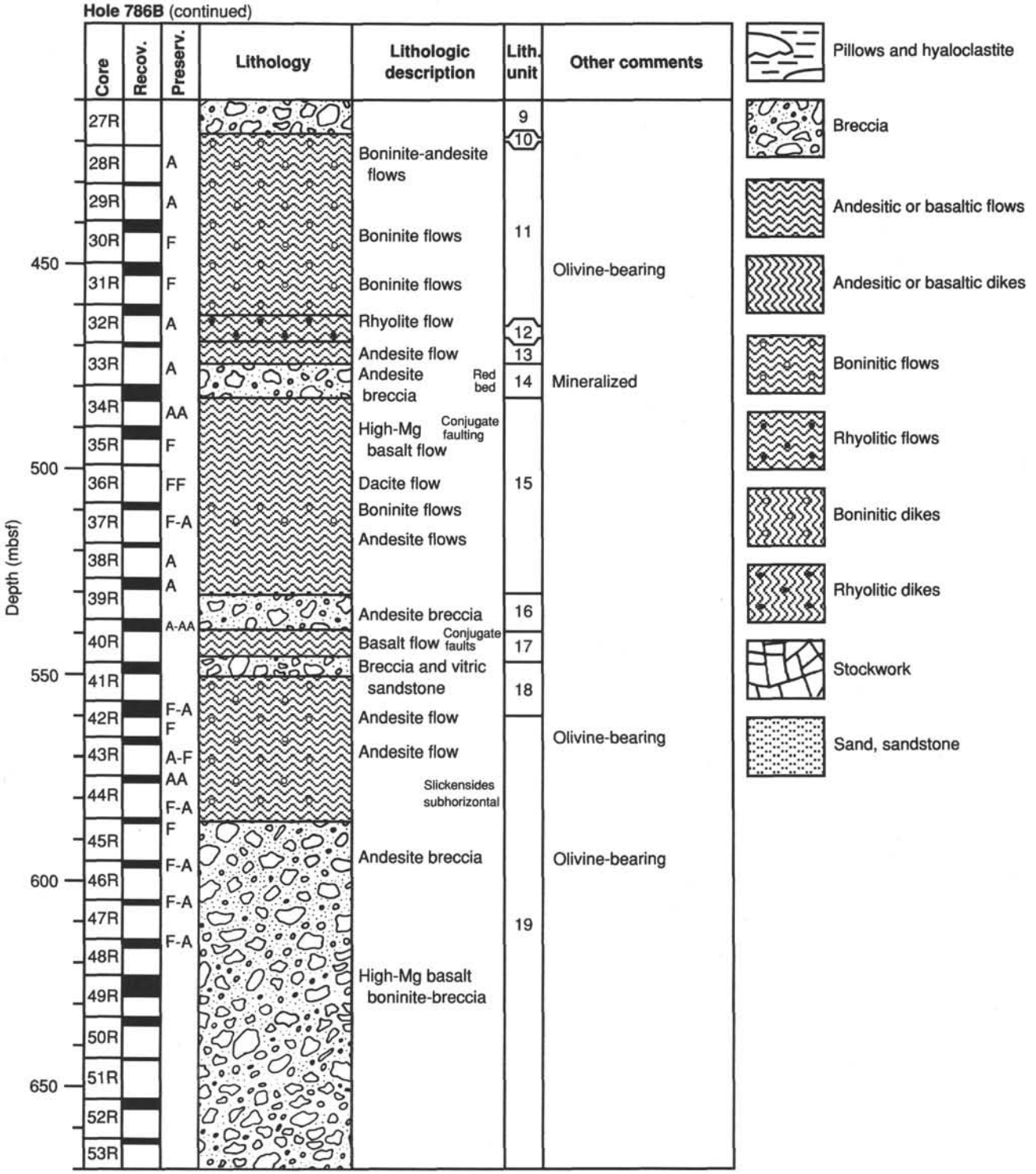

Figure 3 (continued).

ated and altered andesite. A thin veneer of sediment forms the boundary to the underlying unit.

Unit 6

Sections 125-786B-21R-1, 50 cm, to 125-786B-21R-2, 23 cm.

Unit 6 comprises a flow-banded aphyric dacite. The boundary between Units 6 and 7 is placed at the glassy contact of two cooling units, although the incorporation of Section 125-786B-21R-2, 0–23 cm, into this dacite unit cannot be made with certainty without chemical analyses.

Unit 7

Sections 125-786B-21R-2, 23 cm, to 125-786B-22R-1, 27 cm.

Unit 7 comprises glassy aphyric basalt having minor, variable alteration. The lower contact between basalt and the

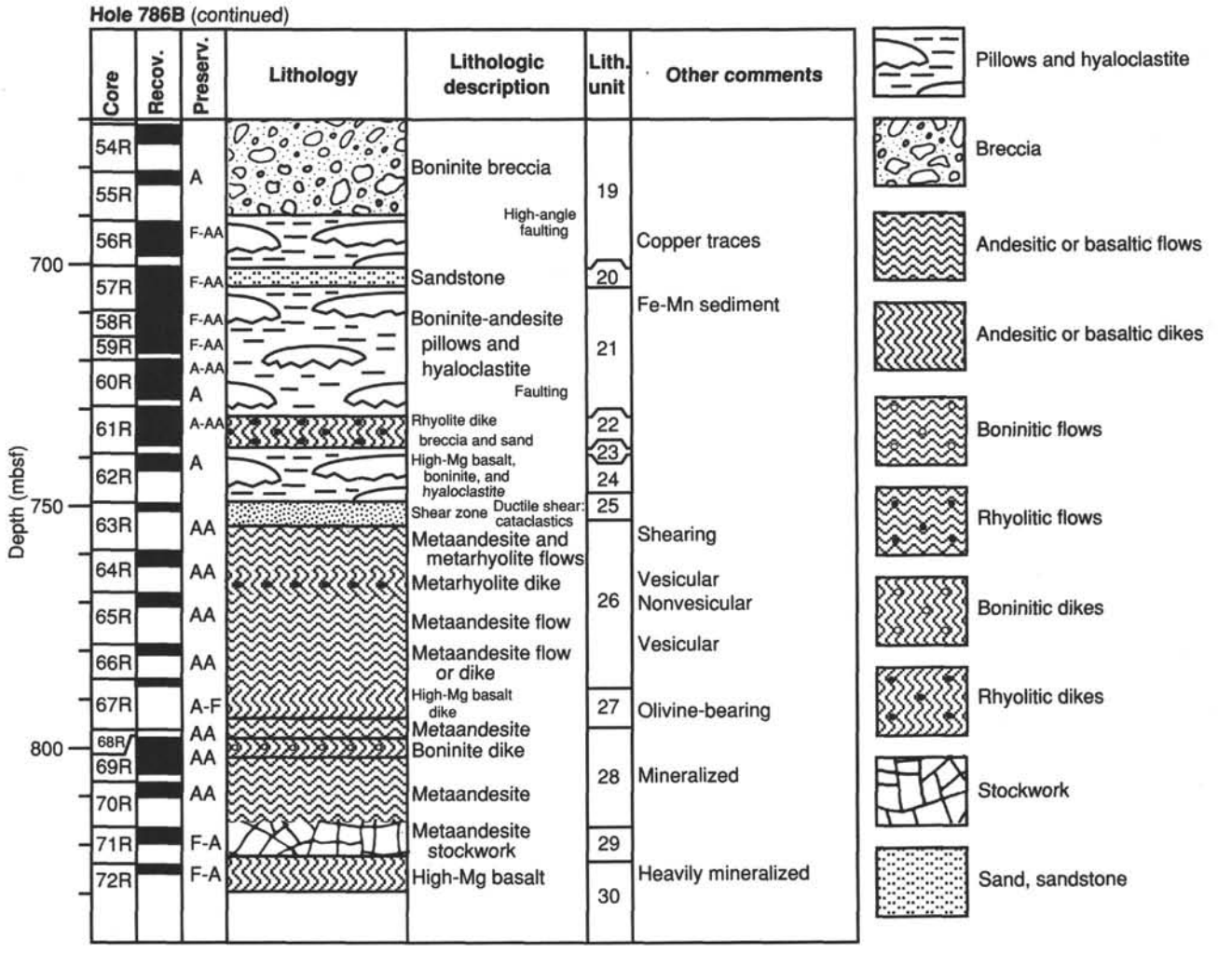

Figure 3 (continued).

underlying sediments of Unit 8 is marked by a thin (12 cm) band of sepiolite.

Unit 8

Sections 125-786-22R-1, 27 cm, to 125-786B-22R-3, 124 cm.

Unit 8 consists of vitric siltstones and sandstones intercalated with a polymictic breccia that contains clasts of pumice and volcanic fragments in a matrix of sand and silt.

Unit 9

Sections 125-786B-23R-1, 0 cm, to 125-786B-27R-1, 110 cm.

Unit 9 is made up of dacite flows with a plagioclase, two-pyroxene, rhyolite breccia at the base (below Section 125-786B-26R-1, 115 cm). The dacite has been variably altered into clays, and vesicles are filled with a white zeolite.

Unit 10

Sections 125-786B-27R-1, 110 cm, to 125-786B-27R-2, 0 cm.

Unit 10 is a thin, glass-rich chloritic sandstone, fining upward, with cross-bedding and lamination at the base. It contains a few clasts.

Unit 11

Sections 125-786B-27R-2, 0 cm, to 125-786B-32R-2, 54 cm.

Unit 11 comprises a series of very phyric (30%) boninites. The boninites contain two pyroxenes and plagioclase with olivine increasingly present toward the bottom of the unit. Clinopyroxene and plagioclase are the dominant phenocryst phases. Alteration has been concentrated along veins and fractures that contain carbonate and possible serpentine. In Sections 786B-31R-1 through 125-786B-32R-1, 73 cm, olivine has been altered to hematite and carbonate, and glass has been largely altered to clay.

Unit 12

Sections 125-786B-32R-2, 54 cm, to 125-786B-33R-1, 0 cm.

Unit 12 is a rhyolite flow, variably altered to clays and chlorite.

Unit 13

Sections 125-786B-33R-1, 0 cm, to 125-786B-33R-1, 35 cm.

Unit 13 consists of olivine-bearing, basaltic andesite that exhibits pervasive hematite alteration localized around olivine

and also disseminated within the groundmass; carbonate-filled veins are common.

Unit 14

Sections 125-786B-33R-1, 65 cm, to 125-786B-34R-1, 145 cm.

The top of Unit 14 consists of a meta-andesite having pyrite mineralization, underlain by a brecciated, flow-banded andesite. The lower part of the unit (Section 125-786B-34R-1, 53–140 cm) is made up of a feldspar-rich, vitric sandstone and siltstone with graded bedding and a possibly baked upper contact. These sediments in turn overlie brecciated andesite having flow banding and pyrite mineralization. Brecciated zones have experienced pervasive alteration to a low-grade metamorphic assemblage.

Unit 15

Sections 125-786B-34R-1, 145 cm, to 125-786B-39R-2, 0 cm.

The top of Unit 15 (Sections 125-786B-34R-1, 145 cm, through 125-786B-34R-4, 101 cm) has been formed by flow(s) of sparsely phyric basalt with phenocrysts of plagioclase, clinopyroxene, and rare orthopyroxene and olivine. Phenocryst contents are higher toward the lower part of this interval. The basalt groundmass has been pervasively altered to a low-grade mineral assemblage, and traces of pyrite occur throughout. Sparsely phyric dacite flows with plagioclase and clinopyroxene phenocrysts are present in Sections 125-786B-34R-4, 101 cm, through 125-786B-37R-1, 80 cm, and olivine-bearing boninite is present in Sections 125-786B-37R-1, 80 cm, through 125-786B-37R-3, 30 cm. Andesite makes up the lower part of the unit. Dacites and andesites are markedly less altered than the more mafic members of this unit.

Unit 16

Sections 125-786B-39R-2, 0 cm, to 125-786B-40R-1, 75 cm.

Unit 16 comprises a series of andesite breccias. Pyrite is disseminated throughout the unit and concentrated along veins that contain zeolites. The groundmass is slightly to moderately chloritized.

Unit 17

Sections 125-786B-40R-1, 80 cm, to 125-786B-41R-1, 0 cm.

Unit 17 consists of orthopyroxene-olivine-phyric basalt, pervasively altered to chlorite and carbonates and cut by veins filled with chlorite, carbonate, and iron oxide.

Unit 18

Sections 125-786B-41R-1, 0 cm, to 125-786B-42R-2, 0 cm.

The top of Unit 18 is an oligomictic breccia having a matrix component that increases in proportion upward. This overlies a laminated vitric sand, and then a polymictic breccia, also with a matrix component that increases upward and then grades into a vitric sand. Clasts in both breccias are andesites. The base of the unit has been formed by an andesite flow.

Unit 19

Sections 125-786B-42R-2, 0 cm, to 125-786B-57R-1, 0 cm.

Various boninite and andesite breccias and flows make up this unit. The top of Unit 19 is marked by the appearance of rare olivine phenocrysts in the andesite flows. Pervasively altered meta-andesite having a low-grade metamorphic assemblage in Section 125-786B-44R-1 forms the transition to the underlying brecciated, olivine-bearing andesite of Sections 125-786B-44R-2, 10 cm, through 125-786B-50R-1. Breccia clasts in Section 125-786B-51R-1 have the composition of high-magnesian basalts, but the phenocrysts of plagioclase (10%–20%) and two pyroxenes (5%–10% each) suggest a close similarity to the andesites. Breccias continue through Section 125-786B-56R-6 with clasts that appear to be boninitic on the basis of the high proportion of orthopyroxene, in the mode of Section 125-786B-55R-6. The boninite breccia of Sections 125-786B-55R-3 through 125-786B-56R-1 contains a trace of native copper. Chlorite and hematite alteration is pervasive. Veins and fractures are characteristically absent, except in the copper-bearing interval.

Unit 20

Sections 125-786B-57R-1, 0 cm, to 125-786B-57R-1, 104 cm.

A fining-upward sandstone with basal graded bedding and local clasts forms Unit 20.

Unit 21

Sections 125-786B-57R-1, 104 cm, to 125-786B-61R-4, 42 cm.

Unit 21 consists of multiple pillow lavas and hyaloclastites of bronzite-boninite and andesite with red sediments between pillows. White and green zeolite and iron oxide fill veins and vesicles. At the base of the unit, a fault breccia forms the contact with Unit 22.

Unit 22

Sections 125-786B-61R-4, 42 cm, to 125-786B-61R-6, 40 cm, and 125-786B-61R-6, 65 cm, to 125-786B-62R-1, 0 cm.

Unit 22 is a rhyolite flow or (more probably) dike or sill, which is locally oxidized to a dark red color and contains glass altered to chlorite.

Unit 23

Sections 125-786B-61R-6, 40 cm, to 125-786B-62R-1, 0 cm.

Unit 23 is a shear zone consisting of breccia and sandstone.

Unit 24

Sections 125-786B-62R-1, 0 cm, to 125-786B-62R-3, 85 cm.

Unit 24 consists of altered boninite or andesite pillows and hyaloclastites, locally high-magnesian basalt in composition, with red sediment between the pillows. Fine filaments of red ferromanganoan sediment are particularly prominent in the hyaloclastites. Clay and chlorite alteration of glass is pervasive. Zeolite and sparse carbonate fill veins.

Unit 25

Sections 125-786B-62R-3, 85 cm, to 125-786B-63R-2, 44 cm, and 125-786B-63R-2, 78 cm, to 125-786B-63R-2, 92 cm.

Unit 25 consists of cataclastic meta-andesites and sandstone in a shear zone. The andesites are largely altered to a low-grade metamorphic assemblage. Orthopyroxene phenocrysts have been largely altered to a chlorite/carbonate assemblage, but some unaltered cores remain. Clinopyroxene is variably altered.

Unit 26

Sections 125-786B-63R-2, 44 cm, to 125-786B-63R-2, 78 cm, and 125-786B-63R-2, 92 cm, to 125-786B-67R-1, 0 cm.

Metadacite and rhyolite flows of low metamorphic grade form this unit. Orthopyroxene has been replaced by chlorite, carbonate, and iron oxide; clinopyroxene has been variably altered to chlorite, and plagioclase is albitized. Vesicles are filled with zeolite, carbonate, and chlorite and locally contain sulfide minerals.

Unit 27

Sections 125-786B-67R-1, 0 cm, to 125-786B-68R-1, 0 cm.

Dikes of basalt and boninite composition make up Unit 27. The dikes show little evidence of chilled margins and have been locally altered to chlorite and carbonate. Olivine has been completely replaced by a chlorite/carbonate assemblage, and clinopyroxene has been variably chloritized. Veins contain carbonate and sulfide minerals.

Unit 28

Sections 125-786B-68R-1, 0 cm, to 125-786B-71R-1, 0 cm.

Unit 28 consists of meta-two-pyroxene-andesite, probably of boninitic composition, with abundant chlorite and carbonates along fractures and extensive sulfide mineralization. One boninite dike, apparently 30 cm thick, also forms part of this unit.

Unit 29

Sections 125-786B-71R-1, 0 cm, to 125-786B-71R-4, 0 cm.

Unit 29 is an argillized, mineralized, andesite stockwork. Andesite has been completely altered to clays, epidote, chlorite, and quartz. Extensive sulfide mineralization is present.

Unit 30

Sections 125-786B-71R-4, 0 cm, to 125-786B-72R-2, 140 cm.

Unit 30 contains fresh, avesicular boninitic glass, possibly intruded as a dike, in a meta-andesite massive flow or dike.

IGNEOUS AND METAMORPHIC GEOCHEMISTRY

Lithologies drilled at Holes 786A and 786B include massive flows, pyroclastic flows and interbedded sediments, massive flows and intrusive sheets, pillow lavas and hyaloclastite flows, and eventually multiple composite intrusive sheets (see "Igneous and Metamorphic Petrology" section, this chapter). Although the metamorphic grade reaches the upper greenschist facies (albite-chlorite-epidote-quartz assemblage) at the base of Hole 786B, most of the extrusive rocks analyzed contain abundant fresh glass. Alteration is therefore thought to have had only a small effect on the concentrations of major elements. A total of 47 samples collected from Site 786 was analyzed on board the ship for abundances of both major and trace elements by XRF spectrometry (see "Explanatory Notes" chapter, this volume). Abundances of major and trace elements are presented in Table 6.

Major-Element Geochemistry

The rock types from Site 786 show a large variation in SiO_2 and MgO (Fig. 4) and hence have been classified on this basis. This classification arbitrarily subdivides the rocks into high- and low-magnesian groups. Although the rock types range from picrites (low SiO_2, >12 wt% MgO) to rhyolites (>70 wt% SiO_2, <2 wt% MgO), the majority of the samples fall into the high-magnesian basalt, boninite, and andesite classification fields. The dispersion on a covariation diagram of magnesium (between 18.5 and 0 wt% MgO) against silica (between 48.5 and 74.5 wt% SiO_2) forms a crescent shape that converges toward both the picrite and the andesite fields. Because the suite of rocks crosses the line of 63 wt% SiO_2 into the dacite and rhyolite fields, the rocks can be inferred to have been derived from parental magmas that were saturated with respect to silica.

Nearly all the rock types at Site 786 contain up to 20 modal% of plagioclase phenocrysts or xenocrysts (see "Igneous and Metamorphic Petrology" section, this chapter). Such large proportions of plagioclase account for the apparent enrichment in aluminum (Fig. 5) and may have been caused by plagioclase accumulation or by a shift in the co-tectic toward plagioclase by an increased water content of the magma. The wide scatter of points on an aluminum-magnesium diagram (Fig. 5) suggests, however, that the modal percentage of plagioclase is independent of the magnesium content of the rock. This scatter may be the result of magma mixing processes (see "Igneous and Metamorphic Petrology" section, this chapter).

Despite the large variations in MgO, SiO_2, and Al_2O_3, all the rocks from Site 786 are characterized by extremely low abundances of these elements and a small range of TiO_2 (from 0.1 to 0.3 wt%). In some rocks, TiO_2 is an order of magnitude less than normal mid-ocean ridge basalt (N-MORB), which has an average TiO_2 content of 1.5 wt%. This suggests that all the rocks may have been derived from a source that was extremely depleted in the incompatible trace elements.

Trace-Element Geochemistry

The characteristically depleted nature of the rocks from Site 786 is reflected by their low abundances of high-field-strength (HFS) elements in general and yttrium and titanium in particular. However, zirconium is variably depleted and the zirconium/yttrium ratio is thus highly variable, ranging from less than 2 to more than 6. The most primitive rocks are also those having the highest abundances of chromium, which ranges from about 220 to 1330 ppm. The accumulation of chromium-rich spinel is probably responsible for abundances of chromium in excess of 1000 ppm; these rocks also have variable amounts of orthopyroxene and olivine phenocrysts (see "Igneous and Metamorphic Petrology" section, this chapter). Two of the factors involved in the petrogenetic history of the rocks are illustrated in the chromium-yttrium diagram in Figure 6. Source effects, either variable depletion or partial melting, generate a subhorizontal array of data points, whereas fractional crystallization produces a subvertical trend. Although large variations in yttrium occur in the primitive rock types, the fractionated rocks exhibit a relatively narrow range of yttrium abundances. The former may be evidence for a range of potential parent magmas related to variable source fertility or variations in partial melting. The latter may be evidence for the generation of the more evolved magmas from a single, homogeneous parental magma. For the majority of primitive rocks at Site 786, the abundance of yttrium is always less than one-half that for N-MORB, which has an average of about 30 ppm yttrium. The HFS-element-depleted nature of the rocks from Site 786 is summarized by N-MORB normalized diagrams for a representative boninite, high-magnesian basalt, and primitive andesite (Figs. 7A–7C). Cerium and phosphorus are near or below their detection limits, and therefore are not included. However, niobium, zirconium, and possibly yttrium may be variably enriched with respect to titanium. The large-ion-lithophile (LIL) elements are enriched in all three representative samples, but their abundances are only slightly higher than those in N-MORB. If the enrichment in LIL elements is derived from

Table 6. Geochemical data, Holes 786A and 786B.

Sample (interval in cm): Rock type:[a]	786A-6X-5, 24–27 Andesite	786A-12X-1, 140–142 Basalt	786A-13X-CC, 27–29 High-Mg basalt	786A-16X-CC, 25–28 High-Mg basalt	786A-17X-CC, 4–6 Picrite	786A-19X-CC, 17–20 Picrite	786A-19X-1, 0–30 High-Mg basalt	786B-1R-1, 61–64 Boninite	786B-2R-1, 58–61 Boninite	786B-3R-1, 94–97 Boninite	786B-5R-2, 70–72 Boninite
Major elements (wt%)											
SiO_2	52.27	51.43	52.45	51.00	48.68	47.53	49.96	60.11	60.88	56.68	50.23
TiO_2	0.82	0.29	0.16	0.21	0.13	0.22	0.20	0.14	0.15	0.15	0.28
Al_2O_3	16.12	17.27	12.15	14.62	11.43	10.70	14.22	12.39	12.37	13.09	14.40
Fe_2O_3 (total)	12.23	8.34	7.92	7.81	9.23	8.97	7.67	7.03	6.8	7.38	8.55
MnO	0.20	0.09	0.01	0.10	0.19	0.16	0.10	0.11	0.11	0.11	0.11
MgO	4.10	5.04	12.78	11.53	14.38	18.84	10.82	7,80	7.05	8.54	7.67
CaO	9.65	8.20	5.50	8.06	6.58	5.76	7.93	6.09	6.07	5.31	10.89
Na_2O	1.03	1.83	1.31	1.57	1.74	1.02	1.32	2.05	2.08	1.46	1.57
K_2O	0.34	1.38	0.83	0.32	0.70	0.41	0.50	0.51	0.55	0.80	1.25
P_2O_5	nd	nd	nd	nd	nd	nd	nd	nd	nd	nd	0.01
LOI	0.84	2.92	5.79	2.41	6.16	5.21	4.66	2.19	2.05	3.78	3.40
Total	98.14	96.84	98.99	97.65	99.23	98.86	97.39	98.48	98.10	98.28	97.36
Mg#	0.37	0.51	0.74	0.72	0.73	0.78	0.71	0.66	0.64	0.67	0.61
Trace elements (ppm)											
Nb	0.6	2.4	2.3	0.8	0.8	1.4	—	2.1	1.8	2.2	0.8
Zr	40	46	27	33	22	21	—	44	45	47	34
Y	24	6.1	5.9	9.4	10.9	8.7	—	7.0	2.2	4.6	12.8
Sr	181	165	100	147	93	64	—	174	178	153	147
Rb	6.1	14.1	13.1	2.5	9.5	7.2	—	6.2	7.4	23	6.4
Zn	113	92	63	68	73	71	—	55	53	61	63
Cu	166	40	52	37	160	23	—	67	72	84	63
Ni	18	85	268	190	215	522	—	99	85	103	170
Cr	23	320	613	506	471	1338	—	374	345	385	333
V	428	356	143	226	194	195	—	177	185	100	237
Tl	5520	1840	1320	1680	1140	1620	—	1320	1320	1380	2280
Ce	26	10	3	3	5	nd	—	12	14	9	nd
Ba	27	36	23	6	8	11	—	37	39	21	18

fluids that were driven off from the slab during subduction dewatering, then this component is not as great as might have been expected for West Pacific subduction-related magmas.

SEDIMENT/FLUID GEOCHEMISTRY

Sediment Geochemistry

Sediments from Site 786 were analyzed on board the ship for inorganic carbon and for total carbon, nitrogen, and sulfur using the techniques described in the "Explanatory Notes" chapter (this volume). The organic carbon content was then calculated by difference. These results are presented in Table 7 and in Figure 8. The $CaCO_3$ content of the sediments varies from less than 1 to 40 wt%, except for a single sample from 102.50 mbsf that contains 67.2 wt%. The organic carbon content decreases from 0.41 wt% near the seafloor to less than 0.05 wt% at about 100 mbsf. The single deep sample, from 154.27 mbsf, contains 0.21 wt%. Nitrogen concentrations generally decrease with organic carbon content and with depth, from 0.22 wt% near the seafloor to less than 0.01 wt% at 14 mbsf.

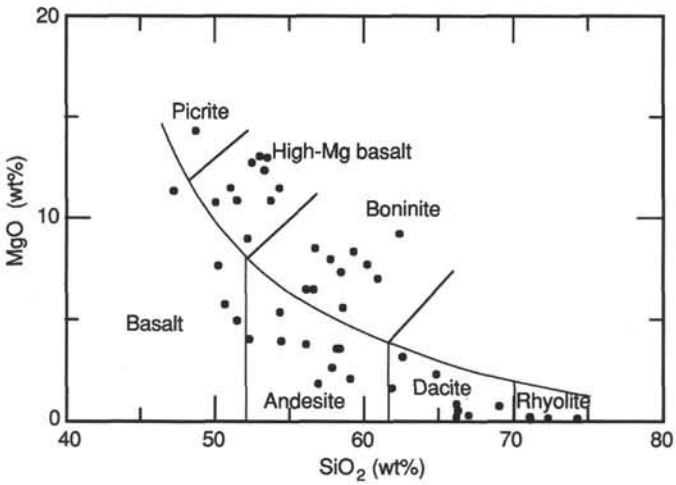

Figure 4. Rock classification based on variation in MgO with SiO_2. The arbitrary separation between high- and low-MgO groups is used to provide a consistent framework of classification.

Fluid Geochemistry

The sediments at Site 786 have uniformly lower concentrations of methane than any of the other eight sites investigated during Leg 125. The concentrations, as measured for 5-cm^3 sediment headspace samples, vary from 8 to 11 μL/L (Table 8). Methane was the only hydrocarbon detected.

Four interstitial-water samples were obtained from 5.98 to 81.25 mbsf in Hole 786A (Table 9). These samples are compared with those from Sites 782 through 785 and with surface seawater in Figure 9. At Site 786, pH varies from 7.6 to 7.9, within the normal range of 7.5 to 8.5 for interstitial waters from deep-sea sediments. Alkalinity and ammonia reach maximum concentrations that are smaller and occur at shallower

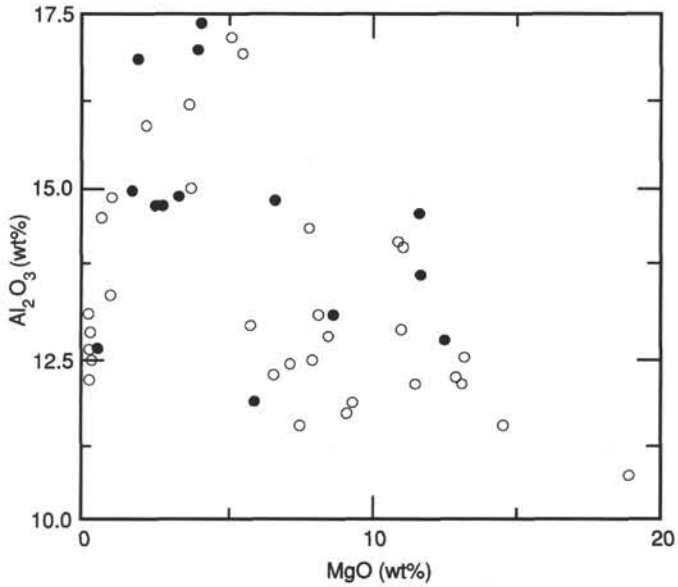

Figure 5. Rocks from Site 786 exhibit a wide variation in MgO vs. Al_2O_3, which may represent variations in the modal% of plagioclase phenocrysts or xenocrysts in the rocks, but not all plagioclase-phyric types have high Al_2O_3. Solid symbols = rocks with plagioclase greater than 10 modal%.

Table 6 (continued).

786B-6R-2, 128–130 High-Mg basalt	786B-8R-1, 45–47 Andesite	786B-9R-1, 10–15 Andesite	786B-11R-1, 122–126 High-Mg basalt	786B-12R-2, 14–16 High-Mg basalt	786B-12R-2, 120–124 Boninite	786B-16R-1, 137–141 Dacite	786B-19R-1, 91–94 Andesite	786B-21R-1, 26–29 Andesite	786B-21R-1, 129–131 Dacite	786B-21R-2, 72–76 Basalt	786B-22R-3, 61–64 Dacite
51.45	54.37	56.09	53.64	54.26	59.24	61.83	58.13	56.85	66.91	50.62	66.14
0.28	0.23	0.24	0.14	0.16	0.12	0.25	0.21	0.27	0.19	0.15	0.17
14.12	17.48	17.07	12.89	13.70	12.78	14.93	16.25	16.95	12.62	11.80	12.13
8.57	7.76	7.43	7.62	8.28	7.11	6.74	7.49	7.70	3.49	8.14	3.29
0.17	0.12	0.11	0.14	0.15	0.12	0.09	0.12	0.10	0.07	0.14	0.06
10.92	3.98	3.83	10.88	11.54	8.38	1.61	3.57	1.85	0.31	5.78	0.11
9.32	7.69	7.52	6.50	7.17	6.72	5.49	7.14	6.56	2.30	13.33	1.96
1.11	2.37	2.07	1.19	1.28	1.56	2.86	2.00	2.80	2.90	1.19	3.58
0.25	0.65	0.57	0.42	0.31	0.44	0.72	0.71	0.85	2.05	0.39	2.38
nd	nd	nd	nd	nd	0.03	nd	nd	0.04	nd	nd	0.02
1.90	2.71	1.97	2.80	2.16	1.53	2.48	2.34	2.91	6.50	5.75	7.97
98.08	97.34	96.88	97.64	98.51	97.99	96.99	97.96	96.88	97.30	97.27	97.06
0.69	0.47	0.47	0.71	0.71	0.67	0.29	0.45	0.29	0.13	0.55	0.05
1.1	0.9	1.6	1.7	1.6	2.1	1.5	1.9	0.9	2.0	1.2	1.5
33	51	53	39	41	37	57	48	58	76	29	76
10.7	16.1	10.4	5.5	5.6	6.5	10	8.7	21	11.8	8.3	13.6
136	227	226	170	185	166	217	214	236	148	150	162
2.9	8.5	6.6	5.8	4.0	6.3	7.2	7.7	11.1	36	7.8	41
68	73	72	71	76	53	65	72	86	49	50	51
69	68	101	40	38	74	91	78	62	68	40	26
223	41	40	159	164	116	9	33	18	6	188	1
501	8	8	471	485	425	6	35	5	0	889	nd
232	236	239	174	153	187	219	226	21	24	185	54
2220	1980	1920	1380	1500	1200	1860	1860	2100	1380	1380	1320
15	8	16	16	3	13	15	13	12	13	13	10
9	17	40	17	25	37	35	31	27	52	20	58

depths than at the other sites, and alkalinity decreases more quickly with depth below its maximum at about 6 mbsf. These changes are consistent with a minimal amount of bacterial sulfate reduction, as indicated by the slight decrease in sulfate with depth. The steep decrease in alkalinity is accompanied by a decrease in silica with depth below 25 mbsf. Like alkalinity, magnesium, potassium, and calcium change more rapidly with depth at Site 786 than at the other sites (Fig. 9). These changes in alkalinity, silica, magnesium, potassium, and calcium probably result from reactions between interstitial water and volcanic material within and below the sediments.

Chlorinity increases by about 2% with depth at Site 786 (Fig. 9), as it does at the other sites. This increase probably results from the increased chlorinity of ocean bottom water during the Pleistocene glaciations, as proposed by McDuff (1985).

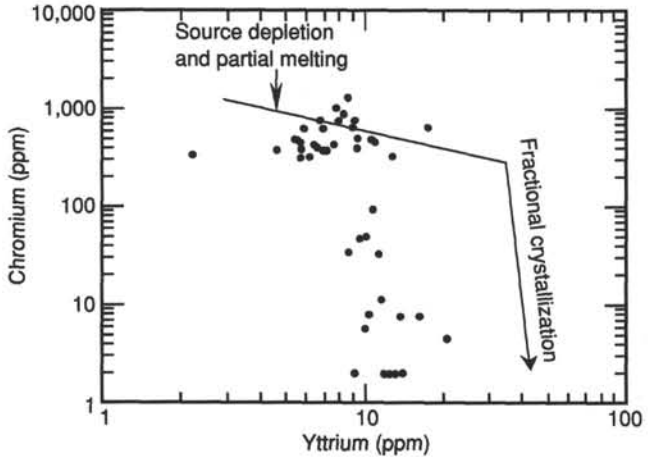

Figure 6. Chromium-yttrium co-variation diagram for volcanic rocks from Site 786. The relatively large variation in yttrium at high chromium indicates a range of primitive liquid compositions that reflects variable source characteristics. The vertical array of data points is a function of crystal fractionation.

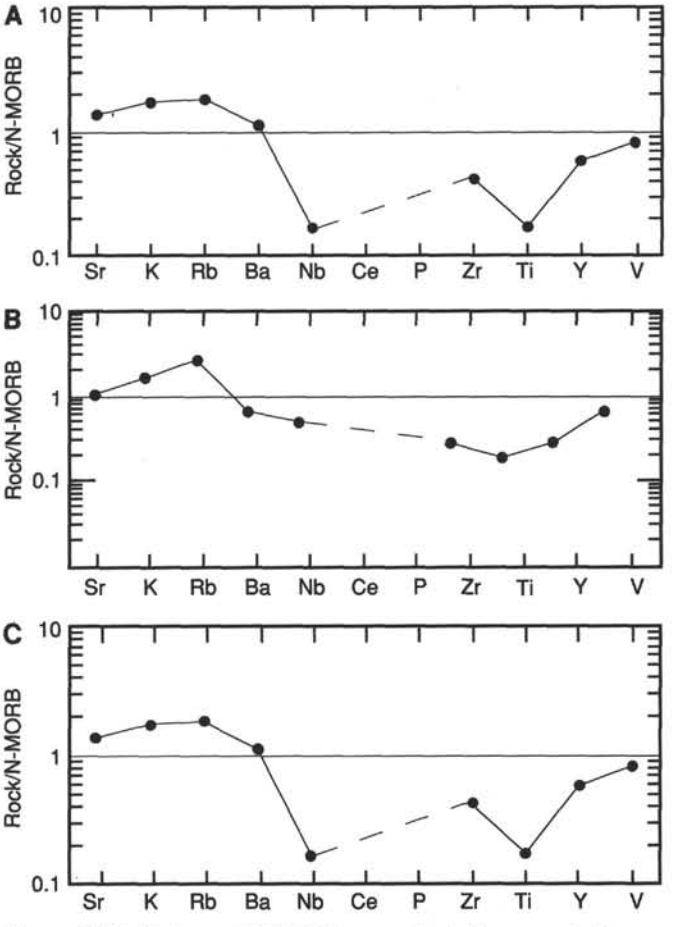

Figure 7. Multi-element N-MORB-normalized diagrams. **A.** Representative high-Mg basalt (Sample 125-786B-5R-2, 70–72 cm). **B.** Representative primitive andesite (Sample 125-786B-40R-2, 54–57 cm). **C.** Representative boninite (Sample 125-786B-11R-1, 122–126 cm).

Table 6 (continued).

Sample (interval in cm): Rock type:[a]	786B-24R-1, 9–12 Dacite	786B-26R-1, 68–70 Dacite	786B-30R-1, 29–31 Boninite	786B-30R-1, 119–121 Boninite	786B-31R-2, 84–86 Boninite	786B-32R-2, 86–88 Rhyolite	786B-34R-3, 45–47 High-Mg basalt	786B-35R-1, 73–76 Dacite	786B-35R-2, 122–126 Dacite	786B-37R-1, 95–98 Boninite	786B-37R-3, 45–49 Andesite	786B-38R-1, 6–8 Andesite
Major elements (wt%)												
SiO_2	66.16	66.24	56.03	58.52	57.71	71.04	52.13	62.48	64.80	56.51	57.75	58.98
TiO_2	0.26	0.26	0.09	0.14	0.10	0.23	0.14	0.20	0.23	0.20	0.20	0.21
Al_2O_3	14.85	14.59	12.20	12.94	13.09	12.85	11.61	14.86	14.72	14.80	14.75	15.93
Fe_2O_3 (total)	5.18	4.74	6.98	6.39	6.47	3.85	7.46	5.74	5.39	7.23	8.05	7.01
MnO	0.07	0.06	0.09	0.09	0.10	0.02	0.12	0.04	0.04	0.08	0.10	0.09
MgO	0.89	0.55	6.52	5.63	8.02	nd	9.00	3.25	2.36	6.53	2.65	2.09
CaO	4.46	3.81	9.83	8.07	8.11	2.88	11.05	5.49	5.00	7.77	5.05	6.68
Na_2O	3.41	3.59	1.71	2.07	1.57	3.35	1.42	3.02	2.93	1.96	2.14	2.05
K_2O	0.82	1.14	0.87	0.070	0.51	1.35	0.58	0.52	0.69	0.47	1.45	1.03
P_2O_5	0.02	nd	nd	nd	nd	nd	nd	nd	nd	nd	nd	nd
LOI	0.44	0.31	4.23	3.43	1.67	1.15	5.44	1.72	1.23	2.29	5.39	2.94
Total	96.52	96.76	98.04	97.94	97.36	96.72	98.34	97.28	97.27	97.82	97.50	97.00
Mg#	0.23	0.17	0.62	0.60	0.68	nd	0.68	0.49	0.43	0.61	0.36	0.34
Trace elements (ppm)												
Nb	1.4	1.8	1.6	1.6	1.6	1.4	1.4	1.6	1.6	1.6	1.4	1.7
Zr	70	75	31	42	34	74	29	56	59	38	44	49
Y	13.7	11.8	5.7	7.6	5.7	12.4	6.8	10.1	9.5	9.3	9.1	9.2
Sr	208	195	195	178	211	173	141	213	201	186	293	229
Rb	7.3	16.1	23	15.8	10.2	43	15.3	7.7	11.4	13.4	29	13.9
Zn	45	40	51	51	63	39	55	48	48	68	61	62
Cu	54	22	29	13	20	20	61	34	33	20	94	66
Ni	7	2	126	127	131	2	277	26	24	149	14	12
Cr	8	0	311	444	381	nd	769	50	47	393	nd	nd
V	185	119	132	142	184	46	160	152	134	185	224	259
Tl	1920	1860	960	1260	1020	1680	1320	1680	1620	1620	1620	1740
Ce	7	10	15	10	11	6	7	0	14	nd	12	13
Ba	84	73	43	45	32	77	11	59	53	34	108	54

STRUCTURAL STUDIES

Normal faults have been observed within the soft sediments of Hole 786A in Sections 125-786A-1H-6, 125-786A-2H-4, and 125-786A-2H-7. In Sections 125-786A-2H-4 and 125-786A-2H-7, the faults cut graded ash layers. In Section 125-786A-2H-7, one of the offset parts of the ash layer is missing. Although the total amount of displacement along the fault cannot be determined, it is at least greater than 25 cm. The faults can be related to local disaggregation processes during normal dewatering of the sediments. They may also indicate regional slope instability, as is probably the case for the set of faults visible in Section 125-786A-1H-6, which may represent a major tectonic feature. The site is near a major fault that has a vertical displacement of a few hundred meters and is evident in seismic sections. A fault crosscuts a volcanic pebble in Section 125-786A-11X-4 at 100 cm. This fault also represents the upper limit of the sediments that contain volcanic pebbles and must therefore be regarded as a major break in the sequence recovered from this hole.

Detailed descriptions and genetic interpretations of all the structural post-depositional features encountered in the volcanic sequence, the volcaniclastic breccias and sandstones, and the interbedded pelagic sediments of Hole 786B are too complex to be presented here. We summarize the most important features as follows:

Core 125-786B-21R: Welded tuffs having a vertical foliation that probably results from flow banding. The attitude of banding may be primary or may indicate post-depositional tectonic tilting.

Core 125-786B-22R: The following observations document a major shear zone:

1. Analysis of relationships of C-S planes in a strongly sheared and flattened pink sepiolite layer in Section 125-786B-22R-1 suggests a normal sense of shear.

2. Primary bedding in sedimentary rocks in Section 125-786B-22R-1 has high-angle (60°–70°) dips. Numerous synsedimentary faults and slump structures in the sediments indicate that syn- to post-depositional tectonic activity and related slope instability had taken place before the major tilting.

3. Welded tuffs in Section 125-786B-22R-2 commonly exhibit vertically oriented flow-banding and syn-consolidation extensional microfaulting. This last observation is consistent with the hypothesis of emplacement along a preexisting slope.

Core 125-786B-27R: Extensional syn-depositional faults and related cross-lamination are in the graded, coarse, green volcanic sandstones in Section 125-786B-27R-1, 50–70 cm.

Core 125-786B-34R: Numerous fractures and calcite-filled veins are visible in Sections 125-786B-34R-2 and 125-786B-34R-3. Dips vary from 45° to 80°. Generally, no displacement took place along the fractures. The veins show multiple orientations.

Core 125-786B-40R: Two fault planes dipping 55° and 65° with slickensided surfaces are observed at 30 cm in Section 125-786B-40R-2. The sense of movement is normal along one fault but is reversed along the other. At 95 cm in the same section, a fault surface dips at 62°, although clear evidence of displacement is not present.

Core 125-786B-41R: Section 125-786B-41R-3 contains welded tuffs with flow lamination and depositional layering dipping at 40° to 50°. "Hot" deformation criteria, such as plastic folding of glass laminae, are common.

Core 125-786B-43R: In Section 125-786B-43R-1 a strong, subhorizontal striation is visible along a plane dipping at 70°. This is the only indicator of strike-slip movement observed at Site 786.

Core 125-786B-56R: Three fault surfaces occur in Section 125-786B-56R-4 between 30 and 80 cm. They show striation rakes on a slickensided surface indicating normal and reverse movements. Fault dips range from 65° to 75°.

Cores 125-786B-58R and 125-786B-59R: Detailed analysis of vesicle distribution within the glassy rims of the boninitic pillow lavas of these two sections suggests a general tilting (40°–50°?) of this volcanic pile (see "Igneous and Metamorphic Petrology" section, this chapter).

Core 125-786B-61R: This core is characterized by tectonic discontinuities within the sequence of andesitic rocks. Faults, fault breccias and cataclastic rocks, powdered rocks from fault gouges, faint pressure-dissolution cleavages, locally abundant veining, and additional high-angle dips of flow banding and flow contacts (up to 60°) are in Sections 125-786B-61R-4 to 125-786B-61R-6. In Section 125-786B-61R-4, steps on a fault plane dipping at 65° indicate normal movement.

Table 6 (continued).

786B-40R-2, 54–57 Basalt	786B-49R-4, 32–37 Andesite	786B-51R-1, 51–55 High-Mg basalt	786B-61R-5, 56–58 Rhyolite	786B-61R-5, 81–84 Rhyolite	786B-62R-3, 40–42 High-Mg basalt	786B-63R-2, 72–74 Rhyolite	786B-65R-1, 17–19 Andesite	786B-66R-1, 88–90 Dacite	786B-67R-1, 63–65 High-Mg basalt	786B-69R-1, 65–67 Boninite	786B-70R-1, 68–73 Boninite
47.23	58.34	53.25	72.30	71.02	53.47	74.29	54.31	68.95	53.00	62.35	58.44
0.22	0.23	0.15	0.24	0.26	0.14	0.17	0.35	0.18	0.16	0.16	0.15
12.06	15.03	12.74	13.12	12.59	12.05	12.41	17.03	13.41	12.46	11.75	11.43
8.05	7.10	8.49	3.26	3.36	8.44	1.92	7.37	4.07	7.54	6.78	6.11
0.14	0.13	0.17	0.05	0.04	0.13	0.01	0.08	0.08	0.14	0.09	0.13
11.40	3.62	12.36	nd	nd	13.04	nd	5.41	0.82	13.08	9.23	7.40
11.90	7.29	7.78	2.49	1.77	5.27	0.45	6.51	2.26	6.70	3.98	4.95
0.89	2.04	1.17	3.35	3.85	2.18	2.51	2.06	2.22	1.28	2.05	2.27
0.26	0.73	0.26	1.11	1.14	0.67	4.98	0.48	3.12	0.21	0.06	0.20
nd	nd	0.08	nd	nd	nd	nd	nd	nd	nd	nd	nd
5.46	2.89	2.01	1.84	1.43	4.33	0.27	3.23	2.36	2.56	4.31	4.66
97.60	97.39	98.43	96.94	95.52	99.20	97.01	93.59	95.10	94.57	96.41	96.74
0.71	0.47	0.72	nd	nd	0.73	nd	0.58	0.26	0.75	0.70	0.68
1.6	1.4	0.5	1.4	2.1	2.2	2.4	1.4	1.7	1.2	2.1	1.6
27	45	37	77	82	34	78	44	74	28	44	45
8.9	10.8	17.4	14.1	14.1	7.8	12.7	11.5	11.2	6.9	8	9.2
136	185	166	121	122	110	47	163	101	137	143	147
5.6	10.1	3.7	18.1	14.6	6.5	51	3.1	34	2.5	0	1.5
57	58	70	45	52	63	41	65	96	58	75	77
27	89	41	56	18	60	63	60	50	56	177	70
374	39	195	3	6	306	1	22	9	296	212	202
650	93	659	0	0	1032	0	11	33	626	748	764
193	245	228	35	41	166	22	267	31	202	156	148
1800	1860	1560	1680	1800	1200	1440	2400	1440	1380	1260	1320
2	9	20	13	11	5	15	10	19	3	10	9
14	46	22	91	93	46	585	46	332	34	39	52

Note: nd = not detected.
[a] Classified according to Figure 4.

Core 125-786B-63R: Section 125-786B-63R-1 contains cataclastic and sheared andesites. Ductile shearing in the interval between 30 and 70 cm is indicated by progressive bending and stretching of andesite breccias. At 66 and 85 cm, a weak, anastomosing, strongly dipping foliation can be seen within the sheared breccias. C-S-like relationships between the cleavage planes are consistent with a normal sense of shear. Both chloritized and primary magmatic minerals are deformed within the shear zone. Slickensided fragments from a fault gouge were recovered from between 95 and 113 cm in this section, and the last sample from this section is a cataclastic andesite having a strongly dipping foliation defined both by pervasive veining and by alignment of broken fragments.

Core 125-786B-69R: The seven sections of this core are characterized by the presence of anastomosing veins and fractures related to hydrothermal brecciation and mineralization. Abundant veins filled with pyrite, quartz, and carbonate dip from 0° to 80° and define a conjugate fracture set. Despite local shearing near vein intersections, no displacement along veins was observed. Fracturing is associated with pods filled with calcite and pyrite. The size and frequency of the pods increase downhole. This fractured zone may represent the upper part or an upper extension of the andesitic stockwork encountered in Core 125-786B-71R.

Core 125-786B-71R: This core contains pervasively fractured volcanic rocks and argillitized and mineralized cataclastites. Pyrite is found in association with quartz and carbonates in anastomosing veins a few centimeters wide. In Section 125-786B-71R-1 the rocks have fractured along variably oriented planes without noticeable displacement. Such features characterize hydraulic fracturing, which is controlled by fluid overpressure. These rocks represent an andesitic stockwork, commonly encountered in arc environments. Sections 125-786B-71R-2 and 125-786B-71R-3 contain intensively argillitized and mineralized fault zones and breccias. The breccias are composed of angular clasts of strongly hydrothermally altered andesites of various colors, ranging from light green to white. The breccias may represent the result of fluid movement along major fractures during the hydrothermal processes or may be fault breccias. At this time, these cataclastic features at Site 786 cannot be related to a particular structural setting or tectonic processes such as normal, reverse, or transcurrent faulting. Two intervals, probably of fault gouge, at 100 and 130 cm in Section 125-786A-71R-2, contain small pieces of slickensided meta-andesite mixed with drill mud.

PALEOMAGNETISM

Magnetic Remanence

Two holes were drilled at Site 786. At Hole 786A, APC/XCB coring penetrated to 166.5 mbsf. There was good recovery of the sediments overlying the volcanic rocks, and many intervals of normal and reversed polarity were identified. No sediments were recovered in Hole 786B. The broken and discontinuous nature of the volcanic rocks in this hole made any magnetostratigraphy impossible.

The natural remanent magnetization of the archive half of each core from Hole 786A was measured using the cryogenic magnetometer. Magnetic intensities range from 1 to 300 mA/m (Fig. 10). Most cores have values of between 10 and 100 mA/m. Intensity does not change systematically downhole. When the cores were demagnetized at the 10-mT level and remeasured, intensities were reduced to about 10% to 30% of their initial values. Discrete samples were also taken from all of the cores in Hole 786A. These samples were measured at levels of 0, 5, 10, and 15 mT. In general, the polarities obtained from these samples agree with the whole-core data (Table 10). Data from whole cores and discrete samples in combination with biostratigraphic data ("Biostratigraphy" section, this chapter) enabled us to construct a tentative magnetostratigraphy for the sediments in Hole 786A (Fig. 11). Only data from the first 55 m of the hole are shown in Figure 11; below this point, correlations are impossible because of poor recovery and sparse biostratigraphic data. The correlations shown are uncertain because of the sparse biostratigraphic data and probable incomplete cleaning of spurious magnetization.

Past research on drill cores from the Philippine Sea Plate (Bleil, 1982) suggests that the Philippine Sea Plate has moved northward with time. Inclination data from Hole 786A were separated into 25-m sections, grouped into 10° intervals, and plotted on histograms (Fig. 12). The data from the intervals between 0 and 25 mbsf and between 25 and 50 mbsf show good bimodal distributions with peaks around +45° and −45°, which suggests that there has been little or no translation since the late Miocene. In the intervals below this, the data are scattered and not bimodally distributed. However, there are

Table 7. Total nitrogen, carbon, inorganic carbon, organic carbon, and carbonate carbon in sediments at Site 786.

Core, section, interval (cm)	Depth (mbsf)	Total nitrogen (wt%)	Total carbon (wt%)	Inorganic carbon (wt%)	Organic carbon (wt%)	$CaCO_3$ (wt%)
125-786A-						
1H-1, 84–86	0.84			4.28		35.7
1H-2, 72–74	2.22	0.22	3.22	2.81	0.41	23.4
1H-3, 76–78	3.76			2.29		19.1
1H-4, 71–73	5.21			2.70		22.5
1H-5, 90–92	6.90			0.27		2.2
1H-6, 51–53	8.01			2.10		17.5
1H-7, 21–23	9.21			1.21		10.1
2H-1, 67–69	10.37			2.92		24.3
2H-2, 73–75	11.93			1.29		10.8
2H-3, 78–80	13.48	0.23	3.05	2.64	0.41	22.0
2H-4, 65–67	14.85			1.72		14.3
2H-5, 73–75	16.43			2.32		19.3
2H-6, 88–90	18.08			3.53		29.4
2H-7, 22–24	18.92			4.45		37.1
3H-1, 75–77	19.95			2.68		22.3
3H-2, 64–66	21.34	0.19	3.58	3.40	0.18	28.3
3H-3, 76–78	22.96			2.51		20.9
3H-4, 75–77	24.45			3.67		30.6
3H-5, 62–64	25.82			2.91		24.2
3H-6, 58–60	27.28			0.08		0.7
3H-7, 44–46	28.64			3.72		31.0
4X-1, 32–34	29.02			3.81		31.7
4X-2, 5–7	30.25	0.22	3.25	2.88	0.37	24.0
4X-CC, 15–17	30.61			3.02		25.2
5X-1, 54–56	38.74			2.49		20.7
5X-2, 54–56	40.24	0.15	3.01	2.93	0.08	24.4
5X-3, 101–103	42.21			2.08		17.3
5X-4, 37–39	43.07			0.35		2.9
6X-1, 59–61	48.19			1.28		10.7
6X-2, 59–61	49.69	0.17	1.61	1.33	0.28	11.1
6X-3, 59–61	51.19			0.50		4.2
6X-4, 59–61	52.69			1.44		12.0
6X-5, 16–18	53.76			0.02		0.2
7X-1, 33–35	57.43			2.34		19.5
7X-2, 33–35	58.93	0.12	1.24	1.04	0.20	8.7
7X-3, 33–35	60.43			1.78		14.8
7X-4, 33–35	61.93			1.64		13.7
7X-5, 33–35	63.43			0.95		7.9
7X-CC, 4–6	64.33			1.28		10.7
8X-1, 48–50	67.58			0.86		7.2
9X-1, 83–85	77.63			0.12		1.0
9X-2, 97–99	79.27	0.12	3.05	2.92	0.13	24.3
9X-3, 93–95	80.73			2.96		24.7
9X-4, 80–82	82.10			2.72		22.7
9X-5, 59–60	83.39	0.14	0.42	0.09	0.33	0.7
9X-5, 98–100	83.78			2.99		24.9
9X-6, 25–27	84.55			4.00		33.3
10X-1, 89–90	87.29			2.12		17.7
10X-2, 82–84	88.72	0.18	2.87	2.76	0.11	23.0
10X-3, 72–74	90.12			3.38		28.2
10X-4, 82–84	91.72			3.57		29.7
10X-5, 82–84	93.22			4.52		37.7
10X-6, 25–27	94.15			2.63		21.9
11X-1, 80–82	96.80			4.72		39.3
11X-2, 83–85	98.33	0.11	4.04	4.04	0.00	33.7
11X-3, 78–80	99.78			2.94		24.5
11X-4, 84–86	101.34			3.81		31.7
11X-5, 50–52	102.50			8.07		67.2
12X-1, 42–44	106.12	0.09	3.27	3.38	0.00	28.2
17X-CC, 27–29	154.27	nd	0.34	0.13	0.21	1.1

Note: nd = not detected. Total sulfur was below the detection limit of 0.06 wt% in all samples analyzed for total carbon, nitrogen, and sulfur.

many more data points between +15° and −15°, which suggests that these rocks may have acquired their magnetization at a lower latitude than their present position. Additional research will be necessary to determine more accurately the translational history for these rocks.

Magnetic Susceptibility

Whole-core magnetic susceptibilities were measured using the multisensor track (MST). A downhole plot of these data is presented in Figure 13. The sediments typically have values between 0 and 19 × 10^{-3} SI units. There are identifiable peaks downhole, but these peaks do not correlate with any major changes in the physical properties of the rocks (see "Physical Properties" section, this chapter).

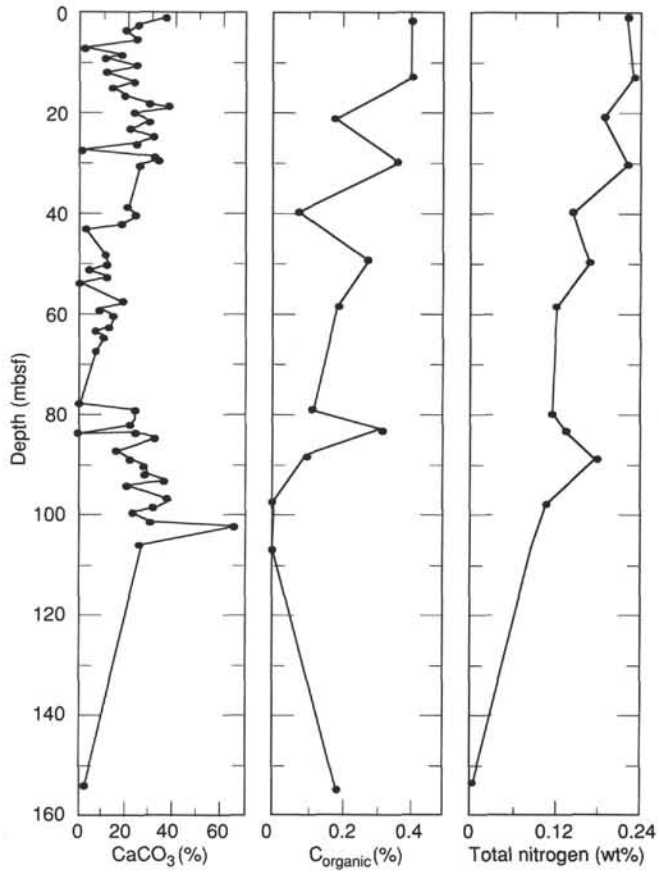

Figure 8. Weight percent of calcium carbonate, total organic carbon, and total nitrogen in sediments at Hole 786A.

SEDIMENT-ACCUMULATION RATES

Estimates of the sediment-accumulation rate for Hole 786A are based on calcareous nannofossils (Table 11), which are used to construct the age vs. depth curve shown in Figure 14.

Sedimentation rates for the middle Eocene through Oligocene are estimated to vary between 1.4 and 0.8 m/m.y. with two possible hiatuses. The hiatuses ("Biostratigraphy" section) are thought to have occurred in the late Eocene and in the early Oligocene. A major hiatus occurred in the early Miocene (7.2 m.y.; "Biostratigraphy" section, this chapter). In the middle and earliest late Miocene, sedimentation rates increased to 4.2 m/m.y., followed by a further increase to 8.6

Table 8. Results of headspace-gas analyses of cores at Site 786.

Core, section, interval (cm)	Depth (mbsf)	Methane (μL/L)[a]	Methane (μM)[b]
125-786A-			
1H-5, 0–5	6.03	9	0.8
2H-3, 0–3	12.72	8	0.7
3H-5, 0–3	25.22	10	0.9
5X-3, 0–3	41.22	10	0.9
6X-4, 0–1	52.11	11	0.9
7X-3, 0–1	60.11	11	0.9
9X-3, 0–1	79.81	10	0.9
12X-2, 0–1	107.21	10	0.9

[a] Microliters of methane per liter of wet sediment, assuming a sample volume of 4.2 cm^3 of sediment.
[b] Micromoles of methane per liter of interstitial water, assuming a porosity of 50%.

Table 9. Composition of interstitial waters from cores at Site 786.

Sample number Core, section, interval (cm)	Depth (mbsf)	Volume (mL)	Squeeze temperature (°C)	Squeeze pressure (psi)	pH	Salinity (R.I., %)	Salinity (calcium, %)	Chlorinity (mmol/kg)	Alkalinity (meq/kg)	Sulfate (mmol/kg)	Sodium (mmol/kg)	Potassium (mmol/kg)
Surface seawater (17 March 1989)					8.25	35.6	34.65	539.2	2.689	27.78	462.0	10.11
1W-1 1H-4, 145–150	5.98	55	3	35,000	7.73	35.4	34.81	541.9	2.921	27.02	464.2	10.05
1W-2 3H-4, 145–150	25.18	85	2	40,000	7.82	35.5	34.85	550.7	1.140	23.81	466.7	9.78
IW-3 6X-3, 140–150	52.05	43	3	36,000	7.61	35.1	35.00	551.7	1.366	24.34	466.0	7.84
IW-4 9X-3, 140–150	81.25	37	4	36,000	7.86	35.1	35.00	552.6	1.209	24.03	468.4	7.92

m/m.y. through the Pliocene. Middle and upper Pleistocene sediments are missing from the succession.

PHYSICAL PROPERTIES

The excellent recovery in Holes 786A and 786B allowed us to make a highly detailed reconstruction of the physical properties of the lithologic sequence at this site. Thermal conductivity, GRAPE bulk densities, index properties (bulk and grain densities, porosity, water content, and void ratio), and electrical resistivity were measured in the sedimentary sections encountered in Hole 786A. The preponderance of voids in the cores precluded the use of the *P*-wave logger for these holes. Thermal conductivity, GRAPE bulk density (on discrete samples), index properties, and compressional-wave velocities of discrete samples were measured for the igneous rocks recovered from Hole 786B. The physical-property measurements are listed in Tables 12 through 14 and plotted in Figures 15 through 19.

Hole 786A

Thermal-conductivity measurements in the sedimentary rocks are scattered about 1 W/mK and show little variation with depth (Table 13 and Fig. 15). Extremely low values (0.127 and 0.171 W/mK) were recorded in cores from the base of the hole, where the probe did not couple well with the sedimentary cores.

Wet-bulk densities measured by the GRAPE sensor on the MST show little variation with depth throughout the sedimentary section (Fig. 16). Densities of sedimentary cores cluster at 1.6 to 1.7 g/cm^3 for the uppermost 100 mbsf. Poor recovery in the interval from 110 to 140 mbsf prevented measurement of GRAPE densities. Rocks from the deepest part of the hole show considerable scatter in bulk density, which may well be related to the brecciated nature of the rocks.

Index properties were measured on discrete samples throughout the hole (Table 12). Bulk densities of sedimentary cores determined from discrete sample measurements are similar to those measured by the GRAPE sensor, and the values are grouped about 1.6 to 1.7 g/cm^3 and show no significant depth variation (Fig. 16). The bulk densities of samples of igneous rock from the base of the hole are higher (1.8 to 2.1 g/cm^3). Grain density also shows little variation with depth in both sediments and igneous rocks and ranges from 2.6 to 2.7 g/cm^3 for both sediment and hard-rock samples.

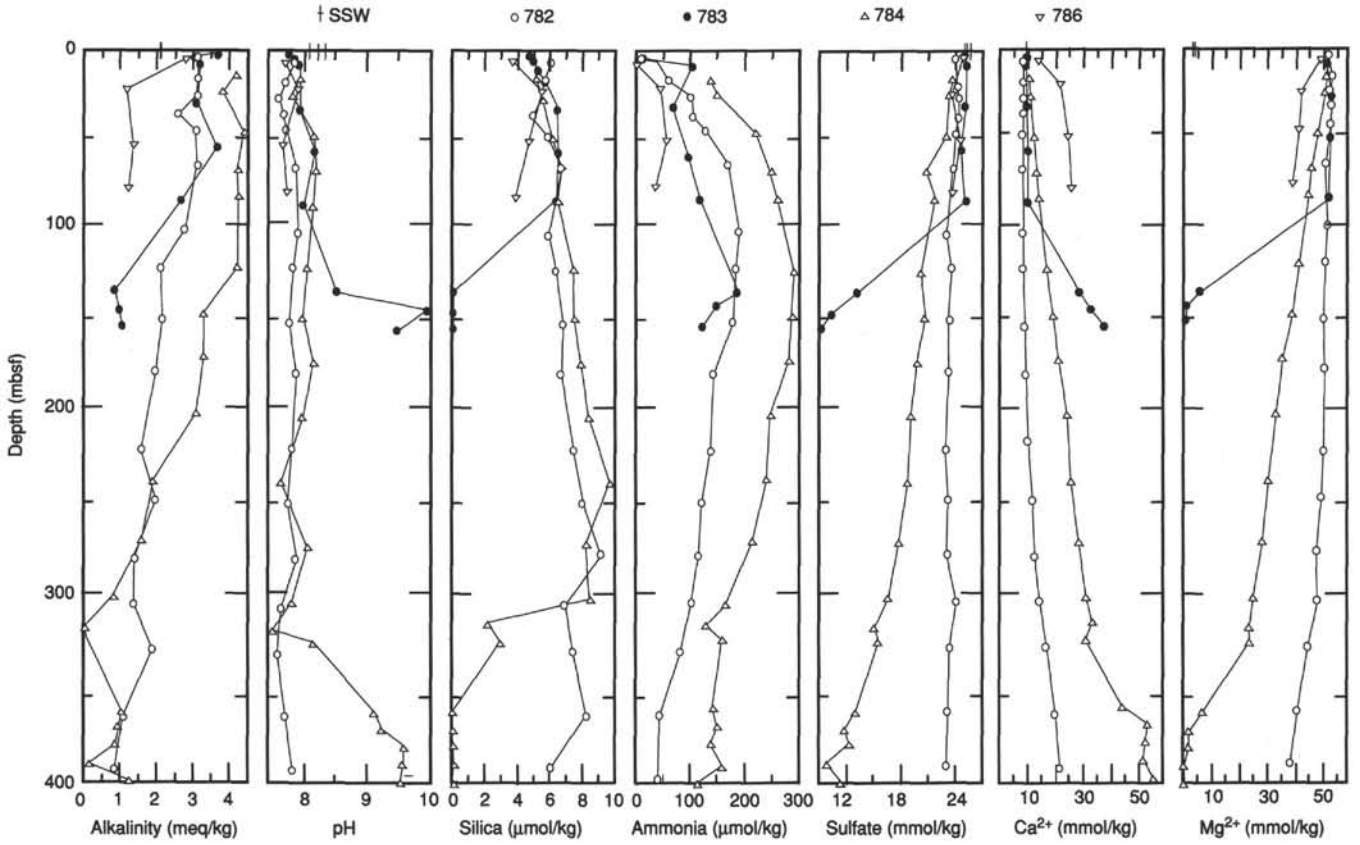

Figure 9. Composition of interstitial waters from sediments at Site 786 (inverted triangles) compared with those from Sites 782 (squares), 783 (diamonds), 784 (triangles), and 785 (X's) and surface seawater collected 22 February and 4 and 17 March 1989 (crosses).

Table 9 (continued).

Calcium (mmol/kg)	Magnesium (mmol/kg)	Bromide (mmol/kg)	Silica (μmol/kg)	Ammonia (μmol/kg)
10.18	52.48	0.830	0	0
14.08	48.24	0.850	385	<12
20.69	40.77	0.866	540	41
24.44	39.06	0.899	467	59
25.00	37.79	0.915	374	37

Where possible, electrical resistivities were measured for every second section of sedimentary material (Table 13). Resistivity may increase with depth, but the data are scattered (Fig. 17).

Hole 786B

Thermal conductivity was measured once per section using the half-slab technique (Table 14). Conductivities ranged from 1.0 to 1.8 W/mK from 150 to 750 mbsf (Fig. 18), but the data show considerable scatter. Below 750 mbsf, the rocks display generally higher thermal-conductivity values (up to 2.5 W/mK). This increase in thermal conductivity corresponds to the boundary between breccias and dikes (see "Igneous and Metamorphic Petrology" section, this chapter).

Discrete measurements of GRAPE density were performed on whole-round core sections, generally twice per section. Density increases with depth from 2.1 to 2.5 g/cm^3 over the 800 m cored (Fig. 18). These data are in good agreement with logging results (see "Downhole Measurements" section, this chapter). Rocks from higher levels in the hole show more scatter than those from deeper levels. The decreased scatter in the data is probably caused by increasing regularity downhole of the core diameter, which allowed us to collect data of higher quality. Index properties do not correlate well with GRAPE and downhole measurements (Fig. 19). Neither bulk density nor grain density shows significant downhole variation. Bulk densities increase from 2.3 to 2.5 g/cm^3, but exhibit a large degree of scatter, probably related to sampling of nonrepresentative rocks. Low bulk densities are recorded for samples from shear zones, where the rocks have significantly higher water contents (see Table 12). Grain densities are nearly constant at 2.7 g/cm^3.

Compressional-wave velocities were measured in two directions in each index-property sample. The A velocity is measured parallel to the split surface of the core, and the B velocity is measured perpendicular to the split surface. The samples measured generally show little seismic anisotropy (Table 14). Velocities range from 3000 to nearly 6000 m/s in each direction, and do not have coherent downhole trends (Fig. 19). The large velocity range is caused by the fractures and microcracks in the samples, which significantly lower compressional-wave velocities.

DOWNHOLE MEASUREMENTS

Hole 786B was logged in five different runs. The first log string consisted of the dual induction tool (DIT), the digital sonic tool (SDT), the natural gamma-ray spectrometry tool (NGT), and the temperature logging tool (TLT) and was run from 449 mbsf up to the end of the drill string. The second string—consisting of the lithodensity tool (LDT), the compensated neutron tool (CNT), NGT, and TLT—was run from a depth of 387 mbsf up to the end of the drill string. These tools were then combined into the Quad string (consisting of the

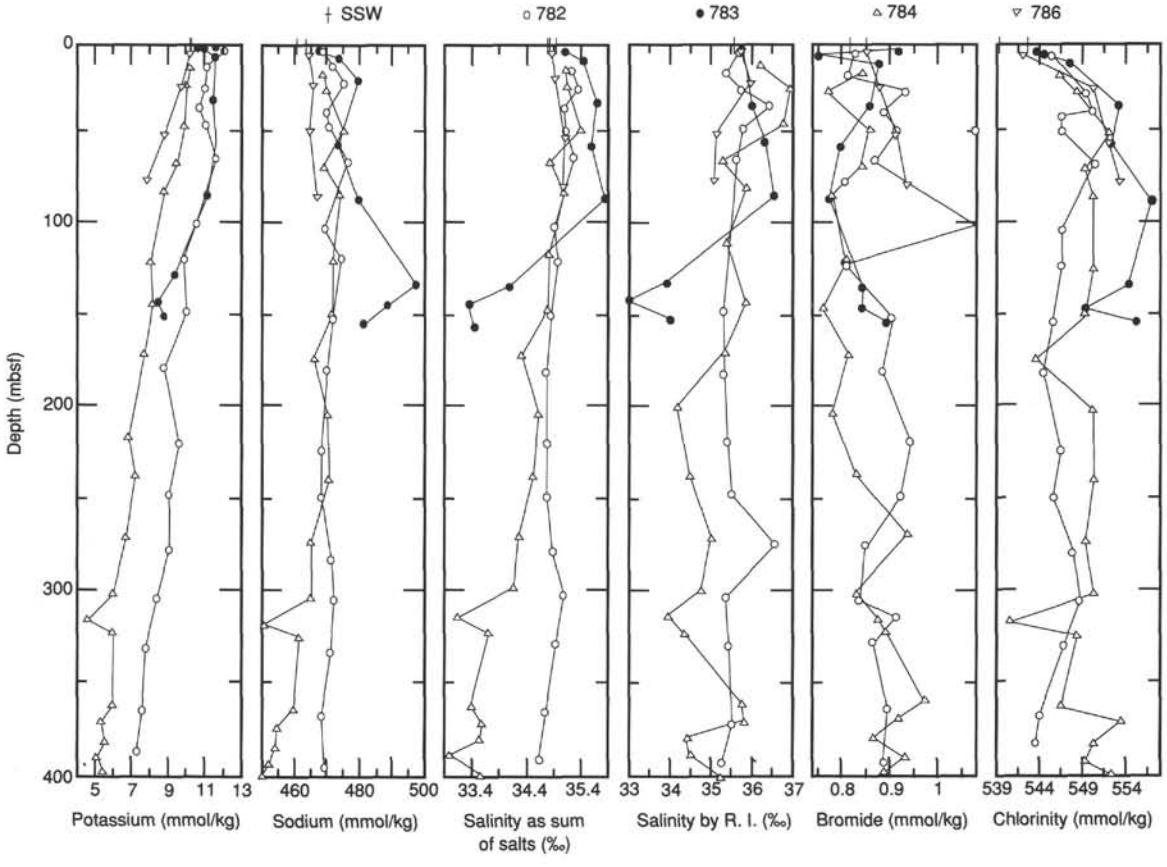

Figure 9 (continued).

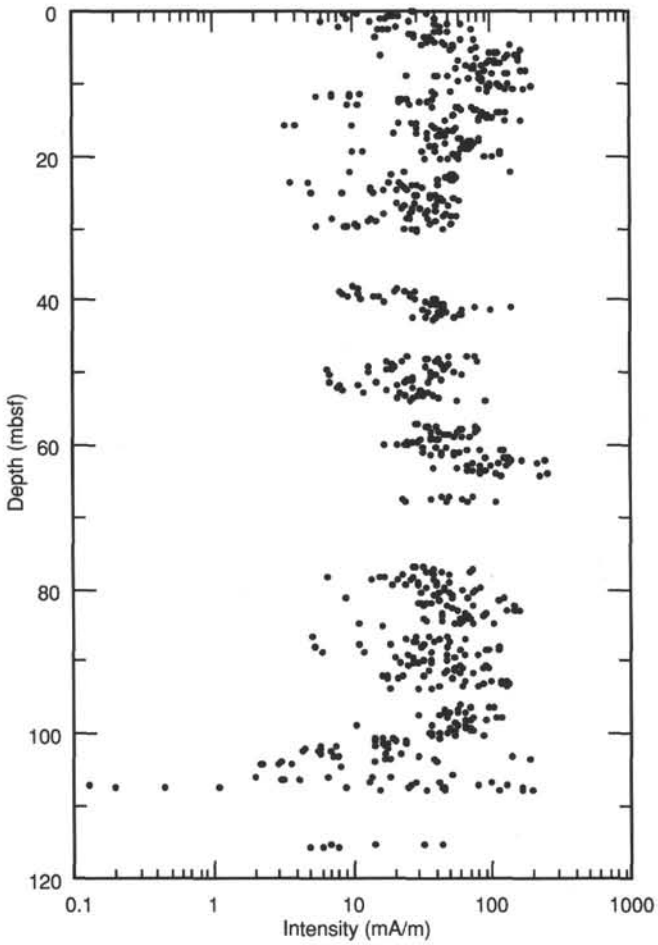

Figure 10. A downhole plot of magnetic intensity for Hole 786A.

DIT, LDT, CNT, SDT, and TLT). This third string was used to log uphole from 821 to 464 mbsf. The fourth run was a geochemical string, consisting of the induced gamma-ray spectrometry tool (GST), the aluminum clay tool (ACT), the NGT, and the TLT, which was run from 821 to 0 mbsf. The fifth logging run was the borehole televiewer (BHTV). After one failure, the tool was run again; 100 m (469–569 mbsf) of the hole was logged before time expired.

Logging results are presented at the end of this chapter. Because of various hole problems, not all logs are continuous throughout the entire hole.

Both lithologic Units I and II, with low percentages of SiO_2 and those of $CaCO_3$ of approximately 5% to 20%, are difficult to distinguish in the logging data. Lithologic Unit III is clearly differentiated from Unit II by the much higher MgO content (~10%), slight decrease in SiO_2, and sharp decrease in $CaCO_3$ in Unit III. The sediment/basement interface at 162.5 mbsf is much less distinct. The only logs that show a significant change at this depth are the bulk density log, which increases to 2.3 g/cm^3, and the porosity log, which decreases to 30%.

Based on the petrology, basement at Hole 786B has been divided into 30 units, some of which are heterogeneous in chemical composition. This large number of units precludes a detailed, unit-by-unit description of the logs here. A more detailed analysis of these logs will appear in the Leg 125 *Scientific Results* volume. In general, the MgO, SiO_2 (upon detailed examination), Al_2O_3, and perhaps sulfur logs are the most useful for distinguishing lithology.

The gamma-ray logs (CGR and SGR) show little variation downhole and average about 20 API units. Certain units stand out with slight variations that are a few API units higher or lower. The most striking feature observed in the gamma-ray logs is an increase of 55 to 70 API units between 752 and 783 mbsf, which is basement Unit 26 (metadacite and rhyolite flows). One dike within the unit has much lower gamma-ray values.

The resistivity logs show a certain amount of variation from unit to unit that is largely controlled by the amount of fracturing and brecciation. Resistivity is about 10 ohm-m in the upper part of the hole and slowly increases to 20 ohm-m at the bottom. Certain intervals, such as from 308 to 358 mbsf, have lower values of 3 to 7 ohm-m. Local variability also changes throughout the hole, with the interval from 468 to 593 mbsf and the zone below 733 mbsf showing increased local variability.

The caliper log shows that the hole is somewhat rugose in the upper part (down to 336 mbsf) with diameters of 0.36 to 0.41 m. The hole is narrower and smoother (from 0.30 m down to 0.25 m) in the lower part of the hole, at 478 mbsf. Data from the interval from 336 to 478 mbsf are unusable.

Bulk density ranges from 2.1 to 2.2 g/cm^3 at the top of the logged interval and 2.4 g/cm^3 at the bottom. Density generally increases with depth, but individual units may show increases or decreases about the trend. Variability can also be enhanced locally, especially at unit boundaries.

Porosity is about 50% at the top of the logged interval and decreases to about 30% at the bottom of the hole. The porosity abruptly decreases between 735 and 740 mbsf, with one small area of increased porosity in an interval with remarkable correspondence to Units 22 (rhyolite dike/sill), 23 (shear zone), and 24 (altered boninite-andesite pillows). The porosity abruptly decreases again at 752 mbsf, in Unit 26 (see the preceding discussion of gamma-ray logs).

The photoelectric effect is 2.9 barns/e at the top of the logged section and 3.2 barns/e at the bottom of the section.

Thorium is low and variable throughout most of the hole and ranges between 0.3 and 1 ppm. Thorium gradually increases to 3 ppm in the interval from 728 to 778 mbsf. Values decrease below that depth.

Uranium values are also low and variable throughout the hole, generally in the range of 0.25 to 0.5 ppm. Values up to 2.0 ppm occur in the interval from 533 to 538 mbsf, which is part of Unit 16, an andesitic breccia.

Potassium values vary somewhat in most of the hole, ranging from 0.5% to 1.0%. The major exception is within Unit 26 between 752 and 783 mbsf, where values range between 2.5% and 4.0%.

A discussion of the elemental logs of MgO, SiO_2, Al_2O_3, sulfur, CaO, and Fe_2O_3 will be presented in the Leg 125 *Scientific Results* volume.

Borehole Televiewer

The ultrasonic borehole televiewer (BHTV) was used to log the interval from approximately 469 to 569 mbsf. Both the high-frequency (1.4 MHz) and low-frequency (400 mHz) transducers were used in logging. The low-frequency transducers gave the best data. Preliminary analysis of the BHTV data indicates breakouts along the N10°E–S10°W direction, which shows the direction of minimum compressive stress. The direction of maximum compressive stress is at right angles to this and is aligned roughly along the orientation of the motion of the Pacific Plate.

SUMMARY AND CONCLUSIONS

Site 786 (proposed Site BON-6C) is located in the center of the Izu-Bonin forearc basin about 120 nmi east of the active volcano Myojin Sho. The objectives of this site were to study (1) the uplift and subsidence history of the forearc basin at this

Table 10. Remanence data for the discrete samples taken from Hole 786A.

Core, section, top of interval (cm)	Natural remanent magnetization			Remanent magnetization (15 mT)			Polarity
	Inclination (degrees)	Declination (degrees)	Intensity (mA/m)	Inclination (degrees)	Declination (degrees)	Intensity (mA/m)	
125-786A-							
1H-1, 142	−46.1	184.3	49.2	−12.4	175.8	7	N?
1H-2, 144	35.2	339.7	176.6	−4.2	163.3	16.2	R
1H-3, 140	56	29.6	21.5	−35.9	178.7	22.6	R
1H-4, 136	40.6	350.8	48.3	−32.7	179	58.3	R
1H-5, 145	32.7	10.8	74.8	−28.3	170.9	35.7	R
1H-6, 112	−0.2	157.1	51	−28.6	181	96.7	R
1H-7, 27	0.5	167.5	18	42.9	103.9	21.9	N
2H-1, 70	47.9	186.5	113.2	51.7	191.1	99.6	N
2H-2, 78	−35.6	27.4	115.6	−44.4	7.1	71.9	R
2H-3, 69	47.8	193	28.6	55.6	180.1	20.5	N
2H-4, 73	57.1	189.3	37.1	58.1	197.9	28.5	N
2H-5, 76	53.9	176.5	73.9	52	175.1	51.7	N
2H-6, 70	33.8	359.9	5.6	37.6	359	4.3	N
2H-7, 33	21.3	340	0.4	14.4	344	0.1	?
3H-1, 70	32.3	53.3	28.9	49.3	26	35.7	N
3H-2, 70	31.7	356.9	156.5	38.7	30.3	86.3	N
3H-3, 70	60.1	65.4	29.3	51.8	23.7	26.1	N
3H-4, 70	50.6	25.1	17.8	35.7	26.2	14.6	N
3H-5, 70	43.7	31.6	21.4	38.2	13.5	13.5	N
3H-6, 70	40	25.2	8.2	40.7	32.1	8.8	N
3H-7, 38	−4.1	227	0.1	−27.7	223.3	0.03	R
4X-1, 69	47.4	5.1	58.3	53.3	5.3	51.3	N
5X-1, 66	40.6	27.9	24.2	48.4	26.7	19.8	N
5X-2, 66	30.1	337.1	28.2	51	328.9	22.5	N
5X-3, 66	−15	242.89	16.3	30.5	220.7	5.2	N
5X-4, 50	10.7	161.9	37.6	61.2	166.6	34	N
6X-1, 87	42.2	185.1	63.2	48.5	182.6	40.2	N
6X-2, 68	37.8	236.2	55.3	39	251.6	34.6	N
6X-3, 68	42	214.6	55.6	42.7	221	39	N
6X-4, 67	3.6	69.1	23.8	−3.5	52.2	20.2	R
7X-1, 59	−33.3	175.7	14.8	53.7	156.8	8.9	N
7X-2, 59	−11.9	181.7	17.2	11.8	158.2	6.5	N
7X-3, 59	−12.5	165	40.4	2.1	152.2	26.9	?
7X-4, 59	−45.8	339.7	62.5	25.4	17.4	39.4	N
7X-5, 59	−38.9	32.4	33.1	−23.7	30.1	14.6	R
8X-1, 55	38.2	193.2	44.8	39.6	211.4	25.9	N
9X-1, 69	15.1	295.4	155	30.3	131.6	12.3	N
9X-1, 69	15.1	295.4	155	30.3	131.6	12.3	N
9X-2, 88	9	1	32	2.5	92.2	16.5	?
9X-3, 30	−38.6	88.6	22.9	−30.7	70.7	13.1	R
9X-4, 85	−8	308	6.5	54.7	219	7.2	N
9X-5, 46	3.2	312.4	43.7	−32.3	88.3	5.5	R
9X-6, 36	−7.5	325.3	28.5	45.7	273	8.7	N
10X-1, 80	38.2	337.2	89.6	50.5	9.2	32.5	N
10X-2, 77	12.7	227.7	207.7	60.8	323.9	16.8	N
10X-3, 63	−22	10.2	176.3	44.9	9.4	21.4	N
10X-4, 89	−2	220.5	222.7	−1	135.8	7.8	?
10X-5, 89	−9	346.4	9.1	7.2	165.3	4.5	?
10X-6, 17	16.2	1.8	32.1	48.5	11.9	9.1	N
11X-1, 43	22.6	353.6	245	47.3	336.3	6	N
11X-2, 96	−2.9	133.2	92.6	55.8	166.6	9.2	N
11X-3, 47	17.4	128.7	14.9	38.4	120.2	7.2	N
11X-4, 92	31.2	163.1	4.1	24	102	5.6	N
11X-5, 90	31.8	266.1	5.5	43.4	255.8	3.2	N

N = normal; R = reversed.

locality; (2) the temporal record of sedimentation, depositional environment, paleoceanography, and the intensity and nature of arc volcanism; (3) the nature and age of the igneous basement to the forearc basin, and (4) the regional stress field of the forearc, microstructural deformation, and large-scale rotation and translation of the forearc. Site selection was based on multichannel seismic records and a short shipboard seismic survey; the site chosen was 5 nmi east of the intersection of line 5 (0510UTC) of *Fred H. Moore* 3505 survey and *Conrad* line 38 (1125UTC). Occupation of the site began at 2015UTC, 1 April, and ended at 0800UTC on 16 April 1989.

Hole 786A (31°52.48′N, 141°13.58′E) was spudded with the APC in a water depth of 3058.1 m at 0815UTC on 2 April. Recovery of 103% was achieved for the 28.7 m drilled before changing to the XCB and drilling an additional 137.8 m with 40.1% recovery, for a total of 166.5 m drilled with 51.0% recovery. Hole 786B (31°52.45′N, 141°13.59′E), in a water depth of 3071.0 m, was washed through 162.5 m of the sedimentary column before recovery of igneous basement began at 162.5 mbsf. Drilling continued to a total depth of 828.6 m using the bionic bit M84F, which showed no signs of failure after 118.4 hr of use when drilling was stopped to begin logging.

Four suites of logging tools were run in Hole 786B. The first suite, consisting of the DIT, SDT, and NGT, was run from 3520.0 mbsl up to the end of the drill string. The second suite, consisting of the LDT, CNT, and NGT, was run from a depth of 3458.1 mbsl up to the end of the drill string. The third logging suite, consisting of the DIT, LDT, CNT, and

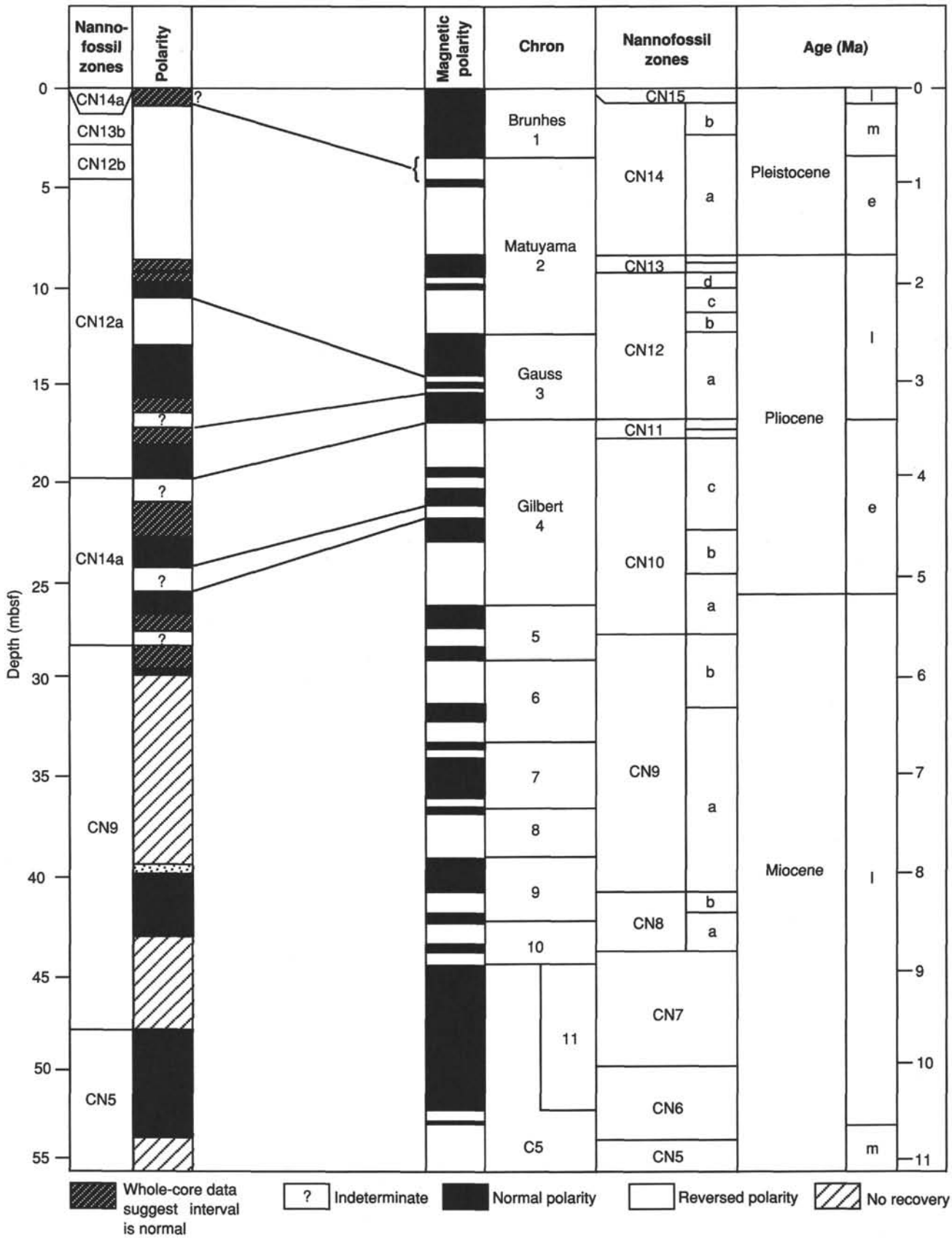

Figure 11. The magnetostratigraphy of Hole 786A for the interval from 0 to 55 mbsf correlated with the polarity time scale of Berggren et al. (1985b).

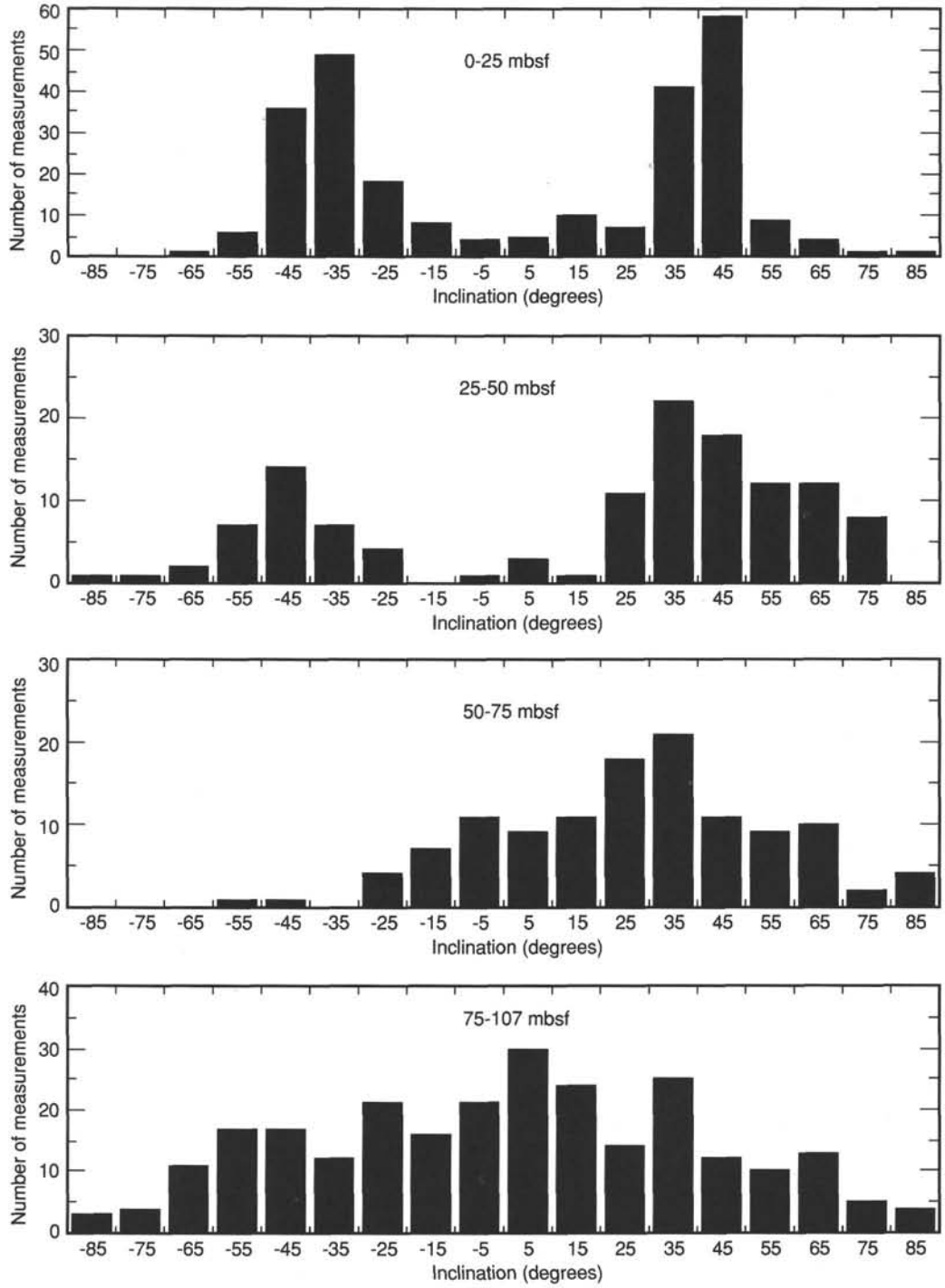

Figure 12. Inclination distribution as a function of depth, Hole 786A.

SDT, was used to log the hole from 3892 up to 3535.2 mbsl. The fourth suite, consisting of the GST, ACT, and NGT, was run from a depth of 3892.0 mbsl to the mud line. The BHTV was deployed for the fifth logging run and logged 80 m of Hole 786B after one failure before logging time expired.

The stratigraphic section recovered at Site 786 is assigned to lithologic Units I through IV (Fig. 3). Units I through III are defined only in Hole 786A, in which the sedimentary sequence was recovered at Site 786. Unit IV is defined in both holes. Unit I (0–83.46 mbsf) comprises 83.46 m of nannofossil marls and clays and is of early Pleistocene to middle Miocene age. It is made up predominantly of nannofossils (up to 70%), with lesser amounts of micrite (trace–40%), foraminifers (trace–30%), clay (5%–7%), sponge spicules (trace–5%), radiolarians (trace–4%), diatoms (trace–3%), and quartz (trace–2%).

Unit II (83.46–103.25 mbsf) is an upper Oligocene to middle Eocene nannofossil marl and nannofossil-rich clay. The unit consists of nannofossils (2%–60%), with lesser amounts of foraminifers (2%–10%), micrite (1%–35%), and radiolarians (trace–2%). Unit II also contains clays (10%–50%) and opaque minerals (3%–15%) with traces of chlorite

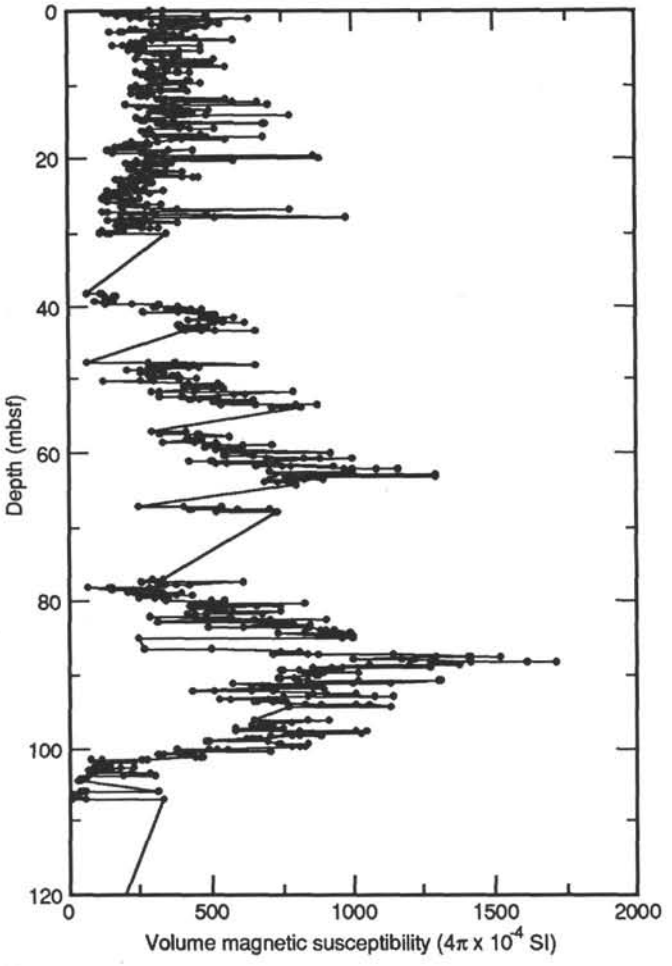

Figure 13. A downhole plot of susceptibility for Hole 786B.

Table 11. Biostratigraphic data used to plot the age vs. depth curve for Site 786 (Fig. 14).

Biostratigraphic event[a]	Depth (mbsf)	Age (Ma)
Calcareous nannofossils		
FO *G. oceanica*	0.2	1.7
FO *D. surculus*	3.9	2.4
LO *D. tamalis*	6.9	2.6
LO *Sphenolithus* spp.	24.5	3.4
LO *A. delicatus*	28.7	3.6
LO *D. quinqueramus*	31.8	5.6
FO *A. delicatus*	41.4	6.5
FO *D. quinqueramus*	47.6	8.3
FO *D. hamatus*	49.5	10.0
LO *D. kugleri*	57.1	10.8
LO *S. heteromorphus*	68.9	14.4
LO *D. bisectus*	85.1	23.7
FO *S. ciperoensis*	92.3	30.1
FO *S. distentus*	94.8	34.1
LO *E. formosa*	95.7	35.1
FO *I. recurvus*	97.7	37.8
LO *C. grandis*	102.9	39.6
FO *S. predistentus*	105.7	42.2
FO *D. saipanensis*	107.5	42.8

[a] FO = first occurrence; LO = last occurrence.

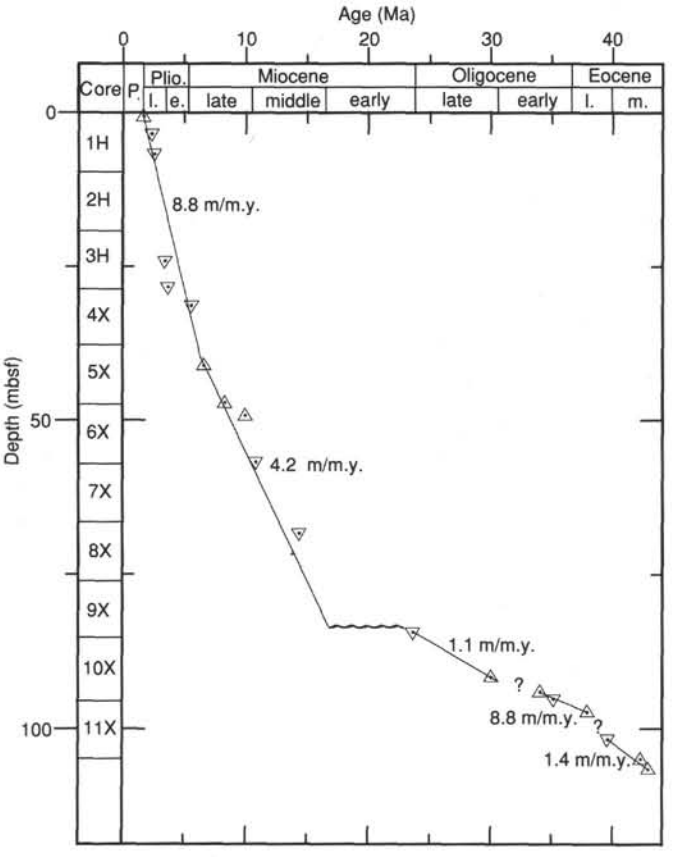

Figure 14. Age vs. depth curve for Hole 786A and estimated sedimentation rates.

and serpentine. Vitric ash and mineral fragments are also present.

Unit III (103.25–124.90 mbsf) is a sequence of volcaniclastic breccia, of middle Eocene age. The sedimentary components of the breccia matrix are nannofossils (up to 65%), clay (10%–50%), micrite (1%–35%), foraminifers (1%–10%), radiolarians (trace–2%), and opaque minerals (3%–15%).

Unit IV (124.9–166.5 mbsf in Hole 786A and 162.5–826.6 mbsf in Hole 786B) consists of volcaniclastic and sedimentary breccias, vitric siltstones and sandstones, lavas, dikes, and pyroclastic flows. Vitric fragments, glass (20%–100%), pyroxene (1%–30%), feldspar (1%–15%), lithic fragments (trace–10%), and amphibole (trace–5%) dominate the detrital component of the sediments; clays (10%–53%) are also present.

Dating is based on calcareous nannofossil, foraminifer, and diatom biostratigraphy. The rocks in the bottom of Hole 786A and the top of Hole 786B are considered to be the same material. Sedimentation rates are highest for the Pliocene (8.6 m/m.y.) and drop (to 4.2 m/m.y.) between the latest Miocene and middle Miocene. A hiatus exists between the middle Miocene and the late Oligocene.

The igneous basement (Fig. 3) consists mainly of massive and brecciated flows, ash flows, and intercalated sediment in its upper part, and pillow lavas and dikes or sills in its lower part. Rock types include high-magnesian basalts, boninites, basalts, andesites, dacites, and rhyolites. There are several prominent shear zones and hydrothermal breccias within the sequence.

Studies of physical properties show that average bulk densities are 1.65 g/cm^3 in the sediments and 1.8–2.1 g/cm^3 in the

the volcanic sequences; the average grain density of 2.65 g/cm^3 varied little between the sediments and the volcanic rocks.

Preliminary interpretation of the paleomagnetic data shows many intervals of normal and reversed polarity. The two intervals between 0 and 50 mbsf show good bimodal distributions with peaks around +45° and −45°, which indicates little translation since the late Miocene. Between 160 and 240 mbsf there is no bimodal distribution, although the many more data points between +15° and −15° suggest translation from a lower latitude.

The principal achievement at this site is the deep penetration of an Eocene volcanic edifice, which will provide (1) a record of the construction and structure of the forearc volcanic basement and (2) the basis for the understanding of early arc magmatism in general and boninite petrogenesis in particular.

REFERENCES

Berggren, W. A., Kent, D. V., and Flynn, J. J., 1985a. Jurassic to Paleogene: part 2. Paleogene geochronology and chronostratigraphy. *In* Snelling, N. J. (Ed.), *The Chronology of the Geological Record*: Geol. Soc. London Mem., 10:141–198.

Berggren, W. A., Kent, D. V., Flynn, J. J., and Van Couvering, J., 1985b. Cenozoic geochronology. *Geol. Soc. Am. Bull.*, 96:1407–1418.

Bleil, U., 1982. Paleomagnetism of Deep Sea Drilling Project Leg 60 sediments and igneous rocks from the Mariana region. *In* Hussong, D. M., Uyeda, S., et al., *Init. Repts. DSDP*, 60: Washington (U.S. Govt. Printing Office), 855–873.

McDuff, R. E., 1985. The chemistry of interstitial waters, Deep Sea Drilling Project Leg 86. *In* Heath, G. R., Burckle, L. H., et al., *Init. Repts. DSDP*, 86: Washington (U.S. Govt. Printing Office), 675–687. Meijer, A., 1980. Primitive arc volcanism and a boninite series: examples from western Pacific island arcs. *In* Hayes, D. E. (Ed.), *The Tectonic and Geologic Evolution of Southeast Asian Seas and Islands, Part I*. Am. Geophys. Union Geophys. Monogr. Ser., 23:269–282.

Ms 125A-114

NOTE: All core description forms ("barrel sheets") and core photographs have been printed on coated paper and bound as Section, near the back of the book, beginning on page 383.

Table 12. Index properties for Holes 786A and 786B.

Core, section, interval (cm)	Depth (mbsf)	Bulk density (g/cm^3)	Grain density (g/cm^3)	Porosity (%)	Water content (%)	Void ratio
125-786A-						
1H-1, 84–86	0.84	1.65	2.43	56.2	36.2	0.56
1H-2, 72–74	2.22	1.73	2.76	59.8	36.7	0.6
1H-3, 76–78	3.76	1.62	2.53	61.3	40.3	0.61
1H-4, 71–73	5.21	1.65	2.66	62.3	40.1	0.62
1H-5, 90–92	6.9	1.51	2.52	67.8	47.6	0.68
1H-6, 51–53	8.01	1.41	2.72	56.7	42.8	0.57
1H-7, 21–23	9.21	1.64	2.54	59.9	38.8	0.6
2H-1, 67–69	10.37	1.59	2.64	65.6	43.9	0.66
2H-2, 73–75	11.93	1.65	2.64	62.3	40.2	0.62
2H-3, 78–80	13.48	1.66	2.76	64.3	41.2	0.64
2H-4, 65–67	14.85	1.63	2.71	64.6	42.1	0.65
2H-5, 73–75	16.43	1.6	2.6	63.9	42.3	0.64
2H-6, 88–90	18.08	1.6	2.64	65	43.2	0.65
2H-7, 22–24	18.92	1.63	2.72	65.7	42.8	0.66
3H-1, 75–77	19.95	1.69	2.71	61.1	38.5	0.61
3H-2, 64–66	21.34	1.66	2.73	63.1	40.3	0.63
3H-3, 76–78	22.96	1.74	2.73	53.4	32.5	0.53
3H-4, 75–77	24.45	1.64	2.66	63	40.8	0.63
3H-5, 62–64	25.82	1.63	2.67	63.7	41.6	0.64
3H-6, 58–60	27.28	1.61	2.62	64	42.3	0.64
3H-7, 44–46	28.64	1.6	2.73	66.9	44.4	0.67
4X-2, 5–7	30.25	1.56	2.71	58.6	46.5	0.69
4X-CC, 15–17	30.61	1.59	2.58	64.4	43.1	0.64
5X-1, 54–56	38.74	1.55	2.73	68.6	46.9	0.69
5X-3, 101–103	42.21	1.66	2.82	64.9	41.5	0.65
5X-4, 37–39	43.07	1.69	2.8	63.3	39.8	0.63
5X-4, 59–61	43.29	1.73	2.98	64.6	39.7	0.65
6X-1, 59–61	48.19	1.7	2.72	60.8	38.1	0.61
6X-2, 59–61	49.69	1.62	2.63	63.5	41.7	0.63
6X-3, 59–61	51.19	1.65	2.76	64.6	41.7	0.65
6X-5, 16–18	53.76	1.63	2.61	62.4	40.6	0.62
7X-1, 33–35	57.43	1.77	2.82	59.1	35.6	0.59
7X-2, 33–35	58.93	1.7	2.83	62.9	39.3	0.63
7X-3, 33–35	60.43	2.15	2.85	77.1	38.2	0.77
7X-4, 33–35	61.93	1.79	2.76	56.7	33.7	0.57
7X-5, 33–35	63.43	1.84	2.82	54.8	31.6	0.55
7X-CC, 4–6	64.33	1.79	2.7	54.9	32.6	0.55
8X-1, 48–50	67.58	1.74	2.71	57.6	35.1	0.58
8X-CC, 6–8	68.18	1.75	2.75	58.2	35.3	0.58
9X-1, 83–85	77.63	1.55	2.69	69	47.3	0.69
9X-2, 97–99	79.27	1.6	2.79	68.1	45.3	0.68
9X-3, 93–95	80.73	1.57	2.66	66.8	45	0.67
9X-4, 80–82	82.1	1.5	2.65	71.1	50.3	0.71
9X-5, 98–100	83.78	1.79	2.98	61.2	36.3	0.61
9X-6, 25–27	84.55	1.79	2.77	56.7	33.7	0.57
10X-1, 88–90	87.28	1.85	2.88	55.8	32	0.56
10X-2, 82–84	88.72	1.67	2.52	57.4	36.5	0.57
10X-3, 72–74	90.12	1.71	2.69	58.9	36.5	0.59
10X-5, 82–84	93.22	1.58	2.51	63.4	42.7	0.63
10X-6, 25–27	94.15	1.79	2.71	54.9	32.5	0.55
11X-1, 80–82	96.8	1.78	2.79	57.9	34.7	0.58
11X-2, 83–85	98.33	1.74	2.78	59.8	36.5	0.6
11X-3, 78–80	99.78	1.38	2.74	79.6	61.1	0.8
11X-4, 84–86	101.34	1.58	2.61	65.3	43.9	0.65
11X-5, 50–52	102.5	1.64	2.81	65.8	42.5	0.66
11X-6, 63–65	104.13	1.92	2.94	53.3	29.5	0.53
12X-1, 42–44	106.12	1.62	2.66	64	41.9	0.64
14X-1, 16–18	125.06	2.05	2.77	41.4	21.4	0.41
15X-CC, 9–11	134.69	1.85	2.66	50.2	28.8	0.5
16X-1, 9–11	144.39	1.54	2.09	52.3	36.1	0.52
16X-CC, 19–21	144.69	2.1	2.86	41.7	21.1	0.42
17X-CC, 27–29	154.27	1.96	2.72	44.9	24.3	0.45
18X-1, 65–67	155.65	2.03	2.73	41.4	21.6	0.41
125-786B-						
1R-1, 61–64	163.11	2.44	2.63	11.4	5	0.11
2R-1, 58–60	170.08	2.51	2.61	6	2.5	0.06
3R-1, 94–97	180.14	2.47	2.86	21.7	9.4	0.22
4R-1, 110–112	190.1	2.7	2.72	1.5	0.6	0.02
5R-1, 1–3	198.61	2.27	2.95	34	15.9	0.34
5R-2, 53–55	200.63	2.4	2.55	9.5	4.2	0.1
6R-1, 38–40	208.58	2.33	2.69	21.6	9.8	0.22
6R-2, 43–45	210.13	2.51	2.73	12.7	5.4	0.13
8R-1, 45–47	228.05	2.25	2.73	28.5	13.5	0.29
9R-1, 10–12	237.2	2.45	2.65	12.9	5.6	0.13
9R-2, 128–129	239.84	2.07	3	47.4	24.3	0.47

Table 12 (continued).

Core, section, interval (cm)	Depth (mbsf)	Bulk density (g/cm^3)	Grain density (g/cm^3)	Porosity (%)	Water content (%)	Void ratio
10R-2, 68–69	248.73	2.46	2.68	13.5	5.8	0.13
11R-1, 22–24	256.52	2.24	2.79	31.7	15	0.32
12R-1, 49–51	266.49	2.24	2.77	30.4	14.4	0.3
12R-1, 49–51	266.49	2.24	2.77	30.4	14.4	0.3
12R-2, 14–16	267.57	2.23	2.57	22.2	10.6	0.22
13R-1, 85–87	276.55	2.46	2.75	16.8	7.2	0.17
13R-2, 70–72	277.83	2.39	2.78	22.1	9.8	0.22
14R-1, 35–37	285.75	2.4	2.69	18	8	0.18
15R-1, 35–37	295.35	2.19	2.65	28.2	13.7	0.28
15R-2, 128–130	297.75	2.11	2.61	32.1	16.2	0.32
16R-1, 78–80	305.38	2.21	2.73	30.7	14.8	0.31
16R-2, 14–16	306.21	2.3	2.47	11.8	5.4	0.12
17R-1, 67–69	314.97	2.33	2.73	24	10.9	0.24
18R-1, 61–63	324.51	2.34	2.6	16.5	7.5	0.17
19R-1, 27–28	333.87	2.36	2.57	14.1	6.4	0.14
20R-1, 71–73	344.01	2.29	2.55	17.1	7.9	0.17
21R-1, 125–127	354.25	2.22	2.43	14.6	7	0.15
21R-2, 86–88	355.3	2.5	2.66	10.2	4.3	0.1
22R-1, 31–33	362.91	1.86	2.52	44.7	25.6	0.45
22R-1, 70–72	363.3	2.05	2.56	33.6	17.4	0.34
22R-2, 62–64	364.71	1.97	2.29	23.7	12.8	0.24
22R-3, 30–32	365.85	1.96	2.12	14.6	7.9	0.15
24R-1, 10–12	382	2.33	2.52	12.5	5.7	0.12
24R-2, 13–15	383.53	2.38	2.54	10.7	4.8	0.11
25R-1, 68–70	392.18	2.41	2.67	14.9	6.6	0.15
26R-1, 65–67	401.85	2.33	2.63	18.7	8.5	0.19
27R-1, 89–91	411.69	2.16	2.73	34.1	16.8	0.34
27R-2, 40–42	412.7	2.25	2.94	36.3	17.2	0.36
28R-1, 98–100	421.38	2.43	2.56	8.6	3.8	0.09
29R-1, 22–24	430.32	2.39	2.77	21.7	9.6	0.22
30R-1, 82–84	440.52	2.48	2.7	13.3	5.7	0.13
30R-2, 70–72	441.9	2.45	2.71	15.6	6.8	0.16
30R-3, 29–31	442.99	2.51	2.61	6	2.5	0.06
31R-1, 106–108	450.46	2.55	2.63	4.7	2	0.05
31R-2, 84–86	451.68	2.64	2.73	5.1	2	0.05
32R-1, 119–121	460.19	2.53	2.62	5.8	2.4	0.06
32R-2, 86–88	461.36	2.34	2.55	13.7	6.2	0.14
33R-1, 18–20	468.88	2.55	2.62	4.2	1.7	0.04
34R-1, 128–130	479.58	2.14	2.3	12.7	6.3	0.13
34R-2, 73–75	480.53	2.6	2.71	6.5	2.6	0.06
34R-3, 45–47	481.65	2.49	2.64	9.3	4	0.09
34R-4, 90–91	483.6	2.55	2.7	9	3.7	0.09
35R-1, 126–128	489.26	2.36	2.46	6.7	3	0.07
35R-2, 41–43	489.91	2.19	2.46	18.9	9.2	0.19
35R-3, 60–62	491.6	2.15	2.28	10.9	5.4	0.11
35R-4, 35–37	492.85	2.04	2.24	16.9	8.8	0.17
36R-1, 63–65	498.33	2.1	2.27	14.1	7.1	0.14
37R-1, 69–71	508.09	2.4	2.68	17.3	7.6	0.17
37R-2, 82–84	509.63	2.44	2.52	5.7	2.5	0.06
37R-3, 14–16	510.45	2.53	2.65	6.9	2.9	0.07
38R-1, 79–81	517.89	2.4	2.48	5.8	2.6	0.06
39R-1, 48–50	527.28	2.3	2.34	17.7	8.2	0.18
39R-2, 65–67	528.95	2.33	2.36	17.3	7.9	0.17
39R-3, 27–29	530.03	2.43	2.62	11.9	5.2	0.12
40R-1, 102–104	537.32	2.59	1.82	89.3	36.6	0.89
40R-2, 46–48	538.03	2.71	2.78	3.9	1.5	0.04
40R-3, 61–63	539.35	2.7	2.78	4.8	1.9	0.05
40R-4, 25–27	540.49	2.53	2.68	9.9	4.1	0.1
41R-1, 61–63	546.51	2.39	2.86	25.7	11.4	0.26
41R-2, 17–19	547.42	2.33	2.66	20	9.1	0.2
41R-3, 9–11	548.84	2.08	2.93	45.1	23.1	0.45
41R-4, 23–25	550.48	2.47	2.71	14.5	6.2	0.14
42R-1, 67–69	556.27	2.55	2.75	11.8	4.9	0.12
42R-2, 67–69	557.77	2.56	2.65	5.6	2.3	0.06
43R-3, 124–126	559.78	2.48	2.59	7.4	3.2	0.07
42R-4, 13–15	560.17	2.61	2.73	7.2	2.9	0.07
43R-1, 30–32	565.3	2.42	2.58	10.2	4.5	0.1
43R-2, 32–34	566.62	2.34	2.61	16.9	7.7	0.17
44R-1, 30–32	574.9	2.68	2.77	5.5	2.2	0.05
45R-1, 53–55	584.83	2.39	2.69	17.8	7.9	0.18
46R-1, 59–61	594.49	2.58	2.88	16.4	6.7	0.16
46R-2, 59–71	596.09	2.41	2.72	18.5	8.1	0.18
47R-1, 101–103	604.51	2.44	2.75	18.2	7.9	0.18
48R-1, 73–75	613.93	2.28	2.65	23.1	10.8	0.23
48R-2, 50–52	615.09	2.43	2.8	20.8	9.1	0.21
49R-1, 32–34	623.22	2.45	2.57	8.1	3.5	0.08

Table 12 (continued).

Core, section, interval (cm)	Depth (mbsf)	Bulk density (g/cm^3)	Grain density (g/cm^3)	Porosity (%)	Water content (%)	Void ratio
49R-1, 82–84	623.72	2.64	2.76	62.8	25.3	0.63
49R-3, 62–64	625.88	2.33	2.67	20.8	9.5	0.21
49R-4, 50–52	627.18	2.39	2.7	18.7	8.3	0.19
50R-1, 24–26	632.74	2.4	2.95	28.9	12.8	0.29
50R-2, 31–33	634.31	2.53	2.81	16.1	6.8	0.16
51R-1, 49–51	642.69	2.47	2.75	16.4	7.1	0.16
51R-2, 6–8	643.76	2.43	2.71	17.6	7.7	0.18
52R-1, 81–83	652.71	2.44	2.97	29	12.6	0.29
52R-2, 143–145	654.83	2.48	2.61	8	3.4	0.08
53R-1, 48–50	662.08	2.69	2.93	12.8	5.1	0.13
53R-2, 55–57	663.65	2.71	2.89	9.7	3.8	0.1
54R-1, 107–109	672.27	2.37	2.76	22.7	10.2	0.23
54R-2, 85–87	673.49	2.58	2.66	5.9	2.4	0.06
54R-3, 65–67	674.79	2.42	2.67	15.7	6.9	0.16
54R-4, 59–61	676.23	2.53	2.74	12.2	5.1	0.12
54R-5, 44–46	677.26	2.64	2.73	5.3	2.2	0.05
55R-1, 49–51	681.29	2.56	2.65	5.5	2.3	0.06
55R-2, 85–87	683.04	2.45	2.66	13	5.6	0.13
55R-3, 90–92	684.53	2.32	2.44	8.9	4.1	0.09
56R-1, 124–126	691.34	2.31	2.48	11.8	5.4	0.12
56R-2, 107–109	692.67	1.93	1.15	94	51.7	0.94
56R-3, 58–60	693.56	2.26	2.49	15.6	7.3	0.16
56R-4, 65–67	695.06	1.99	2.69	42.6	22.8	0.43
56R-5, 79–81	696.7	2.19	2.36	12.8	6.2	0.13
57R-1, 110–112	700.9	2.36	2.63	16.7	7.5	0.17
57R-2, 89–91	702.1	2.34	2.96	32	14.5	0.32
57R-3, 65–67	703.14	2.53	2.95	21.9	9.2	0.22
57R-4, 66–68	704.6	2.67	3.07	19.7	7.8	0.2
57R-5, 50–52	705.75	2.36	2.63	17	7.6	0.17
57R-6, 86–88	707.42	2.19	2.83	35.6	17.3	0.36
57R-7, 70–72	708.76	2.18	2.49	21.1	10.3	0.21
58R-1, 77–79	710.17	2.3	2.49	13.4	6.2	0.13
58R-2, 127–129	712.17	2.3	2.53	16.1	7.4	0.16
58R-3, 83–85	713.05	2.47	2.88	22.3	9.6	0.22
58R-4, 19–21	713.84	2.24	2.45	14.7	6.9	0.15
59R-1, 68–70	715.08	2.36	2.54	11.9	5.3	0.12
59R-2, 86–88	716.5	2.31	2.53	14.2	6.5	0.14
59R-3, 127–129	718.37	2.29	2.5	15.6	7.2	0.16
59R-4, 35–37	718.93	2.35	2.53	12	5.4	0.12
60R-1, 72–74	719.72	2.37	2.58	13.7	6.1	0.14
60R-2, 115–117	721.45	2.53	2.62	5.5	2.3	0.05
60R-3, 94–96	722.69	2.43	2.53	6.3	2.7	0.06
60R-4, 106–108	724.31	2.32	2.42	7.1	3.3	0.07
60R-5, 49–51	725.16	2.41	2.52	7	3.1	0.07
60R-6, 47–49	726.48	2.31	2.42	7.6	3.5	0.08
61R-1, 74–76	729.44	2.34	2.51	10.5	4.8	0.1
61R-2, 29–31	730.49	2.38	2.59	12.4	5.5	0.12
61R-3, 10–12	731.8	2.35	2.56	14	6.3	0.14
61R-4, 82–84	733.83	2.45	2.57	7.6	3.3	0.08
61R-5, 56–58	735.07	2.48	2.62	8.8	3.8	0.09
61R-6, 53–55	736.26	1.95	2.56	40.2	21.9	0.4
62R-1, 34–36	738.74	2.56	2.65	5.6	2.3	0.06
62R-2, 42–44	740.19	2.39	2.58	12.3	5.5	0.12
62R-3, 107–109	742.12	2.42	2.76	19.7	8.7	0.2
63R-1, 83–85	748.83	2.46	2.11	45.8	19.8	0.46
63R-2, 74–76	750.24	2.5	2.7	10.9	4.6	0.11
64R-1, 136–138	759.06	2.48	2.61	8.7	3.7	0.09
64R-2, 90–92	760.04	2.35	2.5	10.4	4.7	0.1
64R-3, 56–58	761.16	2.52	2.6	5.1	2.2	0.05
65R-1, 17–19	767.57	2.66	2.73	4.3	1.7	0.04
65R-2, 37–39	769.27	2.2	2.58	25.1	12.1	0.25
65R-3, 52–54	770.89	2.22	2.37	11.2	5.4	0.11
66R-1, 88–90	777.98	2.31	2.5	13.3	6.1	0.13
66R-2, 80–82	779.34	2.48	2.56	5.2	2.2	0.05
66R-3, 34–36	780.3	2.41	2.53	8.2	3.6	0.08
67R-1, 35–37	787.05	2.44	2.55	7.1	3.1	0.07
68R-1, 9–11	796.39	2.45	2.54	6	2.6	0.06
69R-1, 78–80	798.08	2.55	2.61	4.1	1.7	0.04
69R-2, 24–26	798.93	2.34	2.66	19.7	9	0.2
69R-3, 130–132	801.1	2.37	2.56	12.4	5.5	0.12
69R-4, 51–53	801.81	2.46	2.69	14.3	6.2	0.14
69R-5, 63–65	803.09	2.48	2.59	7.3	3.1	0.07
69R-6, 75–77	804.66	2.37	2.62	15.8	7.1	0.16
69R-7, 30–33	805.63	2.43	2.54	8.9	3.9	0.09
70R-1, 5–7	806.95	2.45	2.56	7.3	3.1	0.07
70R-2, 5–7	808.45	2.45	2.58	8.3	3.6	0.08

Table 12 (continued).

Core, section, interval (cm)	Depth (mbsf)	Bulk density (g/cm^3)	Grain density (g/cm^3)	Porosity (%)	Water content (%)	Void ratio
70R-3, 117–119	811	2.48	2.69	12.6	5.4	0.13
70R-4, 49–51	811.68	2.46	2.72	15.6	6.8	0.16
71R-1, 115–117	816.75	2.23	2.5	18.8	8.9	0.19
71R-2, 106–108	818.16	2.33	2.58	17.4	8	0.17
71R-3, 107–109	819.59	2.21	2.54	21.5	10.3	0.22
71R-4, 71–73	820.65	2.53	2.64	7	2.9	0.07
71R-5, 16–18	821.6	2.51	2.59	4.9	2.1	0.05
72R-1, 87–89	824.47	2.55	2.62	4.4	1.8	0.04
72R-2, 80–82	825.9	2.32	2.5	12.3	5.6	0.12

Table 13. Physical properties for Hole 786A.

Core, section, interval (cm)	Depth (mbsf)	Thermal conductivity (W/mK)	Resistivity (ohms)	Formation factor
125-786A-				
1H-1, 75	0.75	1.004		
1H-2, 75	2.25	1.079		
1H-3, 75	3.75	0.971		
1H-4, 75	5.25	0.965		
1H-5, 75	6.75	0.778		
1H-6, 75	8.25	0.999		
1H-CC, 10	9.63	0.77		
2H-1, 75	10.45	0.959		
2H-2, 75	11.95	0.934		
2H-3, 75	13.45	0.894		
2H-4, 75	14.95	0.914		
2H-5, 75	16.45	0.97		
2H-6, 75	17.95	1.01		
2H-7, 27	18.97	1.035		
2H-CC, 22	19.5	1.028		
3H-1, 75	19.95	1.026		
3H-2, 75	21.45	0.991		
3H-4, 75	24.45	1.042		
3H-5, 75	25.95	1.036		
3H-6, 75	27.45	1.069		
3H-7, 34	28.54	0.935		
3H-CC, 8	28.97	0.933		
5X-1, 68	29.38	1.019		
4X-2, 19	30.39	0.954		
4X-CC, 22	30.68	1.006		
5X-1	38.4		23.3	2.72
5X-1, 69	38.89	1.057		
5X-2, 69	40.39	0.997		
5X-2	41.3		27.9	3.26
6X-1	47.9		23.5	2.74
6X-1, 50	48.1	0.788		
6X-2, 50	49.6	0.962		
6X-3	0.8		25.9	3.02
6X-3, 50	51.1	1.037		
6X-4, 40	52.5	0.873		
7X-1	57.13		38.1	4.45
7X-1, 65	57.75	1.039		
7X-3	60.2		24.5	2.86
7X-3, 65	60.75	1.066		
7X-5	63.35		27.7	3.23
7X-5, 65	63.75	1.099		
8X-1	67.25		34.1	3.98
8X-1, 65	67.75	0.994		
9X-1, 65	77.45	0.715		
9X-1	77.8		17.5	2.04
9X-3, 65	80.45	0.915		
9X-3	82.26		24	2.8
9X-5	83.1		18.5	2.16
9X-5, 65	83.45	0.987		
9X-5	83.6		40	4.67
10X-1	86.7		51.5	6.01
10X-1, 75	87.15	0.947		
10X-3, 75	90.15	0.921		
10X-3	90.26		42.5	4.96
10X-4, 75	91.65	0.997		
10X-5, 75	93.15	0.838		
10X-5	93.2		28	3.27
10X-6, 29	94.19	1.019		
11X-1, 75	96.75	1.037		
11X-1, 75	98.25	0.93		
11X-3, 75	99.75	0.834		
11X-5, 75	102.75	1.017		
11X-6, 56	104.06	0.854		
12X-1, 63	106.33	1.001		
12X-2, 20	107.4	0.944		
12X-CC, 24	107.82	0.127		
15X-CC, 10	134.7	0.822		
16X-CC, 35	144.85	0.171		

Table 14. Physical properties for Hole 786B.

Core, section, interval (cm)	Depth (mbsf)	Thermal conductivity (W/mK)	Compressional-wave velocity	
			A direction (km/s)	B direction (km/s)
125-786B-				
1R-1, 60–62	163.1	1.17	5.27	5.01
2R-1, 56–58	170.06	1.643	5.59	5.34
3R-1, 89–91	180.09	1.194	3.77	
4R-1, 52–54	189.52	1.194		
4R-1, 110–112	190.1		5.64	5.82
5R-1, 1–3	198.61		3.25	3.33
5R-2, 53–55	200.63		4.4	4.5
6R-1, 38–40	208.58		3.64	3.45
6R-2, 43–45	210.13		3.96	3.96
8R-1, 45–47	228.05		3.84	3.44
9R-1, 10–12	237.2		4.32	4.34
10R-1, 110–112	247.7		3.78	3.63
10R-2, 16–18	248.21	1.353		
11R-1, 22–24	256.52		3.68	3.58
11R-1, 60–62	256.9	1.215		
12R-1, 46–48	266.46	1.359	3.32	3.36
12R-2, 14–16	267.57		3.75	3.62
13R-1, 82–84	276.52	1.081	5.25	4.79
12R-2, 66–68	277.79	1.243	4.65	4.34
14R-1, 31–33	285.71	1.04	5.28	5.26
15R-1, 33–35	295.33	0.776	4.09	3.77
15R-2, 126–128	297.73	0.975	3.17	3.14
16R-1, 75–77	305.35	1.101	3.74	3.76
16R-2, 12–14	306.19	1.235	4.2	4.03
17R-1, 64–66	314.94	1.472	3.24	3.61
18R-1, 61–63	324.51		4.45	4.19
19R-1, 10–12	333.7	1.04		
20R-1, 77–79	344.07	1.042	4.2	4.21
21R-1, 97–99	353.97	1.28	4.11	4.05
12R-1, 125–127	354.25		4.56	3.74
22R-2, 62–64	364.71		3.72	3.97
22R-2, 107–109	365.16	0.957		
22R-3, 30–32	365.85		3.75	3.74
22R-3, 46–48	366.01	0.949		
24R-1, 10–12	382		4.19	4.44
24R-2, 11–13	383.51	1.728	4.94	4.66
25R-1, 63–65	392.13	1.529	3.98	4.17
26R-1, 61–63	401.81	3.928	3.7	3.99
27R-1, 86–88	411.66	0.916	3.23	3.28
27R-2, 37–39	412.67	1.176		
28R-1, 96–98	421.36	1.692	4.48	4.5
29R-1, 17–18	430.27	1.162	3.59	3.51
30R-2, 65–67	441.85	1.375		
30R-1, 75–77	440.45	1.412	3.73	3.91
30R-2, 70–72	441.9		4.11	4.16
30R-3, 21–23	442.91	1.468	4.48	4.43
31R-1, 102–104	450.42	1.345	4.43	4.37
31R-2, 78–80	451.62	1.619	4.5	4.51
32R-1, 119–120	460.19		4.39	4.42
34R-1, 64–66	478.94	1.671		
34R-2, 80–82	480.6	1.574		
34R-3, 108–110	482.28	1.761		
34R-4, 78–80	483.48	1.69		
35R-1, 115–117	489.15	1.505		
35R-2, 24–26	489.74	2.332		
35R-2, 41–43	489.91		3.67	3.67
35R-3, 57–59	491.57	1.619	3.86	3.58
35R-4, 31–33	492.81	1.732	3.75	3.75
36R-1, 60–62	498.3	1.716	3.67	3.73
37R-1, 67–69	508.07	1.403	3.96	3.7
37R-2, 82–84	509.63		4.33	4.27
37R-3, 11–13	510.42	1.533	4.21	4.27
38R-1, 74–76	517.84	1.072	4.87	4.96
39R-1, 44–46	527.24	1.263	3.99	4.02
39R-2, 64–66	528.94	1.018	4.04	4.1
39R-3, 25–27	530.01	1.192	4.69	4.43
40R-1, 98–100	537.28	1.332		
40R-1, 120–124	537.5		4.06	4.1
40R-2, 41–43	537.98	1.34		
40R-2, 46–48	538.03		4.25	4.34
40R-3, 54–56	539.28	0.924	4.73	4.73
40R-4, 25–27	540.49		4.03	3.97

Table 14 (continued).

Core, section, interval (cm)	Depth (mbsf)	Thermal conductivity (W/mK)	Compressional-wave velocity	
			A direction (km/s)	B direction (km/s)
41R-1, 61–63	546.51		4.06	4.02
41R-2, 17–19	547.42		4.05	3.89
41R-2, 122–124	548.47	1.194		
41R-3, 9–11	548.84		2.66	2.7
41R-4, 23–25	550.48		4.54	4.53
42R-1, 15–17	555.75	0.816		
42R-1, 67–69	556.27		5.06	5.03
42R-2, 67–69	557.77		4.56	4.44
42R-3, 90–92	559.44	1.824		
42R-3, 124–126	559.78		4.37	4.5
42R-4, 13–15	560.17		4.33	4.47
43R-1, 30–32	565.3		4.05	
43R-1, 38–40	565.38	1.911		
43R-2, 34–36	566.64	1.57	3.6	3.6
44R-1, 30–32	574.9		4.46	4.35
45R-1, 53–55	584.83		4.34	4.27
46R-1, 56–58	594.46	0.853	4.43	4.42
46R-2, 65–67	596.05	1.2	4.81	4.12
47R-1, 98–100	604.48	1.046	4.47	4.62
48R-1, 67–69	613.87	1.182	3.65	3.64
48R-2, 45–47	615.04	1.135	3.76	3.72
49R-1, 32–34	623.22	1.19	3.46	3.44
49R-2, 77–79	624.72	1.042	4.81	4.71
49R-3, 60–62	625.86	1.168	3.74	3.87
49R-4, 50–52	627.18		4.57	4.51
50R-1, 24–26	632.74		4.14	4.03
50R-2, 31–33	634.31		4.38	4.47
51R-1, 49–51	642.69		4.43	4.54
51R-1, 59–61	642.79	1.235		
51R-2, 6–8	643.76		4.27	4.19
52R-1, 81–83	652.71		3.94	3.87
52R-2, 140–145	654.83		4.85	4.88
53R-1, 128–130	662.88	1.257		
54R-1, 75–77	671.95	2.248		
54R-1, 107–109	672.27		3.9	3.81
54R-2, 64–66	673.28	1.164		
54R-2, 85–87	673.49		5.11	5.28
54R-3, 60–62	674.74	1.131	3.91	3.82
54R-4, 55–57	676.19	1.343	4.6	4.61
54R-5, 44–46	677.26		5.18	5.35
55R-1, 45–47	681.25	1.379	5.15	5.27
55R-2, 85–87	683.04		4.29	4.25
55R-3, 87–89	684.5	1.332	4.08	3.99
56R-1, 114–116	691.24	1.399		
56R-1, 124–126	691.34		4.16	4.32
56R-2, 100–102	692.6	1.373		
56R-2, 107–109	692.67		3.56	3.62
56R-3, 56–58	693.54	1.458	3.79	3.65
56R-4, 60–62	695.01	1.145	2.75	2.72
56R-5, 73–75	696.64	1.178	3.93	3.84
57R-1, 1–3	699.81	1.198		
57R-1, 12–14	699.92		3.1	3.19
57R-1, 107–109	700.87	1.273	3.14	3.2
57R-2, 83–85	702.04	1.261	4.06	3.92
57R-3, 57–59	703.06	1.316		
57R-4, 59–61	704.53	1.223		
57R-4, 65–67	704.59		3.52	
57R-5, 51–53	705.76	1.186	3.7	3.63
57R-6, 53–55	707.09	1.093		
57R-6, 86–88	707.42		3.24	3.34
57R-7, 85–87	708.91	1.204		
58R-1, 77–79	710.17		4.08	4.1
58R-1, 107–109	710.47	1.125		
58R-2, 53–55	711.43	1.15		
58R-2, 127–129	712.17		3.94	3.75
58R-3, 47–49	712.69	1.278		
58R-3, 83–85	713.05		3.14	
58R-4, 19–21	713.84		3.56	3.58
58R-4, 89–91	714.54	1.432		
59R-1, 68–70	715.08		4.5	4.24
79R-1, 92–94	715.32	1.249		
59R-2, 93–95	716.57	1.353	3.65	3.84
59R-3, 34–36	717.44	1.328		
59R-4, 35–37	718.93		4.24	4.12

Table 14 (continued).

Core, section, interval (cm)	Depth (mbsf)	Thermal conductivity (W/mK)	Compressional-wave velocity	
			A direction (km/s)	B direction (km/s)
60R-1, 44–46	719.44	1.213		
60R-1, 72–74	719.72		4.03	3.89
60R-2, 37–39	720.67	1.143		
60R-2, 115–117	721.45		5.3	5.27
60R-3, 69–71	722.44	1.292		
60R-3, 94–96	722.69		4.93	4.71
60R-4, 91–93	724.16	1.316		
60R-4, 106–108	724.31		4.39	4.44
60R-5, 35–37	725.02	1.399		
60R-5, 49–51	725.16		4.43	4.44
60R-6, 47–49	526.48		4.33	4.33
60R-6, 130–132	727.31	1.334		
61R-1, 68–70	729.38	1.304	4.2	4.4
61R-2, 26–28	730.46	1.542	3.95	4.11
61R-3, 1–3	731.71	2.053	3.45	3.5
61R-4, 71–73	733.72	2.053		
61R-4, 82–84	733.83		4.41	4.53
61R-5, 54–56	735.05	1.85	4.41	4.45
61R-6, 53–55	736.26		2.56	
62R-1, 31–33	738.71	1.858	4.47	4.51
62R-2, 31–33	740.08	1.757	3.74	3.66
62R-3, 104–106	742.09	1.332	3.5	3.45
63R-1, 20–22	748.2	1.253		
62R-1, 83–85	748.83		4.38	4.49
63R-2, 70–72	750.2	1.763	4.66	4.73
64R-1, 126–128	758.96	2.423		
64R-1, 145–147	759.97		4.84	4.84
64R-2, 93–95	760.07	2.265	4.65	4.68
64R-3, 56–58	761.16		4.71	4.77
65R-1, 5–7	767.45	1.759		
65R-1, 17–19	767.57		4.71	4.7
65R-2, 37–39	769.27		4.12	4.1
65R-2, 68–70	769.58	2.151		
65R-3, 52–54	770.89		4.11	4.09
65R-3, 38–40	770.75	2.147		
66R-1, 88–90	777.98		4.01	3.99
66R-1, 95–97	778.05	2.177		
66R-2, 70–72	779.24	2.488		
66R-2, 80–82	779.34		4.78	4.7
66R-3, 34–36	780.3		4.39	4.45
66R-3, 43–45	780.39	2.358		
67R-1, 33–35	787.03	2.252	4.17	4.09
68R-1, 1–3	796.31	1.862	4.99	4.93
69R-1, 69–71	797.99	1.613		
69R-1, 78–80	798.08		3.99	3.93
69R-2, 22–24	798.91	1.676	3.34	3.43
69R-3, 25–27	800.05	1.97		
69R-3, 130–132	801.01		3.86	3.69
69R-4, 35–37	801.65	2.07		
69R-4, 51–53	801.81		4.2	3.51
69R-5, 52–54	802.98	2.173		
69R-5, 63–65	803.09		4.24	4.17
69R-6, 71–73	804.62	1.574	4.18	4.2
69R-7, 33–35	805.66	1.613		
70R-2, 64–66	809.04	1.787		
70R-3, 60–62	810.43	1.706		
70R-4, 23–25	811.42	2.198		
71R-1, 103–105	816.63	2.198		
71R-2, 106–108	818.16		3.4	3.49
71R-2, 126–128	818.36	2.415		
71R-3, 107–109	819.59		3.21	3.25
71R-3, 130–132	819.82	2.177		
71R-4, 43–45	820.37	2.212		
71R-4, 71–73	820.65		4.53	4.44
71R-5, 10–12	821.54		4.83	4.75
72R-1, 80–82	824.4	2.236	4.78	4.75
72R-2, 76–78	825.86	1.761	3.72	3.62

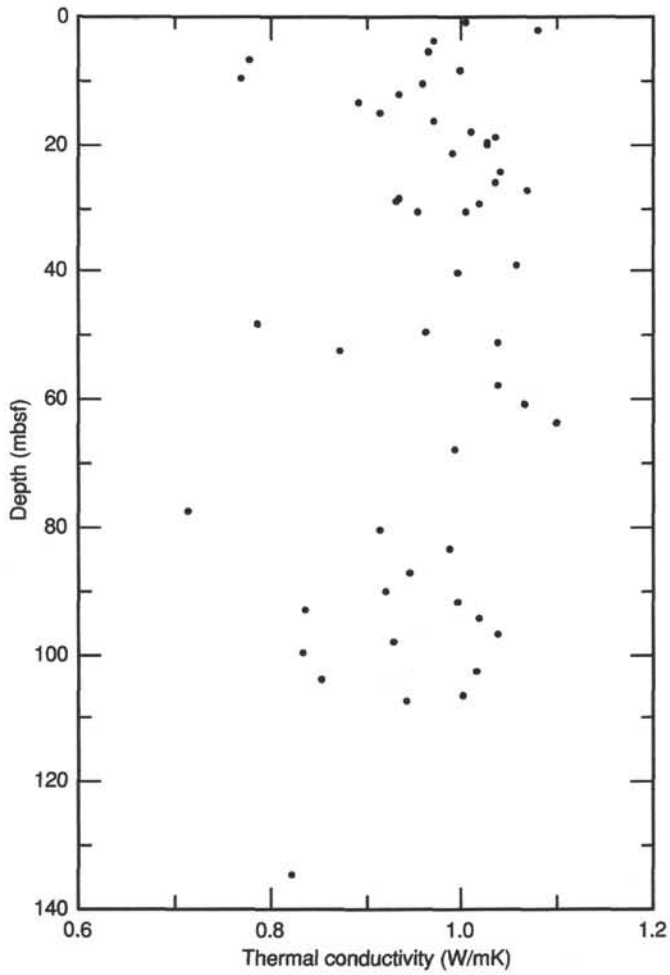

Figure 15. Thermal conductivity vs. depth for Hole 786A (the large degree of scatter in the data from the base of the hole is probably caused by measurement of irregularly shaped hard rocks).

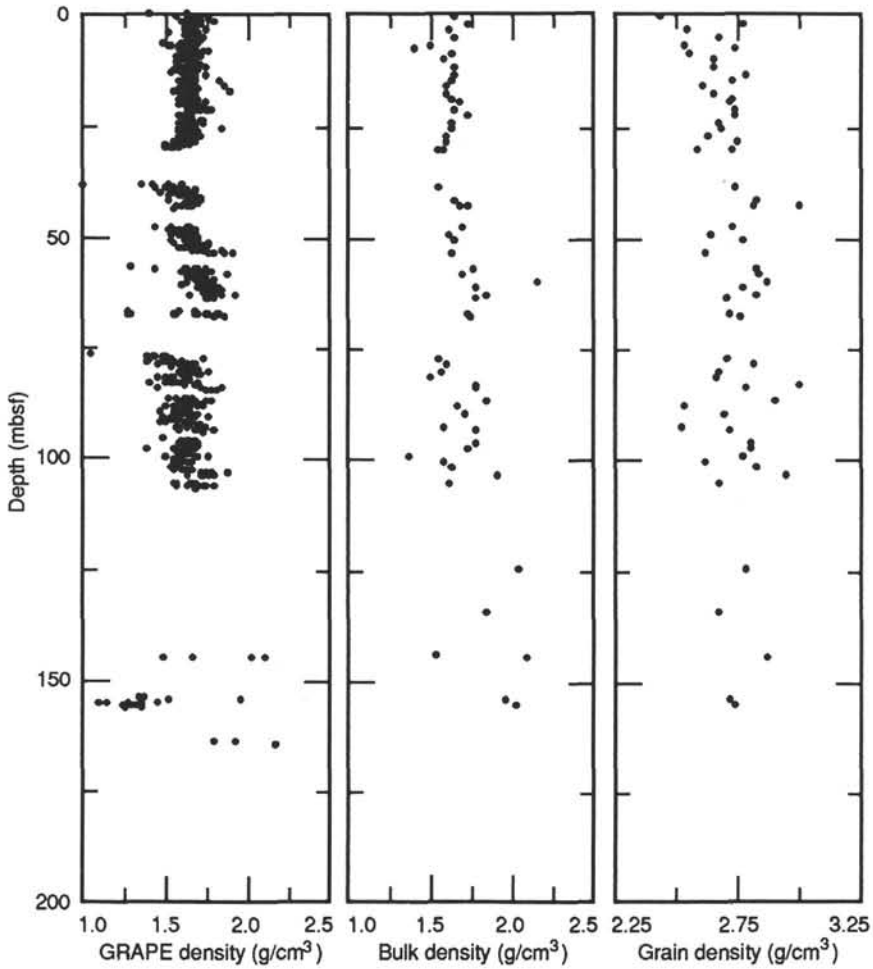

Figure 16. Bulk density (determined by GRAPE), bulk densisty (determined by discrete samples), and grain density vs. depth for Hole 786A.

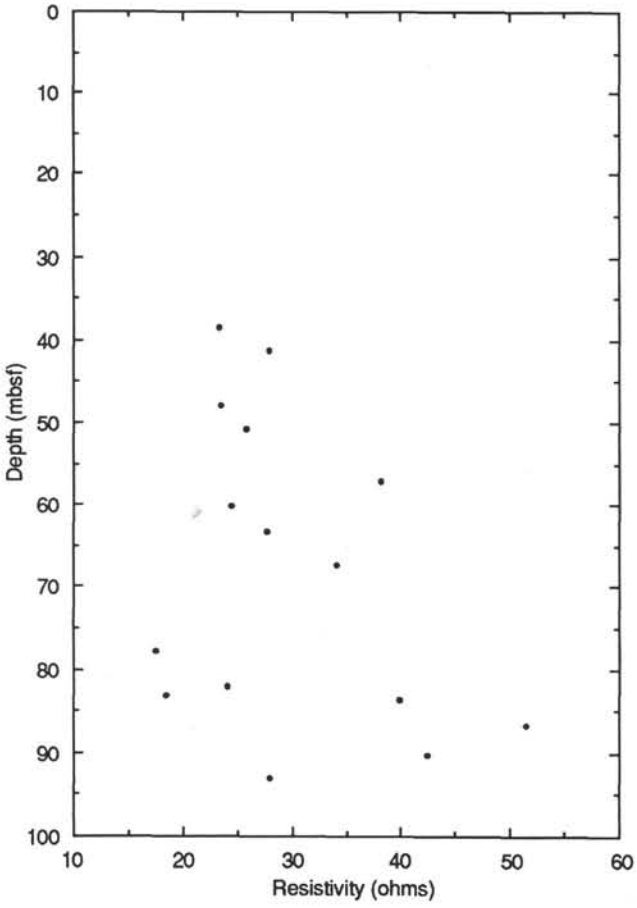

Figure 17. Resistivity vs. depth for Hole 786A.

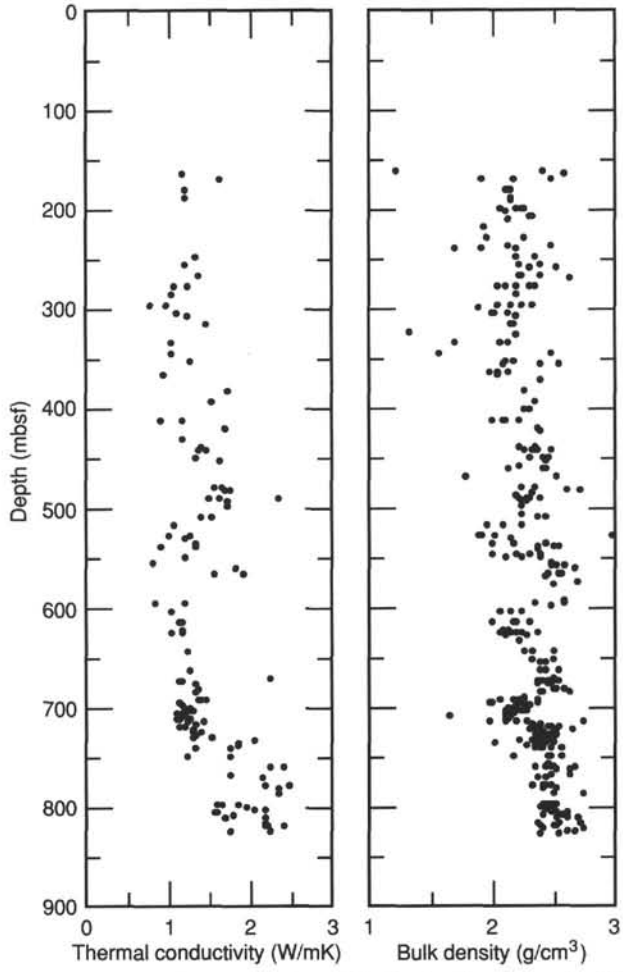

Figure 18. Thermal conductivity and bulk density (determined by 2-min GRAPE counts) vs. depth for hard rocks from Hole 786B.

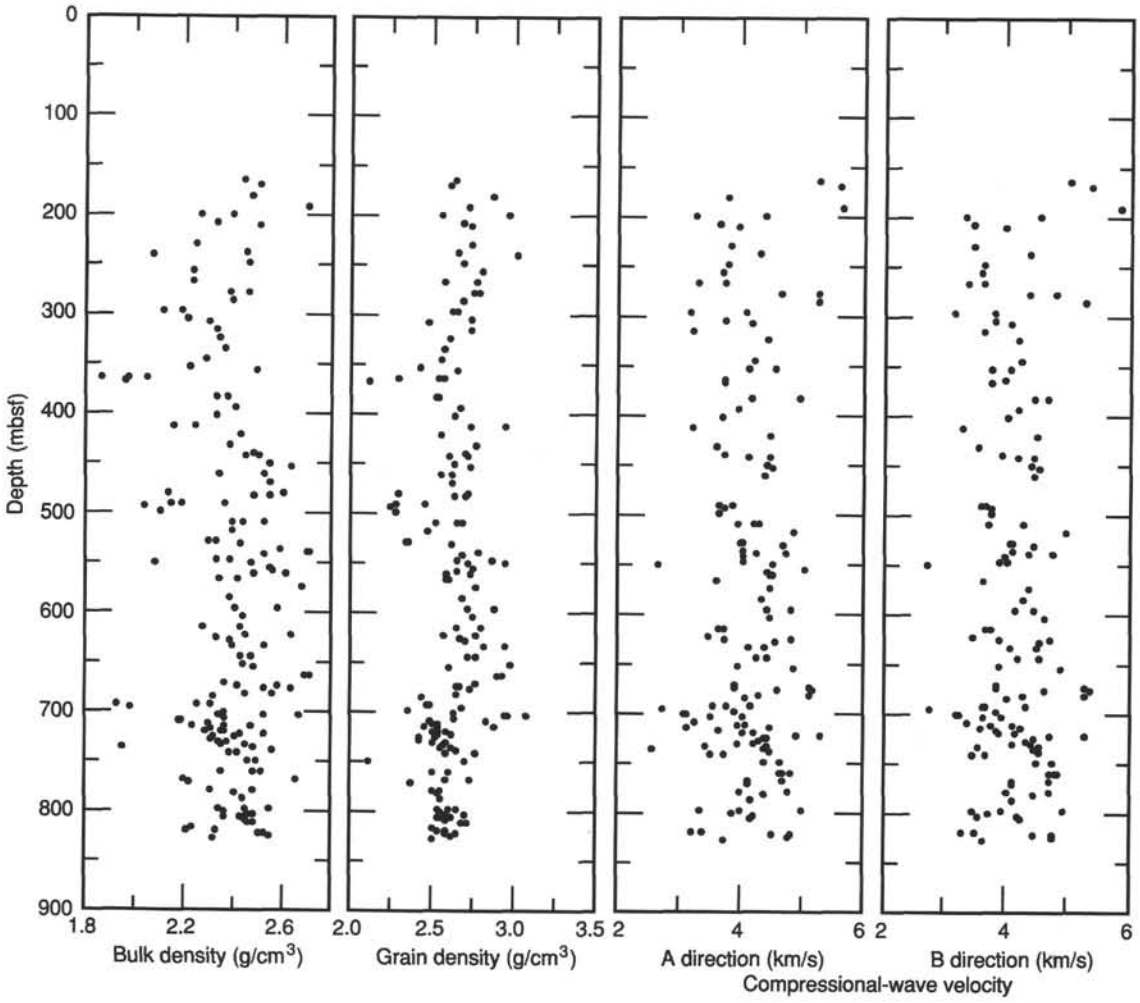

Figure 19. Bulk density, grain density, and compressional-wave velocities measured on the Hamilton Frame apparatus vs. depth for Hole 786B. The velocities in the orthogonal directions are nearly equivalent and show a high degree of scatter, which is related to microcrack effects.

Summary Log for Site 786

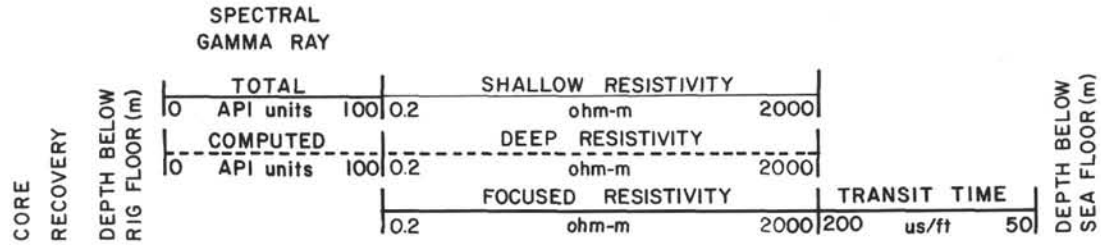

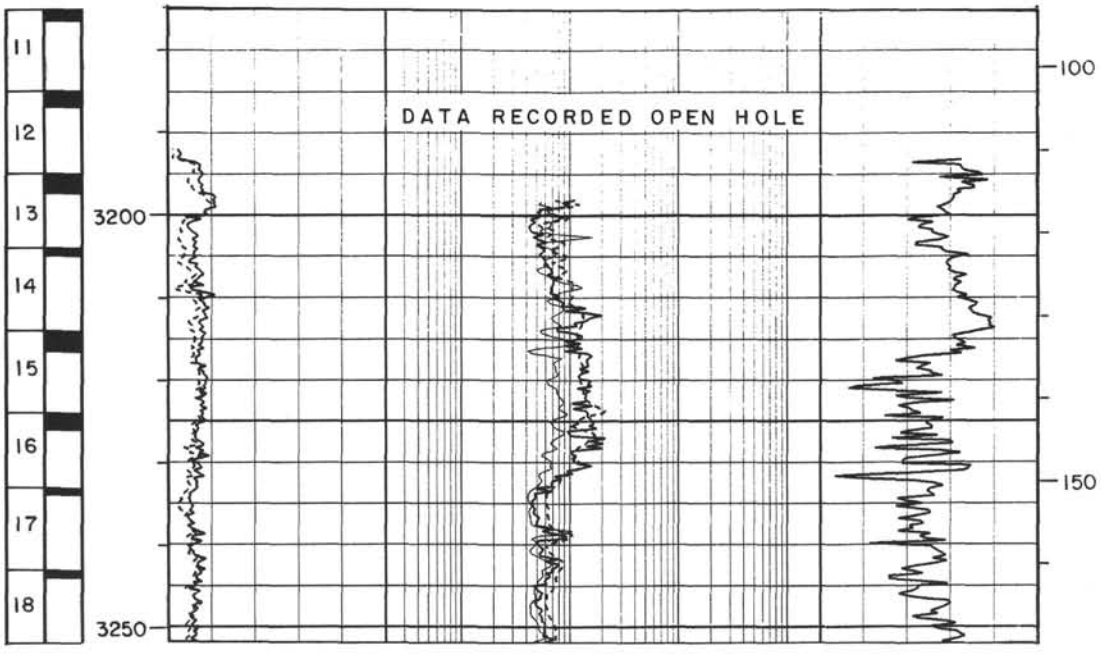

Summary Log for Site 786 (continued)

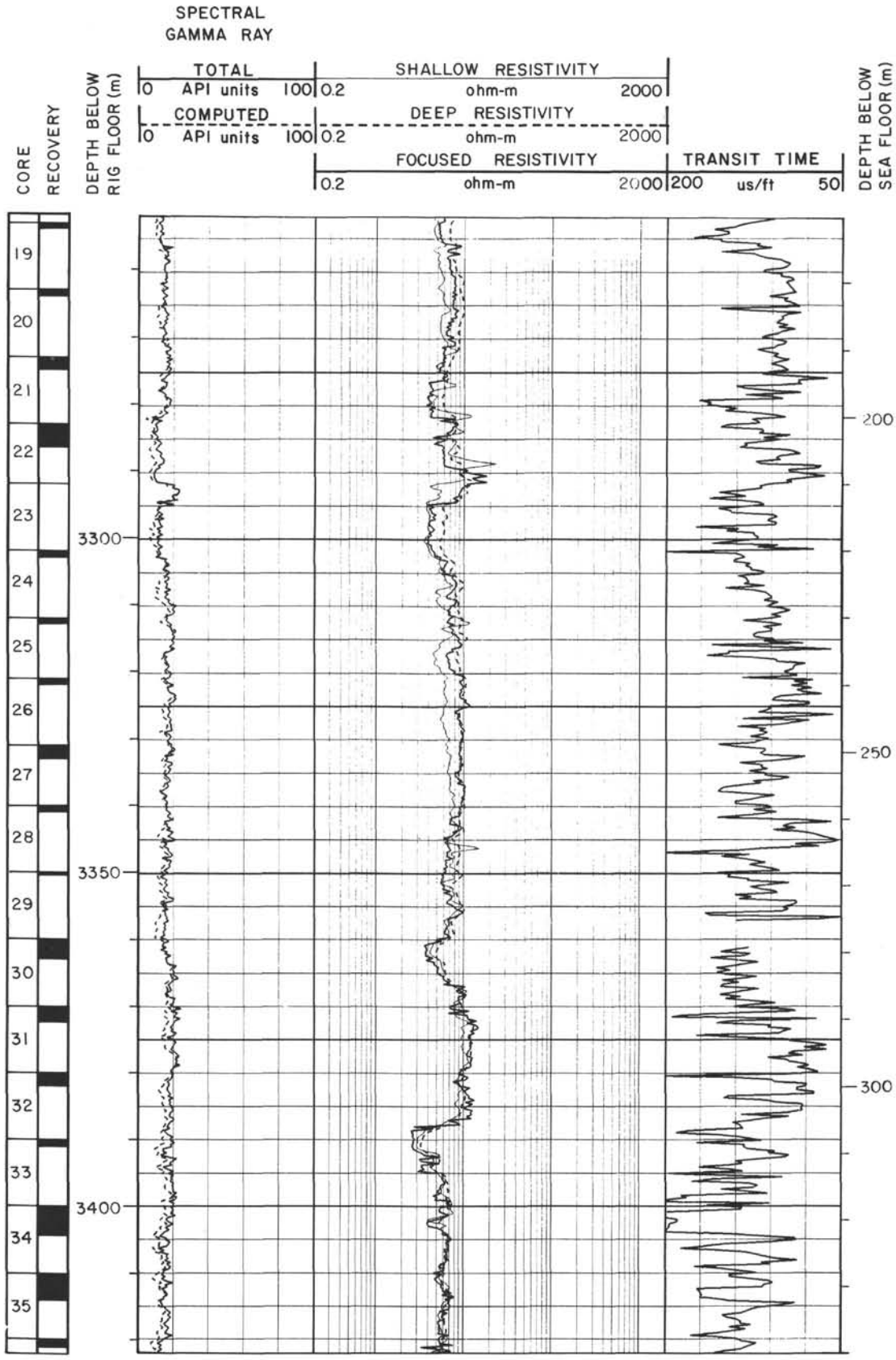

Summary Log for Site 786 (continued)

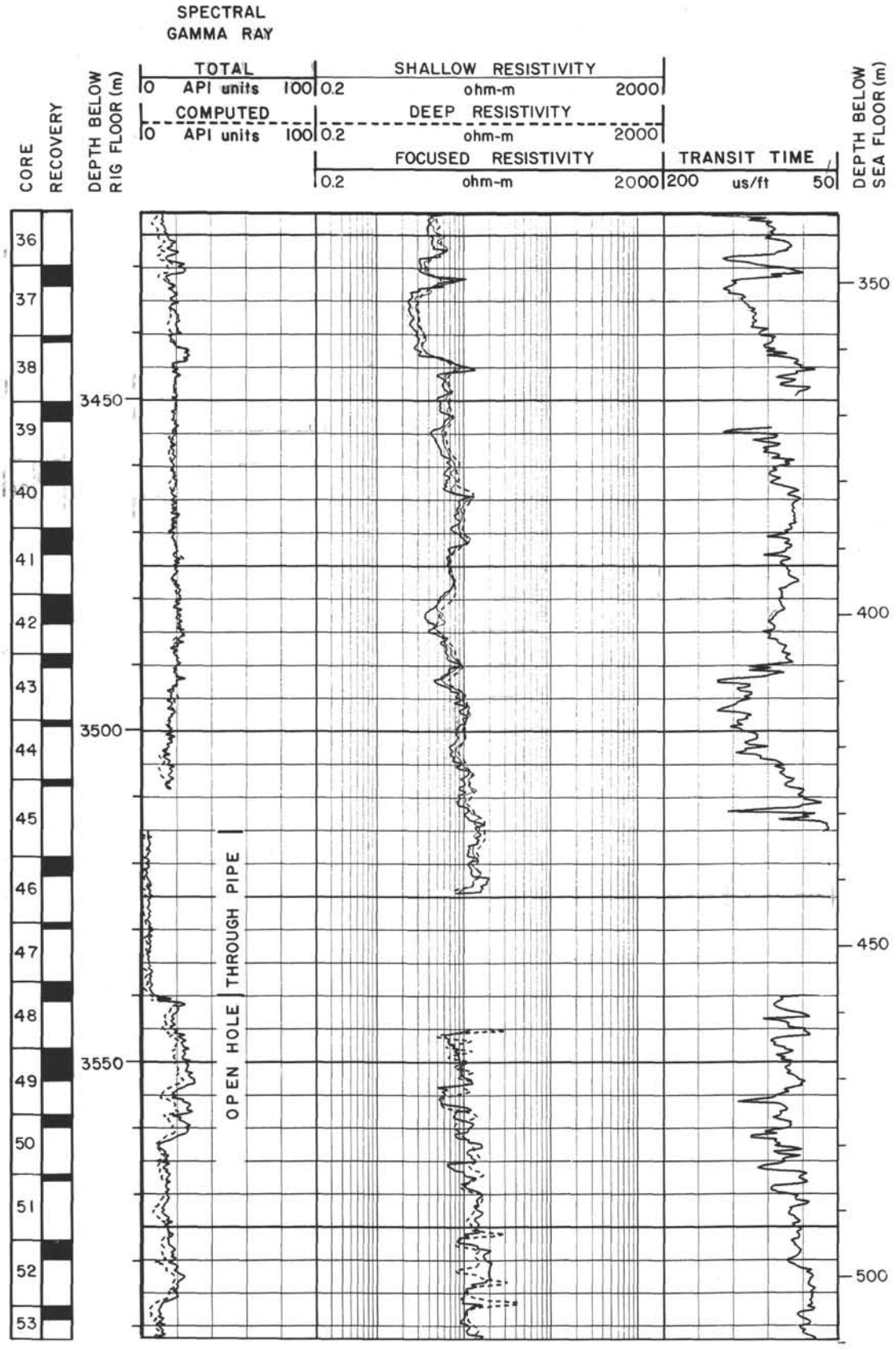

Summary Log for Site 786 (continued)

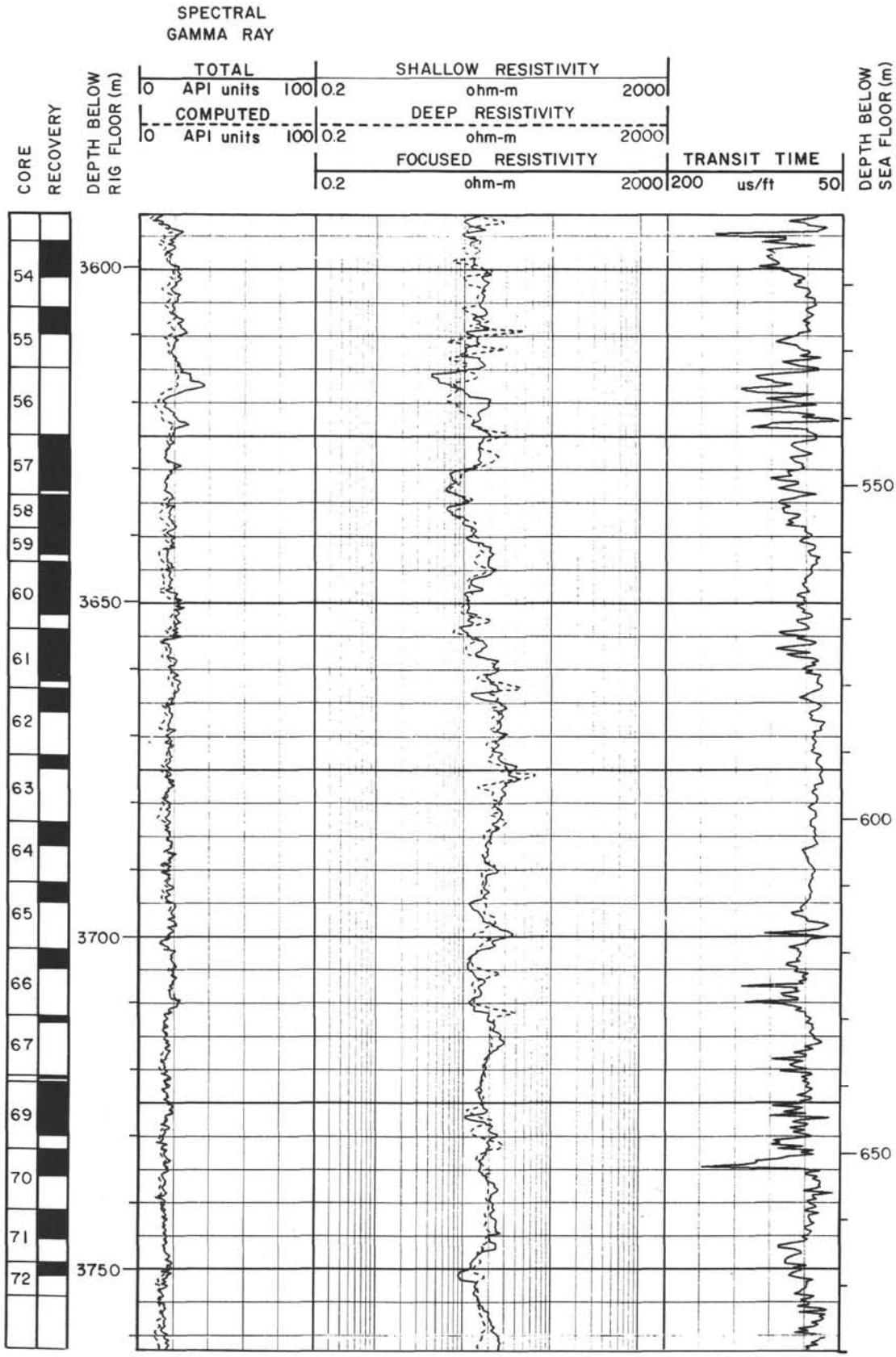

Summary Log for Site 786 (continued)

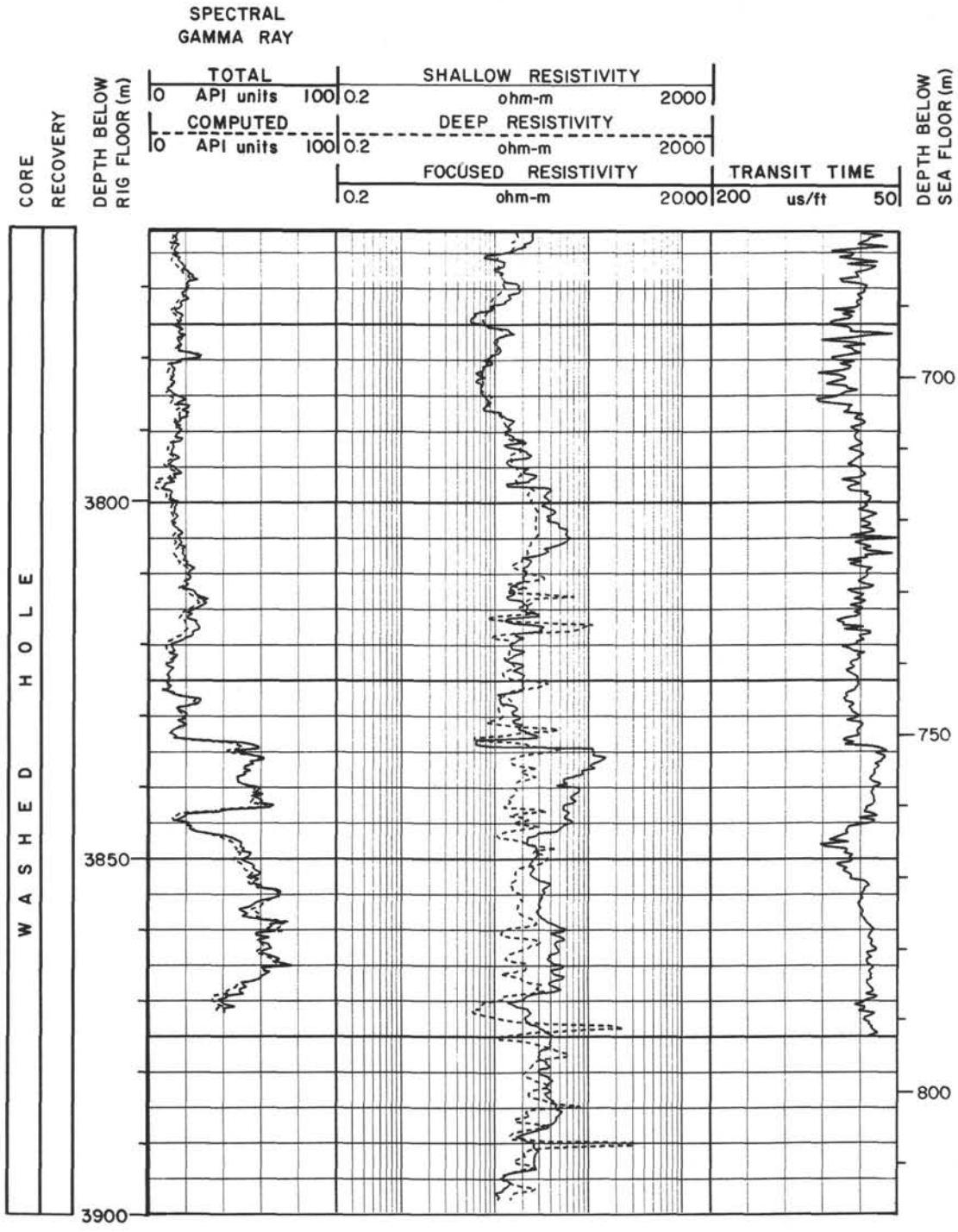

Summary Log for Site 786 (continued)

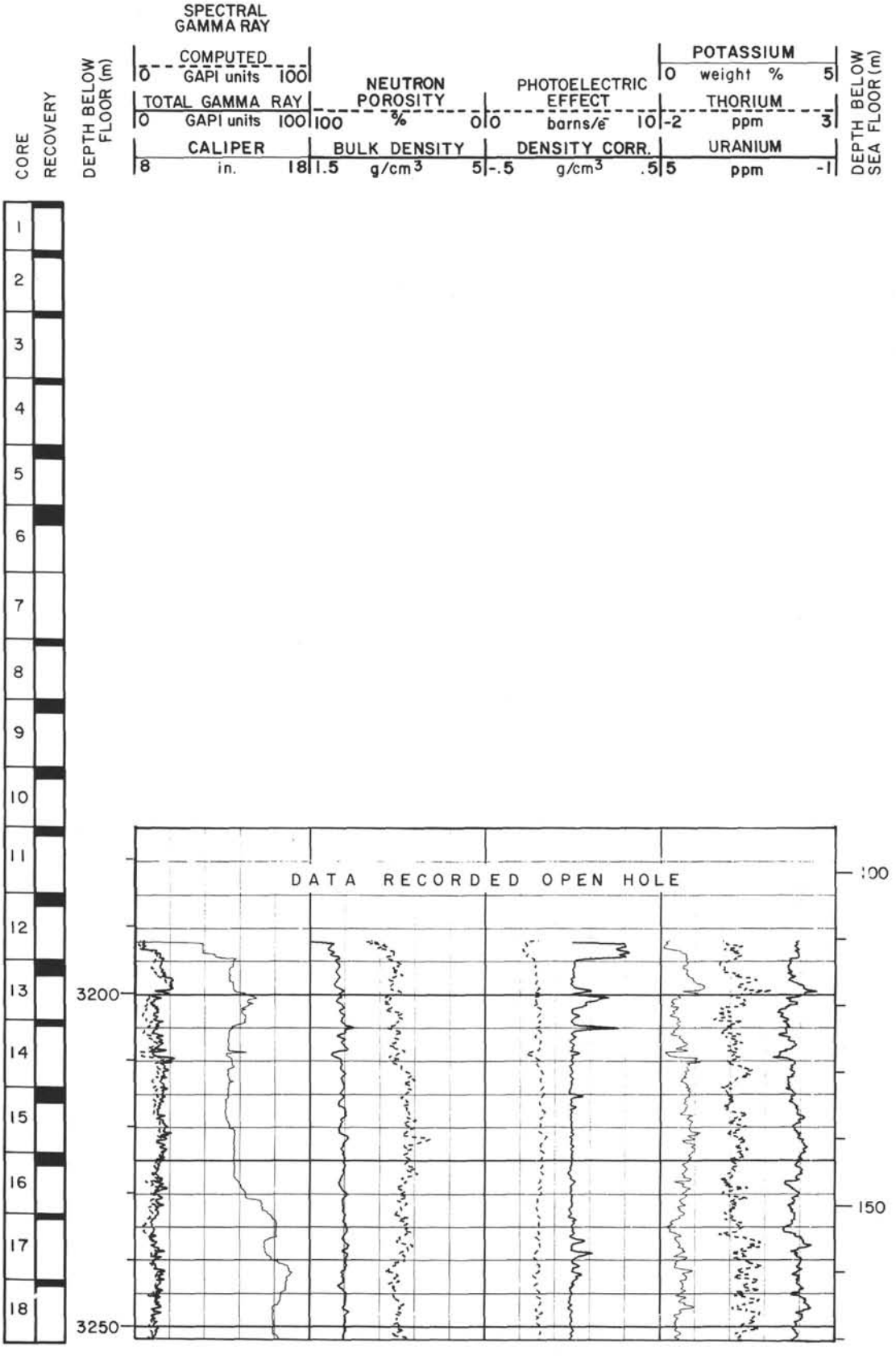

Summary Log for Site 786 (continued)

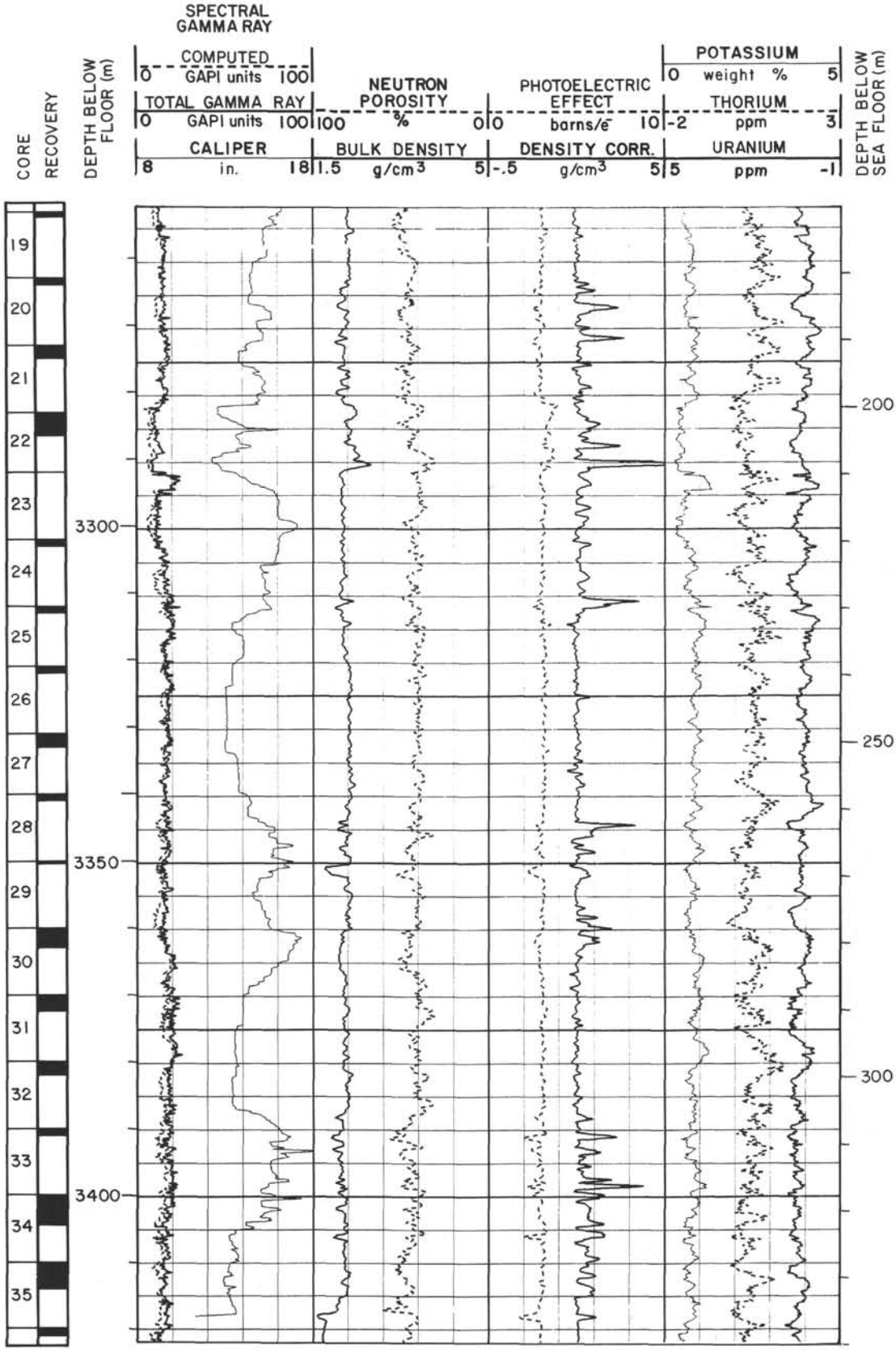

Summary Log for Site 786 (continued)

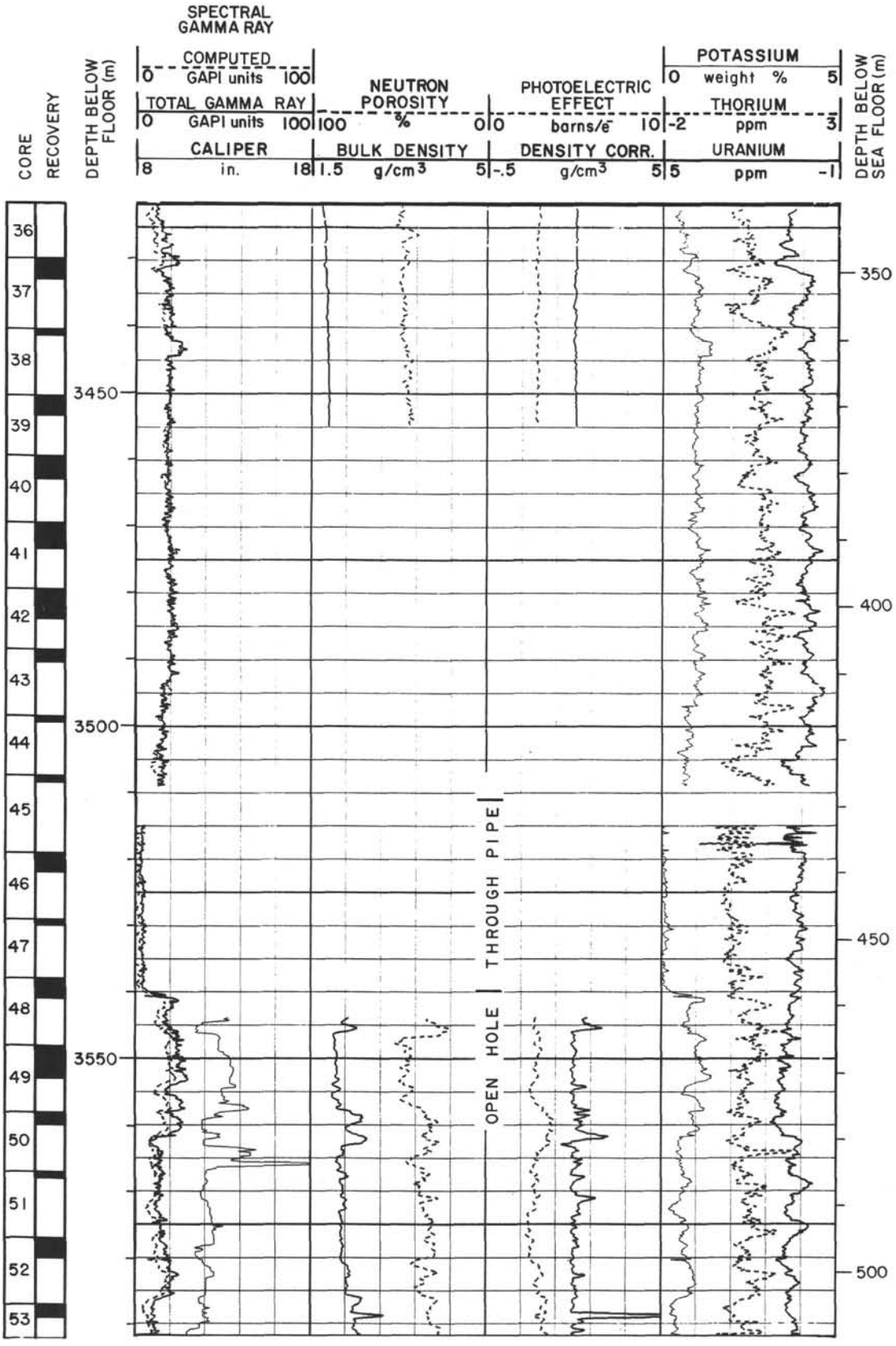

Summary Log for Site 786 (continued)

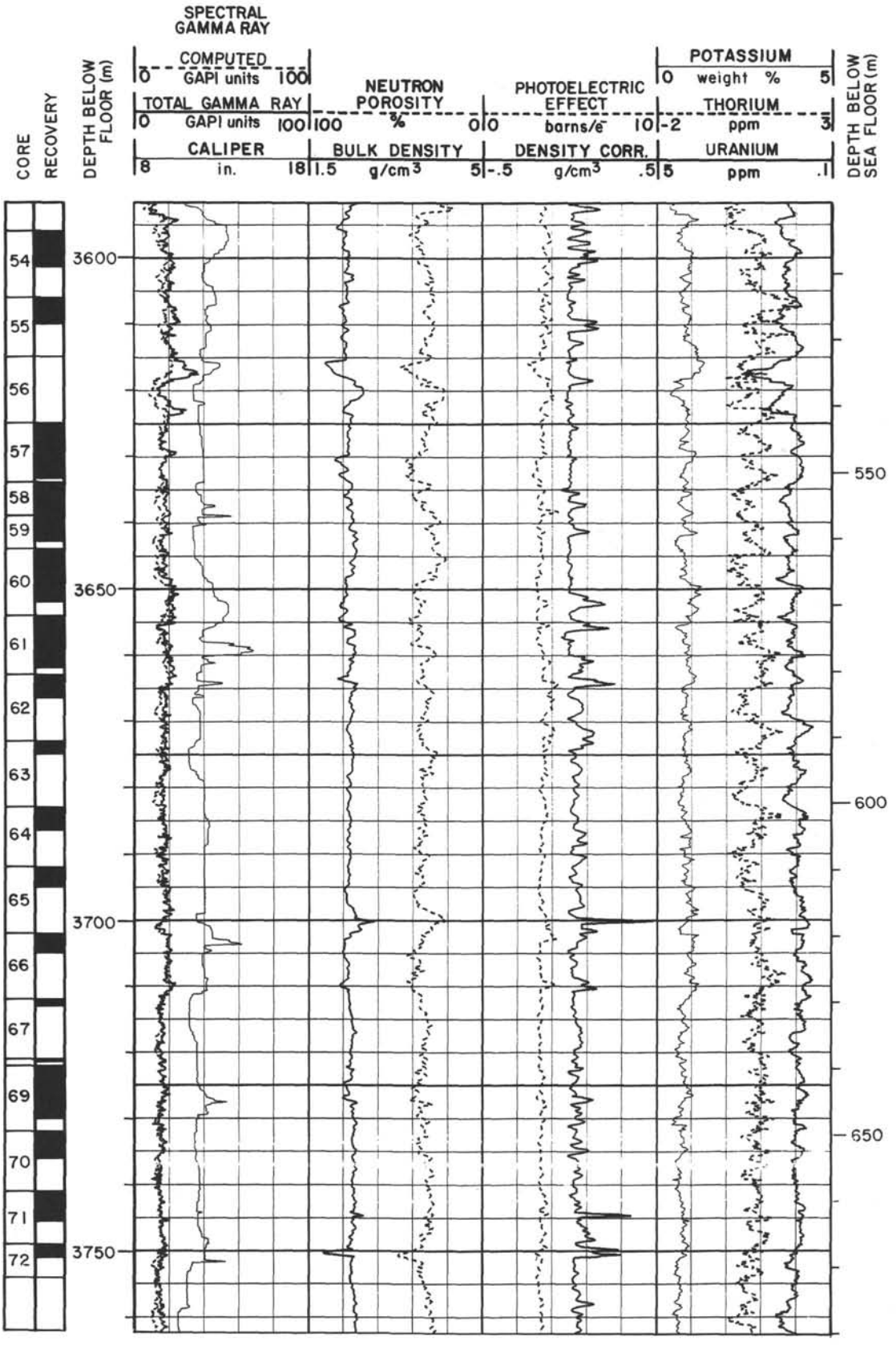

Summary Log for Site 786 (continued)

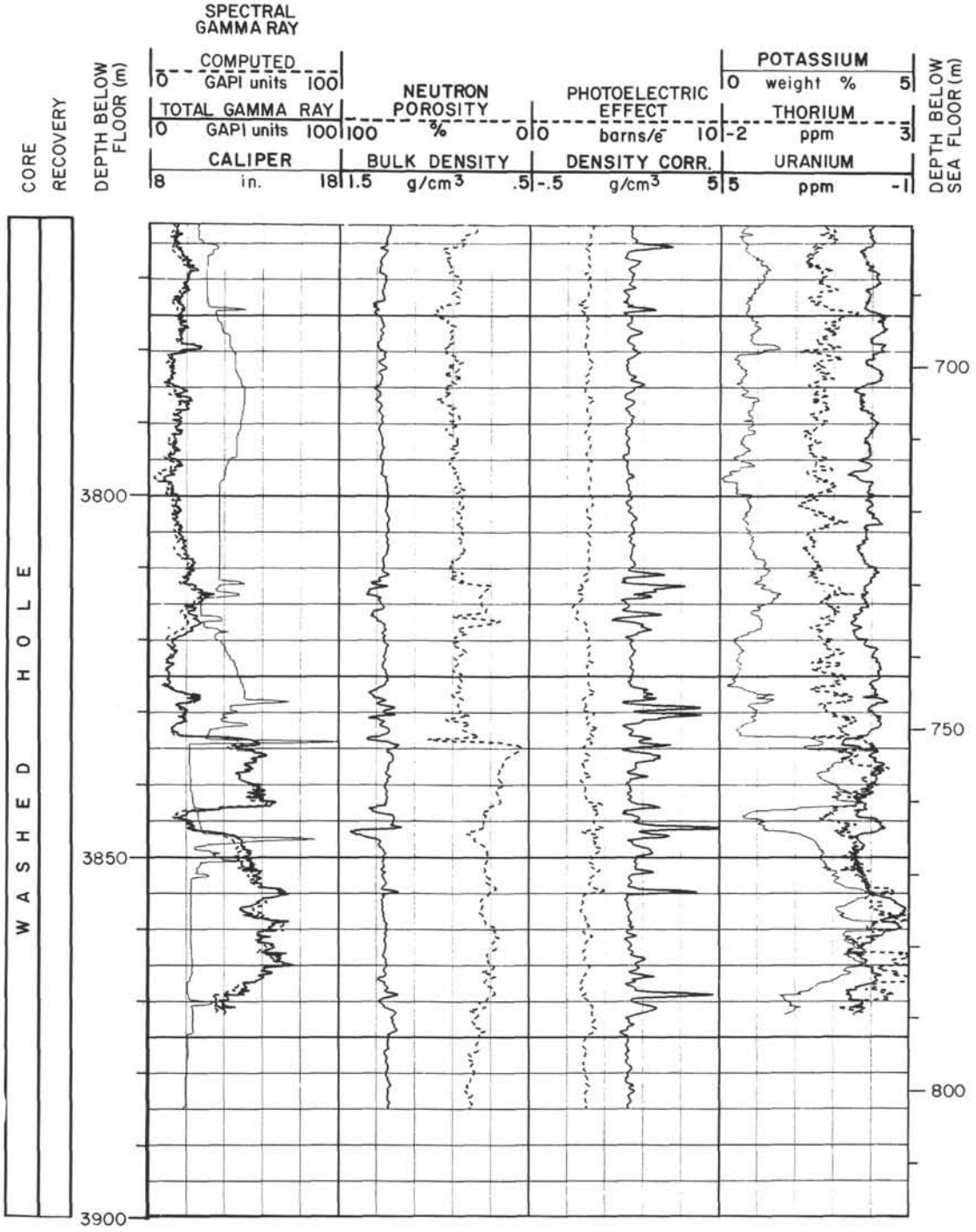

Summary Log for Site 786 (continued)

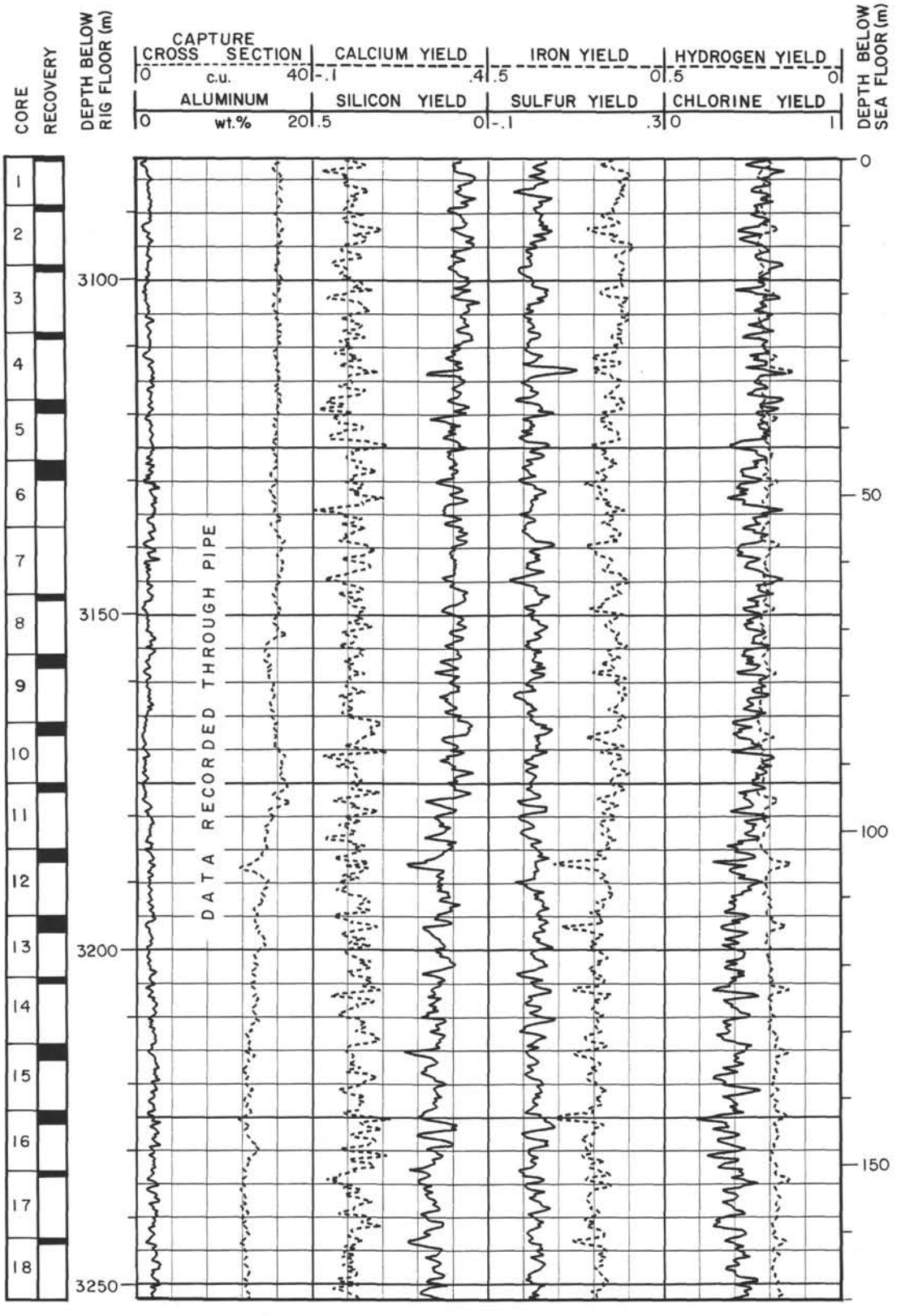

Summary Log for Site 786 (continued)

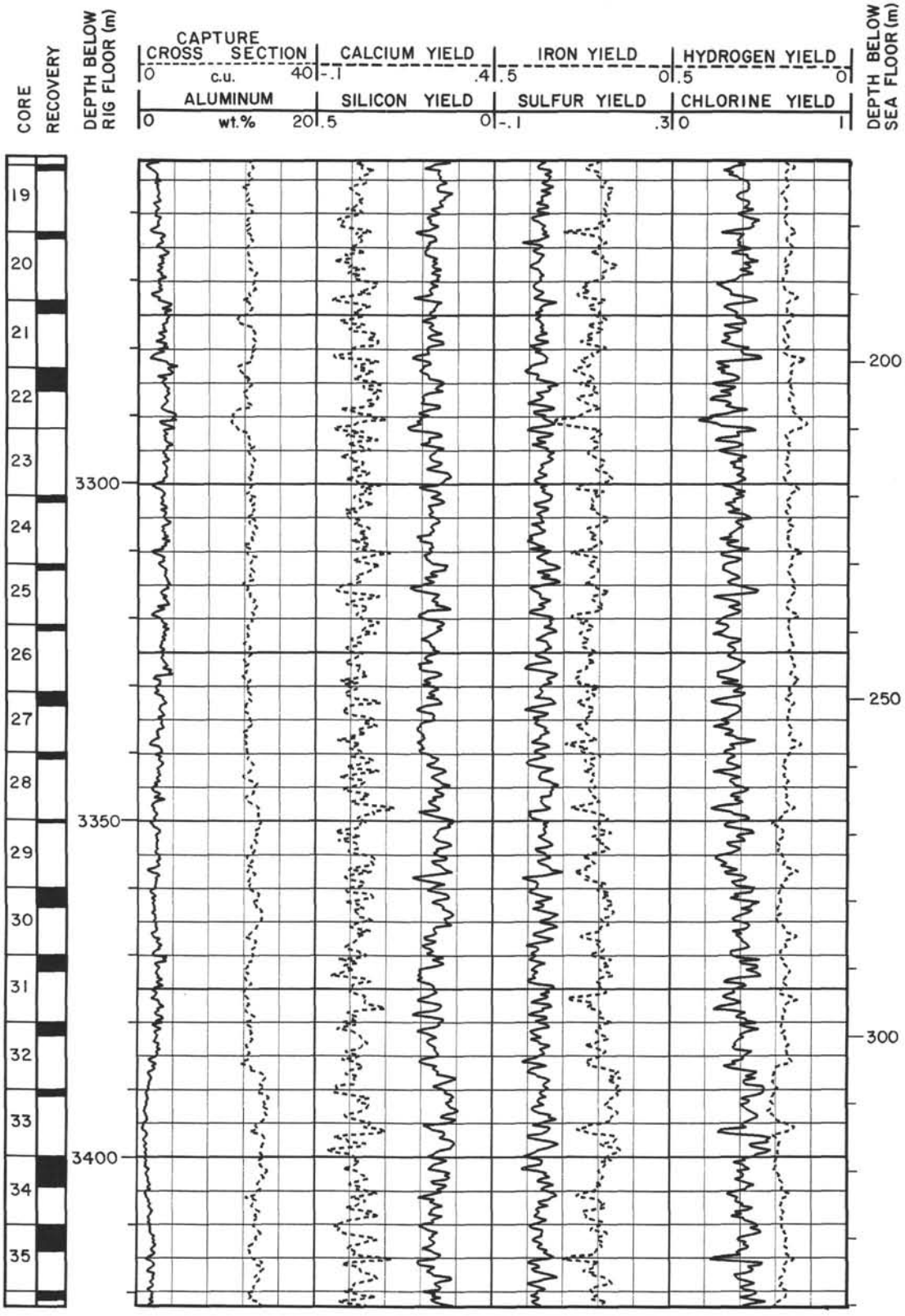

Summary Log for Site 786 (continued)

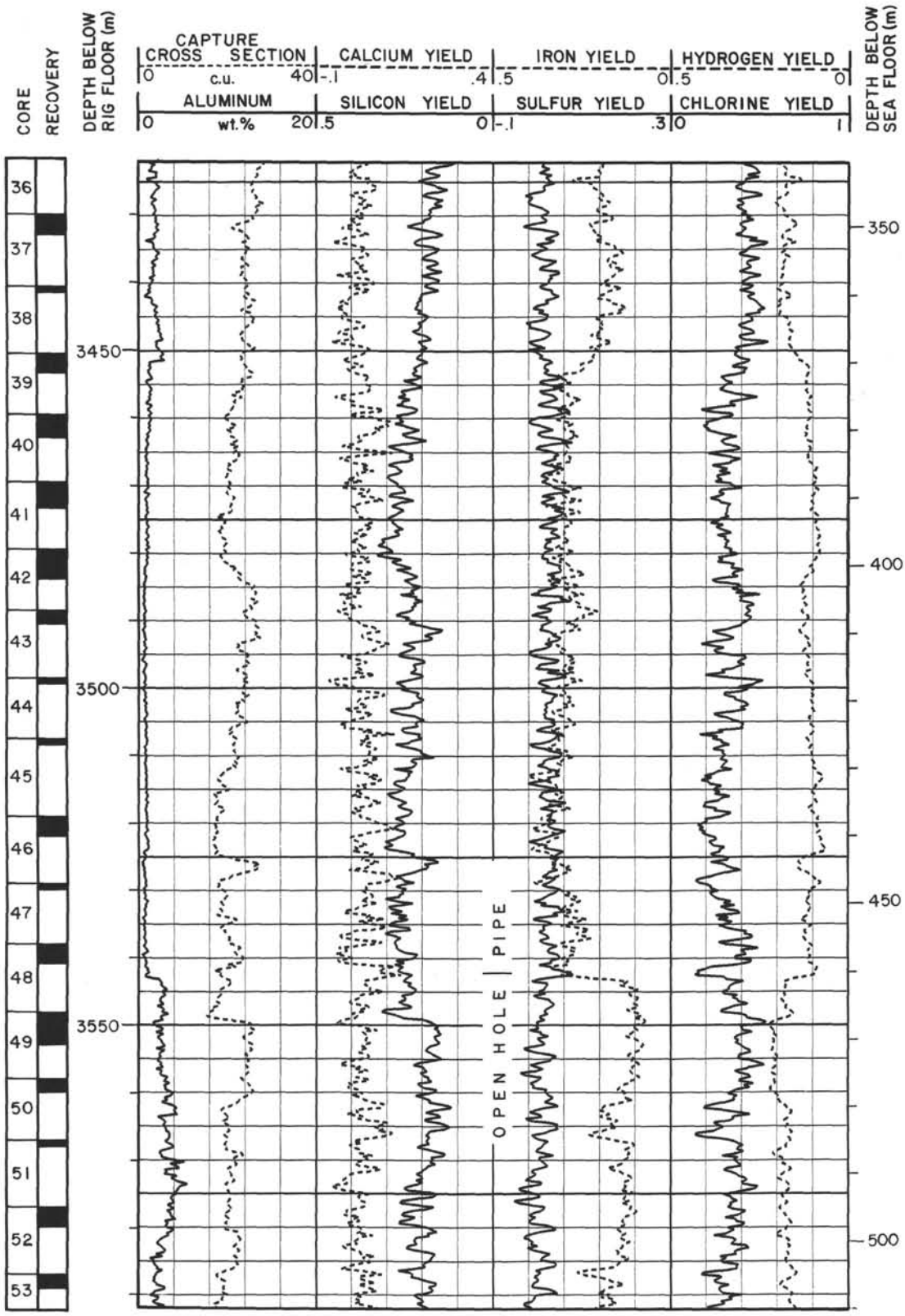

Summary Log for Site 786 (continued)

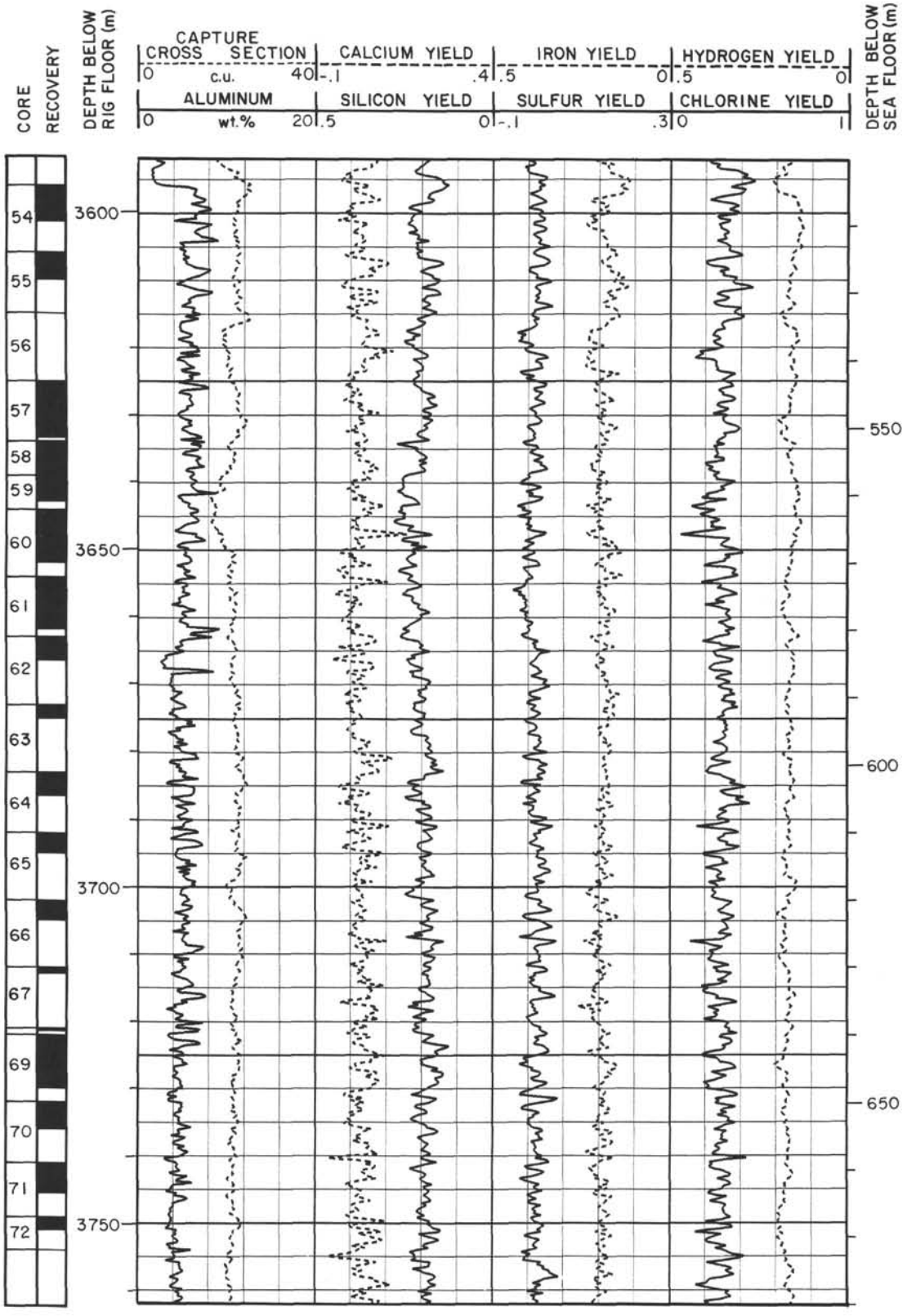

Summary Log for Site 786 (continued)